PREPARATION OF PLATE TYPE CATALYST AND DESIGN OF TUBE WALL REACTORS

（プレート状触媒の調製と管壁型反応器の設計）

DEPARTMENT OF CHEMICAL ENGINEERING
DIVISION OF CHEM. & BIO. SCI. AND TECH.
TOKYO UNIV. OF AGRI. & TECH.

Kyu MURATA

1996

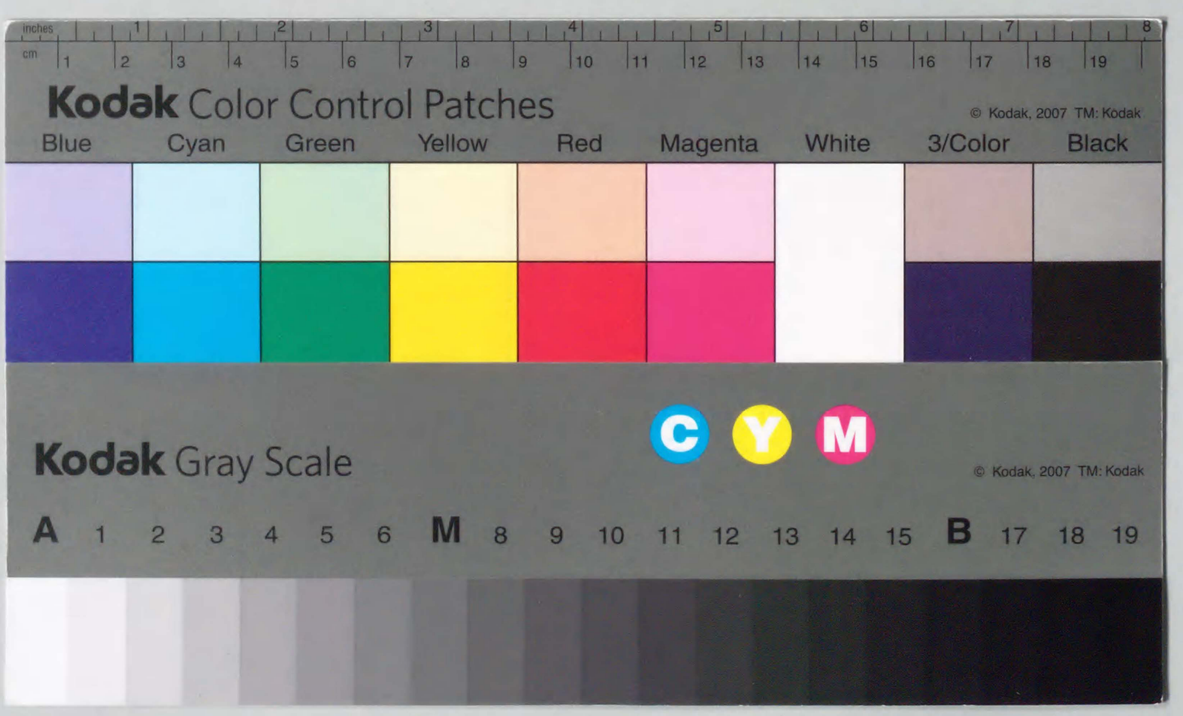

PREPARATION OF PLATE TYPE CATALYST AND DESIGN OF TUBE WALL REACTORS

（プレート状触媒の調製と管壁型反応器の設計）

DEP. OF CHEMICAL ENGINEERING
DIV. OF CHEM. & BIO. SCI. AND TECH.
TOKYO UNIV. OF AGRI. & TECH.

KYU MURATA

1996

Acknowledgments

The studies presented in this thesis are the summaries of the author's work carried out during 1990-1995 at the KAMEYAMA laboratory, department of Chemical Engineering , division of Chem. & Biol. Sci. and Tech., Faculty of Engineering, Tokyo University of Agri. & Tech.

Many thanks must begin with my parents, young brother, grandfathers and grandmothers. This thesis would not have been possible without their continuous encouragements and assistance. I would like to express my appreciation to my parents for giving me opportunity to go on to doctor course.

I would like to acknowledge the continuing guidance and encouragement of Professor Kameyama. His helpful suggestions with respect improved this study.

The through and helpful comments of the reviewers on preliminary versions of the article are gratefully acknowledged.

The comments of Professor Kabe provided many insights into preparation of plate type catalyst.

I wish to thank Professor Matsuoka for helpful suggestions and comments.

I am indebted to Assistant Prof. Kokugan for valuable comments and criticisms.

I wish to express my gratitude to Assistant Prof. Nagai for valuable advise.

I would like to express my gratitude to Dr. Yamamoto for frequent, stimulating and helpful discussions.

I gratefully acknowledge helpful discussions with Dr. Gastauer on several points in the paper.
I am indebted to Ms. Eliska of Tokyo Univ. of A&T and Mr. Christopher Watkins of JGC Corp. for their assistance in checking my English.

I wish to thank Prof. Saitoh and Dr. Yamashita for many helpful suggestions during the course of this work.
I am indebted to Dr. Matsumoto of JGC Corp. for drawing attention to catalysts and reactors. I am pleased to acknowledge the helpful discussion to Mr. Shibata, Mr. Taneda and Mr. Yasutomi of JGC Corp.
Several helpful discussions about anodic oxidation with P.E. Kuroda, Prof. Baba and Dr. Ono are gratefully acknowledged.

This work is supported in part by a Grant-in-Aid for scientific research from the Ministry of Education, Japan and IDEMITSU KOSAN Co.,LTD.

I wish to thank JGC Corp. for generous financial assistance for 4 years. I wish to thank Dr. Hashitani, Mr. Akatsuka and Mr. Kunoh of JGC Corp. for their encouragement for this work.
My special thanks are due to Mr. Higashi Deputy Manager of Chemical 1 group and members of Chemical 1 group of Project systems division of JGC Corp.

It is a pleasure to acknowledge the hospitality and encouragement of the member of Kameyama lab. This study is based on the former works of Mr. Yamaseki and Mr. Inoue. I would like to acknowledge the considerable assistance of them.

I wish to thanks Mr. Ichimura for his assistance and Mr. Toyoshima for the preparation of plate type catalysts. I also acknowledge the assistance of Mr. Terai for measurements of pore size distributions and Mr. Saitoh for EPMA analysis.

Thanks are due to my many colleagues with whom I have discussed this problem. Especially, I am grateful for help, encouragement and inspiration provided by Mr. Nagasawa, Mr. Shiizaki, Mr. Hirano and Mr. Imagawa.

It would be inappropriate to list all of them and their contributions, but I would like to express my gratitude.
Only the errors and omissions are entirely my own.

Final thanks go to all the friends and loved one on whose support and love I depend and to whose warm and lively companionship. I happily return now that this thesis is complete.

1996 February Kyu MURATA

CONTENTS

CHAPTER 3 THE PREPARATION METHODS OF THE PLATE TYPE CATALYST USING OXALIC ACID

CHAPTER 4 EFFECTIVENESS FACTOR OF THE PLATE TYPE CATALYST

CAPTIONS TO FIGURES

Chapter

1

Introduction and Basic Concepts

1 BACKGROUND

New energy sources must be developed in response to growing worldwide demand for energy and man's commitment to the environment. Since it is impossible to satisfy all energy demand with new energy sources immediately, new systems of highly efficient use of fossil energy must be developed.

The Japanese "HEAT PUMP TECHNOLOGY CENTER" reported recently that conventional heat pumps can save about 1 % of the total energy consumption in JAPAN. To reduce energy consumption still more, new heat pump systems, such as chemical heat pumps, are needed.

Chemical heat pumps are one new system for highly efficient use of energy. Chemical heat pumps transfer solar energy, geothermal heat and thermal waste heat into chemical substances by chemical reaction and upgrade their potential heat by raising the temperature.

1.1 Chemical heat pumps

(1) Definitions of Chemical Heat Pumps [17)32)33)]

Chemical heat pumps involve processes which use exo- and endothermic reverse chemical reactions. The chemical heat pumps can store industrial waste heat or natural heat such as solar energy and upgrade such heat by raising the temperature.

These processes are useful, since they enable us to:

1) Use energy highly efficiently
2) Control working temperature easily, and
3) Store and transport energy in the form of stable chemical substances without energy loss

Therefore, the early realization of their practical use is expected in the fields of large

scale industries and energy usage.

Many kinds of reactions are considered for chemical heat pumps:

1) Hydrogenation, isomerization and hydration
2) Adsorption of condensed vapor by liquids and solid salt
3) Mixing of different species of liquids
4) Adsorption of gas into porous material
5) Hydrogenation of metal
6) Formation of clathrate compounds

Each reaction has common problems of a way to supply reaction heat efficiently.

(2) Chemical heat pumps using organic substances [1)4)-16)19)21)22)30)31)]

Isopropanol/Acetone/Hydrogen (IAH) cycle and Cyclohexane/Benzene/Hydrogen (CBH) system are types of chemical heat pumps using organic substances.

IAH cycle with reaction couple of isopropanol dehydrogenation and acetone hydrogenation has been proposed (**Figure 1.1**). Fundamental studies such as catalyst, reactor, efficiency etc. have been undertaken at Saito laboratory at Tokyo Science university and Kameyama laboratory at TOKYO Univ. of Agri. & Tech. Recently, a bench-scale plant was constructed by JGC corporation under contract from NEDO (**Figure 1.2**).

CBH system with reaction couple of cyclohexane dehydrogenation and benzene hydrogenation has been also proposed (**Figure 1.3**). Feasibility studies have been done in some laboratories, but fundamental study has been undertaken at Kameyama lab. at TOKYO Univ. of Agri. & Tech.

(3) Cyclohexane/Benzene/Hydrogen chemical heat pump system [33)20)]

The CBH chemical heat pump combines compressive work and a reaction couple of benzene hydrogenation at 623 K, 20 atm and cyclohexane dehydrogenation at 473 K, under 1 atm. The system is hopefully a way to realize efficient use of many kinds of waste heat such as;

1) Thermochemical hydrogen production process

2) Methanol fuel cells
3) Several technologies using sunshine.

The reaction couple is expressed as equation (1.1).

$$C_6H_6 + 3H_2 \Leftrightarrow C_6H_{12} + 206\ kJ/mole \qquad (1.1)$$

Several applications of CBH chemical heat pump have been proposed.

1) Back up system for the UT-3 thermochemical hydrogen process as a heat and hydrogen storage system (**Figure 1.4**) [15].
2) Utilization for the world energy network (WE-NET) system that transports hydrogen produced elsewhere to Japan.
3) Combination of IAH cycle and CBH cycle. Here it would be possible to raise the temperature level of heat, available at 353 K, up to a temperature of about 623 K (**Figure 1.5**).
4) Back up system for fuel cell as a heat storage system.

1.2 Role of wall type reactor and plate type catalysts

To realize the efficient use of many kinds of heat, a wall type reactor is required. In the wall type reactor, the endothermic or exothermic reaction takes place on the catalyst wall. The reaction heat is recovered and supplied simultaneously through the reactor wall without exergie loss.

In the wall type reactor, catalyst layer is formed on the surface of the reactor wall. The following are requirements of the catalyst to create this reactor:

1) High thermal conductivity to avoid exergie loss
2) High catalytic reactivity to achieve small sized reactor
3) High selectivity for reaction, for high efficiency of the CHPs.
4) High durability and easy reactivation, for low running cost of the CHPs
5) Technique to prepare various shapes of the catalyst, to make wall type reactor from commercial heat exchangers

Many techniques have been proposed to prepare a catalyst layer on the reactor wall. These are ;

1) Spray or coating of catalyst on reactor wall [25)2)3)]
2) Galvanizing of catalyst metal [18)]
3) Leaching of Raney alloy [28)29)]
4) Anodic oxidation and hot water treatment method [19)22)]

These methods, except the anodic oxidation method, have critical defects of low reactivity and omission of catalyst.

In this thesis, anodic oxidation and hot water treatment [19)31)14)] is adopted as the preparation method of the plate type catalyst.

1.3 Anodic oxidation [23)24)26)27)]

Anodic oxidation of aluminum is widely known and applied in many areas of surface treatment for;

1) Stabilizing or coloring the surface
2) Creating non-conductive film of electrolytic capacitor
3) High-density magnetic film for data storage

Yamada et. al. have reported the effect of anodic oxidation on controlling porosity or morphology of alumina. They also studied catalytic reactivities of the alumina layer stripped from the aluminum plate.

Heat conductivity of this anodized alumina/aluminum catalyst is ten times higher than conventional alumina pellet catalyst [19)31)]. It is possible to use commercial aluminum and aluminum and stainless clad plate as base material [12)13)].

2 PURPOSE

Main purpose of this thesis is preparation of plate type catalyst and design of tube wall type reactors for practical use in the CBH-CHP. The following require study

ahead of practical usage of this technique:

1) Development of preparation technique of a plate type catalyst by the combination of anodic oxidation of commercial aluminum plate of 99.5% purity and successive hot water treatment.
2) Prevention of deterioration of catalytic reactivity.
3) Development of catalysts in shape of tube-wall, fin-tube and plate-fin reactors.
4) Examination of performance of the tube wall reactor, compared with that of a fixed bed reactor, by calculating temperature and conversion distributions inside the reactor.
5) Proposal of improvement of process flow and operating conditions for heat storage/release operating mode.

3 ORIGINALITY

(1) Preparation method of plate type catalyst

Preparation conditions of $Pt/Al_2O_3/Al$ plate type catalyst with high reactivity were established. Catalyst thickness more than 300 μm and porosity up to 0.7 were possible, by controlling thickness and porosity of anodized alumina layer.

(2) Durability of plate type catalyst

Quality analysis of plate type catalyst under cyclohexane dehydrogenation was conducted and deactivation model was proposed. Long life test up to 1000 h was studied using integral reactor. The conversion change with time was illustrated using this model.

(3) Design of plate type catalyst

As contributors to effectiveness factor, optimum thickness and structure of plate type catalyst layer were proposed. The optimum thickness depends on reaction conditions and kind of reaction.

(4) Design of tube wall reactor

Mass transfer in tube wall reactor developing laminar flow was experimentally studied. According to the results, a simulator of the tube wall reactor was made. Optimum design of tube wall reactor, demonstrating both small and large duty, was proposed.

(5) Improved process flow and operating conditions

Improvement of the process flow of CBH-CHP bringing tube wall reactor into full play is proposed. Operating conditions for heat storage or release operating mode are also proposed.

4 STRUCTURE

This thesis consists of 3 main parts over 10 chapters.

Chapter 1 Introduction and Basic Concepts

Background, purpose, originality and structure of this doctor thesis are written.

Part 1 Preparation of Plate Type Catalysts [34)35)36)37)41)]

Preparation method, effectiveness factor and durability of plate type catalyst are studied in **Chapters 2-5**.

Part 2 Design of Wall Type Reactors [38)39)40)]

Mass transfer in the tube wall reactor, simulation of tube wall reactor and performance of the tube wall reactor are studied in **Chapters 6-8**.

Part 3 Chemical Heat Pump System With Tube Wall Reactors

Performance of cyclohexane/benzene/hydrogen chemical heat pump system

including heat storage/release operating mode are studied. Operating parameters are also studied in **Chapter 9**.

Chapter 10 Conclusions

Conclusions of each chapter and lists of published papers and presentations are shown.

References

1) Aramaki,I., K.Yamamoto, H.Kameyama,:Preprints of the 20th Autumn Meeting The Soc. of Chem.Engrs, JAPAN, SM304, 1987
2) Arashi, N. : *Kagaku Kogaku Ronbunshu*, 6, 5, 476(1980)
3) Arashi, N. : *Kagaku Kogaku Ronbunshu*, 10, 3, 359(1984
4) Itoh,M., K.Yamamoto, H.Kameyama,: Preprints of the 52nd Annual Meeting of The Soc. of Chem. Engrs, JAPAN, G202, 1987
5) Itoh,M., K.Yamamoto, H.Kameyama,: Preprints of the 21st Autumn Meeting The Soc. of Chem.Engrs,J APAN, SO313, 1988
6) Yamaseki,K., K.Yamamoto, H.Kameyama,: Preprints of the 21st Autumn Meeting The Soc. of Chem.Engrs, JAPAN, SN114, 1988
7) Yamaseki,K., K.Yamamoto, H.Kameyama,: Preprints of the 22nd Autumn Meeting The Soc. of Chem.Engrs, JAPAN, SM304, 1989
8) Inoue,M., K.Yamamoto, H.Kameyama,: Preprints of the 54th Annual Meeting of The Soc. of Chem. Engrs, JAPAN, L115, 1989
9) Okumura,H., K.Yamamoto, H.Kameyama,: Preprints of the 22nd Autumn Meeting The Soc. of Chem.Engrs, JAPAN, SM103, 1989
10) Okumura,H., K.Yamamoto, H.Kameyama,: Preprints of the 27th Nensho Symposium, 1989
11) Inoue,M., K.Yamamoto, H.Kameyama,: Preprints of the 23rd Autumn Meeting

The Soc. of Chem.Engrs, JAPAN, SB201, 1990

12) Yamanaka,R., K.Yamamoto, H.Kameyama,: Preprints of the 55th Annual Meeting of The Soc. of Chem. Engrs, JAPAN, E101, 1990

13) Yamanaka,R., K.Yamamoto, H.Kameyama,: Preprints of the 23rd Autumn Meeting The Soc. of Chem.Engrs, JAPAN, SB202, 1990

14) Yamaseki, K., K.Yamamoto, H.Kameyama, *Kagaku Kougaku Ronbunshu*,17, 267-272, 1991

15) Kameyama et.al, Hydrogen Energy, IX,1, 93-102, 1992

16) Kameyama,H.,M.Inoue,H.Okumura,I.Sasaki,*Kagaku Kougaku*, 55, 1991

17) Fujii, S., H. Kameyama, T. Kawahara, K. Yoshida, J. of Chem. Eng. Japan, 10, p.224-228 (1976)

18) Fukuhara, N. and A. Igarashi:Preprints of the 23rd Autumn Meeting of The Soc. of Chem. Engrs, Japan, Kanazawa, p.156 (1990)

19) Hashioka,T., S. Kosedo, M. Itoh, K. Yamamoto and H. Kameyama :Chem. Let., 1987, 1067 (1987)

20) Kashiwagi, T.et al.:"Kouseinou Chemical heat pump oyou jireishu",SCIENCE FORUM,1991

21) Kameyama, H., M. Yamashita and Y. Saitoh:Shokubai, 31, 5, 285 (1989)

22) Kameyama, H. and M. Itoh: Chem. Eng.(JPN), 34, 4, 58 (1989)

23) Keller, F., M.S.Hunter and D.L.Robinson: J.:Electrochem, Soc., 100, 411 (1953)

24) Koda, M., H. Takahashi and M. Nagayama: *Kinzoku Hyoumen Gijutu*, 33, 5, 242, (1982)

25) Kubo, O. : *Jidousha Gijutsu*, 47, 5, 70(1993)

26) Ono, S.:*Keikinzoku*, 40, 10, 729 (1990)

27) Shimura M. and T. Fukushima:*Kinzoku Hyoumen Gijutu*, 27, 10, 480 (1976)

28) TAKEOKA S. : *Kagaku Kogaku*, 45, 433 (1981)

29) TAKEOKA S. : Hyoumen, 24, 143 (1986)

30) Yamaseki, K.:Master's Thesis,1990

31) K. Yamaseki, K. Yamamoto and H. Kameyama, *Kagaku Kougaku Ronbunshu*, Vol.17, pp.267-272 (1991).

32) Yoshida, K., H. Kameyama, Proc. of 1st hydrogen energyconf,1,p.6A51 (1976)

33) Yoshida, K.et al.: "Chemical heat pump sekkei handbook", SCIENCE FORUM, 1985

34) Murata, K., K. Yamamoto and H. Kameyama: Study of Method of Preparing a Plate-Type Catalyst by Anodic Oxidation and Hot-Water Treatment, *Kagaku Kogaku Ronbunshu*, 19, 1, p.41(1993)

35) Murata, K. and H. Kameyama: Application of the Anodized Alumina Plate to the Wall Type Catalyst, *Hyoumen Gijutsu*, 47, 2, (1996)

36) Murata, K. and H. Kameyama: Effectiveness Factor of $Pt/Al_2O_3/Al$ Plate Type Catalyst, submitted to *Hyoumen Gijutsu*

37) Murata, K. and H. Kameyama: Deactivation and Durability of the $Pt/Al_2O_3/Al$ Plate type catalyst for the Chemical Heat Pump, under preparation

38) Murata, K. and H. Kameyama: related to mass transfer of the tube wall catalyst, under preparation

39) Murata, K. and H. Kameyama: A Study of a Tube-Wall Reactor with Heat Exchanger Function, *Kagaku Kogaku Ronbunshu* , 19, 5, p.849(1993)

40) Murata, K., K. Yamamoto and H. Kameyama: Performance of a Tube Wall Type Reactor for Transforming Heat Energy Into Chemical Energy Efficiently,Int. J. Hydrogen, 21, 3, p.201- (1996)

41) Terai, S., K. Murata, K. Yamamoto and H. Kameyama; *Kagaku Kogaku Ronbunshu*, 21, 6, p.1069- (1995)

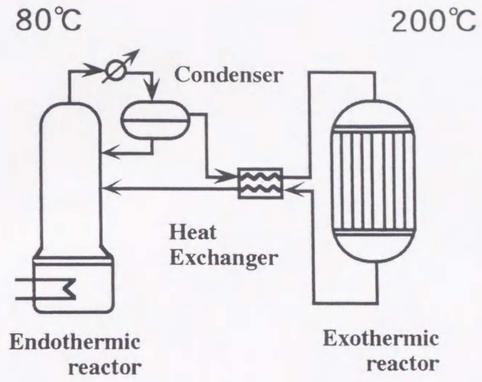

Figure 1.1 Process flow of Isopropanol/Acetone/ Hydrogen (IAH) cycle

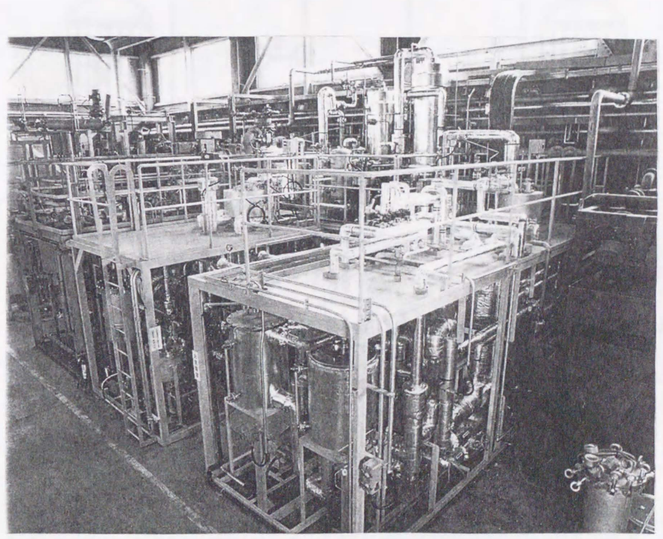

Figure 1.2 Photograph of pilot plant of IAH cycle constructed by JGC Corporation under contract from NEDO

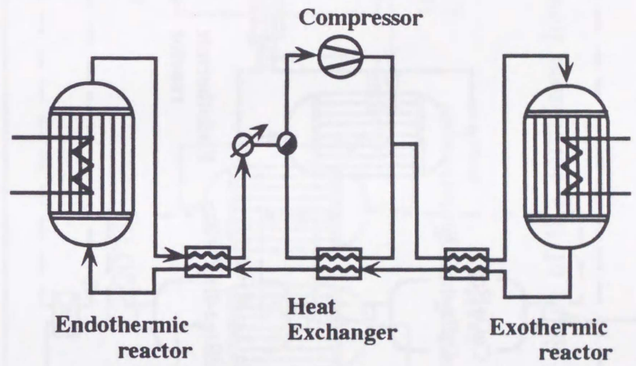

Figure 1.3 Process flow of Cyclohexane/Benzene/ Hydrogen (CBH) system

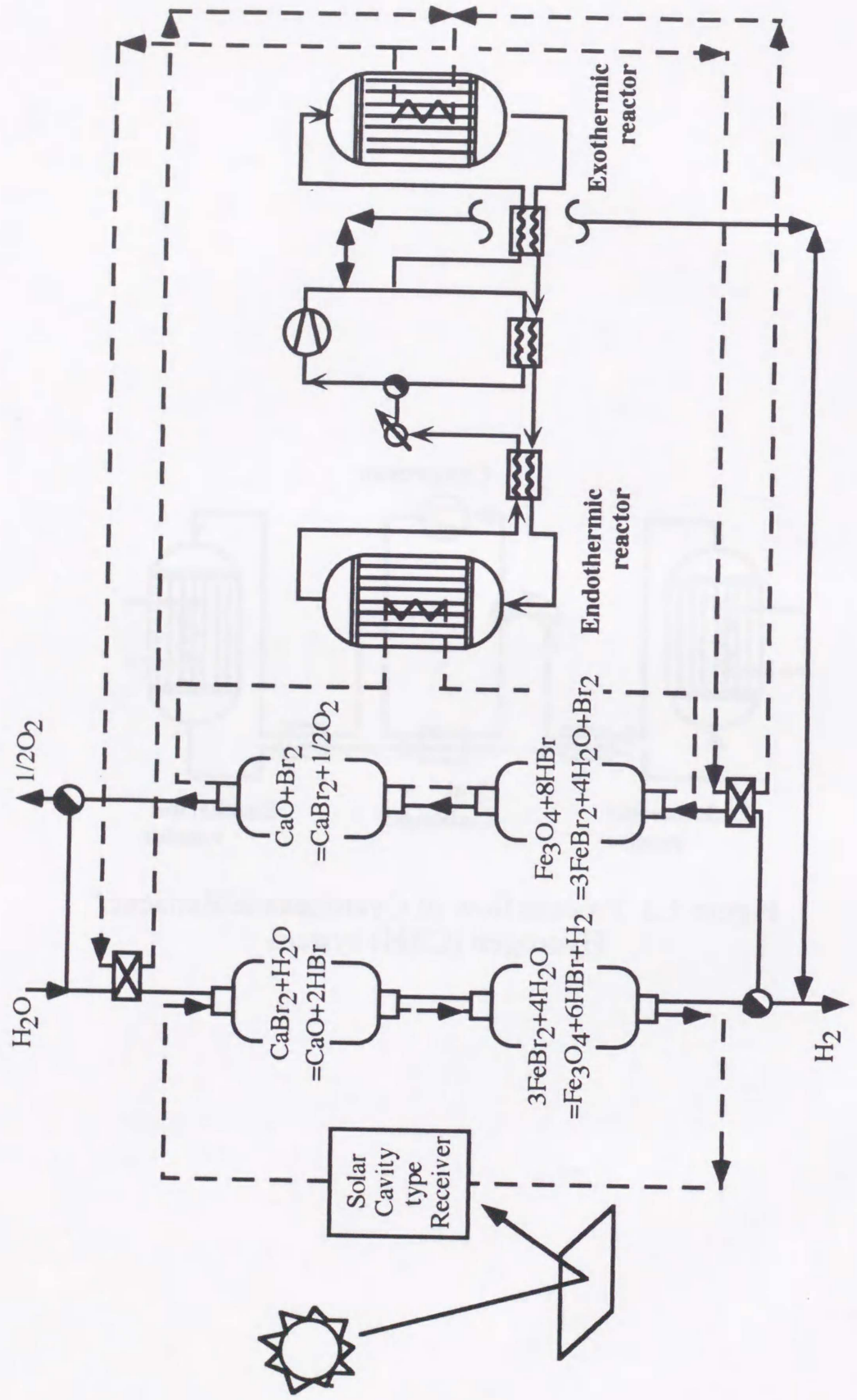

Figure 1.4 CBH system as heat recovery and hydrogen storage system for UT-3 thermochemical hydrogen production process

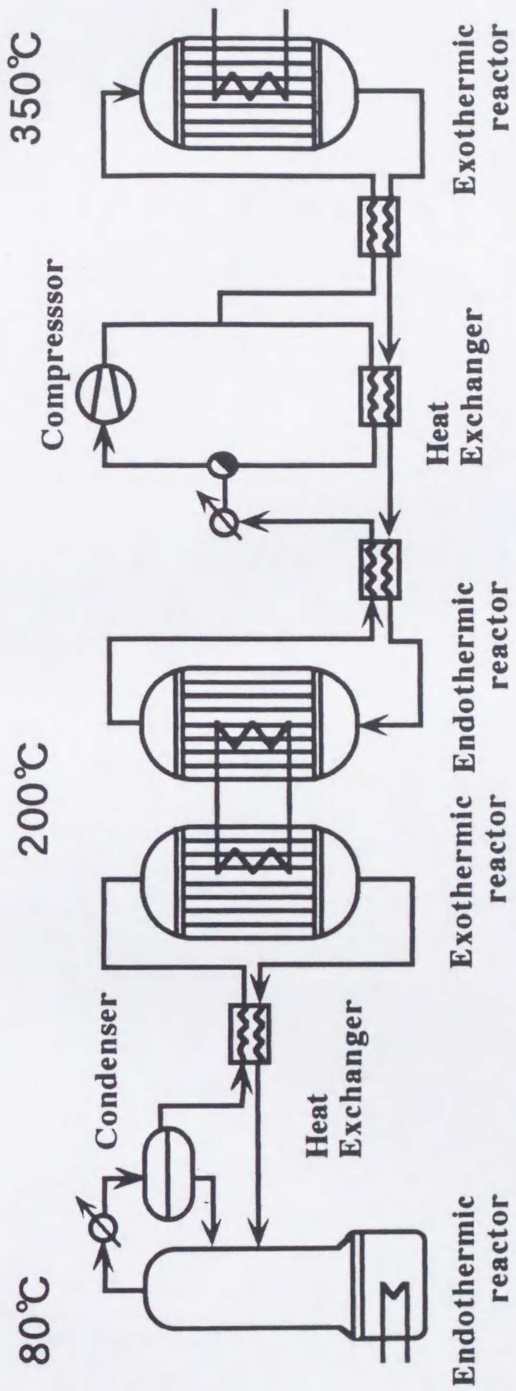

Figure 1.5 Flow sheet of the combined heat pump cycle

Chapter

2

The Preparation Method Of The Plate Type Catalyst Using Chromic Acid

INTRODUCTION

In the fixed bed reactor, it is difficult to keep reaction temperature the same throughout the radius. This is because thermal conductivity of packed catalyst is low and contact thermal resistance of catalysts is large. The distribution of reaction temperature in radius, which is called hot spots in case of an exothermic reaction, causes side reactions, difficulty in controlling the reaction and damage of the catalyst.

To dissolve the weak points of the fixed-bed reactor, plate type catalyst whose catalyst layer is directly formed on the metal body of reactor wall is proposed (see Figs 8.7, 8.9 p.159) [3]. A reactor equipped with this type of catalyst is called a wall type reactor. In the wall type reactor, distribution of reaction temperature is not observed, due to its high thermal conductivity [1]. The wall type reactor can serve as a heat exchanger, since the catalyst is expected to exhibit high thermal conductivity and low pressure loss.

Other preparation methods of plate type catalyst have been reported, such as anodic oxidation method, spray method, galvanizing method and leaching method of Raney alloy. The methods other than anodic oxidation have a fatal defect, i.e. the catalytic reactivity is low and the catalyst layer is detached from metal body easily.

A $Pt/Al_2O_3/Al$ plate type catalyst was prepared by anodic oxidation followed by hot water treatment and calcination of a commercial aluminum plate. Alumina catalyst support is produced by anodic oxidation and subsequent hot water treatment which impregnates Pt as a catalyst species. BET surface area of the alumina layer is increased by calcination after the hot water treatment. This catalyst has high thermal conductivity and the catalyst layer did not detach from the metal body after a long period of reaction test. A reactor equipped with this type of catalyst can serve as a heat exchanger due to the high thermal conductivity and low pressure loss.

The basis for the production of plate type catalyst was established as

followings 1)2)4)5)9).

1) Development of the preparation method by the combination of anodization of aluminum plate of 99.99 % high purity and successive hot water treatment (HWT). Maximum thickness of catalyst layer was 10 μm.
2) Development of a catalyst in the shape of a tube with spiral plate inside for the exothermic hydrogenation of benzene, using commercial aluminum.

In this chapter, the best conditions for catalyst preparation using chromic acid for anodic oxidation are identified.

1 EXPERIMENTAL

1.1 Preparation of the catalyst

(1) Anodic oxidation (AO)

The experimental apparatus of anodic oxidation is shown in **figure 2.1**. The raw materials used were high quality aluminum (99.99 % in purity and 0.1 mm in thickness) and the commercial aluminum plate (JIS A1050: 99.5 % in purity, 0.3 mm in thickness). A piece of the plate (from 40 x 140 mm to 240 x 240 mm) was pre-treated in 20 wt% aqueous solution of NaOH for 3 min., and in 30 wt% HNO_3 for 1 min., successively. The plate was anodized in 2.5-4.0 wt% of chromic acid aqueous solution at current density of 19-2000 A/m2, at 283-313 K and for 2-24 h with copper plate as cathode. The anodized plate was rinsed with water, and then dried at 623 K for 1 h.

(2) Hot water treatment (HWT)

In this process, platinum is impregnated in the alumina layer by hot water treatment. The experimental apparatus was shown in **figure 2.2**.

The hot water treatment was conducted in H_2PtCl_6 solution of 0.2-1.0 Pt-g/L at pH 11.4 (controlled by ammonia), at 353 K and for 1-4 h. The plate was rinsed with deionized water, soaked in 0.3 wt% KCl solution at room temperature for 20 min and rinsed with deionized water again. Then, the plate was dried at room temperature and then calcined in air at 623 K for 1 h.

1.2 Characterization of the catalyst

(1) Thickness of alumina layer

ISOSCOPE MP-2 (Helmut Fischer) was used to measure the thickness of alumina film.

(2) BET surface area

The surface area and pore size distribution of the catalyst were determined with BET apparatus.

(3) Platinum content

Quantity of platinum content was measured by atomic absorption spectroscopy (Shimazu AA-680).

(4) Platinum dispersion

Platinum dispersion was determined by CO pulse method 8).

(5) EPMA analysis of the cross section of the catalyst

Platinum distribution in the alumina layer was measured by X-ray microanalyser (XMA).

1.3 Measurement of catalytic reactivity

In this study, we evaluated catalytic reactivity by cyclohexane dehydrogenation which is used for endothermic reaction of CBH-CHP 4).

The chemical reaction is expressed in equation(2.1).

$$C_6H_{12} + 206\ kJ/mole \overset{473K}{\Leftrightarrow} C_6H_6 + 3H_2 \qquad (2.1)$$

The flow type reactor (**figures 2.3, 2.4**) was used as **a differential reactor. 0.1-0.15 g of the catalyst and small aluminum tips as dilutor was packed in pyrex reaction tube of 10 mm in diameter. The height of the catalyst bed was 15 mm.** Activation of the catalyst was performed by oxidation in air at 623 K for 12 h and reduction in hydrogen stream at 623 K for 2 h before the reactivity test. Dehydrogenation reactivity was studied at 473 K, 0.1 MPa. Cyclohexane which is purified by raney nickel catalyst [7] is diluted by nitrogen (dilution ratio was 10) flowed at a rate of 7.5 ml-cyclohexane/h and the concentrations at inlet and outlet gases of the reaction tube were determined with GC equipped with FID (Shimazu GC-8A).

2 RESULTS AND DISCUSSION

2.1 SEM analysis of prepared catalysts

Figure 2.5 shows SEM analysis of cross section and surface of anodized alumina layer and following hot water treatment. Alumina layer with 10 μm was formed on the both side of aluminum layer.

After anodic oxidation, pores more than 50 nm in radius were formed. Roughness factor (RF=BET surface area / apparent surface area) was about 450-700 [BET-m^2/m^2]. After hot water treatment and calcination, the pore radius changed to about 2 nm and BET surface area increased. Roughness factor increased more than 10000 [BET-m^2/m^2]. Platinum impregnated within the porous alumina layer and Pt/Alumina catalyst layer was formed.

2.2 Conditions of anodic oxidation

(1) Purity of aluminum

Effects of aluminum purity on the physical properties of catalyst and the catalytic reactivity were studied. Two materials were used. One is high purity aluminum (99.99 % in purity) and the other is commercial aluminum (99.5 % in purity, JIS-A1050). Plate type catalysts were prepared under the same conditions and the physical properties are shown in **table 2.1**. The results of reaction test are shown in **figure 2.6**. The results are shown as follows:

Table 2.1 Physical properties of catalysts prepared by using high purity alumina and commercial alumina

Cat	(a)	(b)
Al purity	99.99%	99.5%(JIS A-1050)
AO condition	Cr 2.5 wt%, 303 K, 12 h	
HWT condition	1.0 g-Pt/L, 353 K, 2 h	
Thickness of Al_2O_3	20 μ m	10 μ m
R.F.	11500	6700
Pt contents	1.72 g/m^2	1.1 g/m^2
Pt dispersion	0.72	0.51
Pt area	1.24 g/m^2	0.56 g/m^2

1) The thickness of catalyst layer using high purity aluminum was 20 μm

which was two times thicker than that of commercial aluminum. It has been reported that the purity of aluminum affects the thickness of anodized alumina layer [6]. Therefore, impurity in the aluminum is expected to prevent anodization.

2) Roughness factors of each catalyst were proportional to the thickness of the catalyst layer in spite of the purity of aluminum. This means the RF per unit volume is the same and the structure of the catalyst layer is considered to be also the same.

3) Platinum content per unit RF of each catalyst is the same and it seems that chemical properties of the catalyst prepared using commercial aluminum are the same as that prepared using high purity aluminum.

4) Catalytic reactivity is proportional to the catalyst content and the impurity of the catalyst seems to have no effect on the reaction.

The purity of aluminum has an effect on the thickness of anodized alumina layer but it has no effect on the catalyst content and the catalytic reactivity. To utilize the plate type catalyst, it is necessary to use a cheap material like commercial aluminum. Therefore, I used commercial aluminum and studied preparation conditions of the plate type catalyst, prepared by anodic oxidation and hot water treatment.

(2) Concentration of chromic acid solution

Effects of the concentration of chromic acid solution (2.5-3.5 wt%) on the thickness of the anodized alumina layer are illustrated in **figure 2.7**. Current density was 19 A/m^2 and anodized time was 12 hr. It is clear that the thickness of alumina layer is irrelevant to the reactivity. In this work, chromic acid solution of 2.5 wt% was used, to keep cost minimal for waste water treatment and electrolyte.

(3) Temperature and oxidation time

Figure 2.8 shows a change in thickness of alumina layer at 12 h of anodization, according to temperature of the electrolyte bath. The temperature was changed between 288 K and 311 K. The thickness showed a peak of 20 μm at 298 K.

Figure 2.9 shows the changes in thickness of the alumina film with time of anodization at 298 K and 303 K. The thickness increased with time at first, then kept a constant value related to the temperature. The constant value shows that the rates of production and dissolution of the film are kept equal at that temperature. The maximum thickness at 303 K and 293 K were 10 and 30 μm, respectively.

(4) Dissolution of anodized alumina layer

Figure 2.10 shows changes in thickness with dissolution time. The thickness decreased linearly with dissolution time. The dissolution rate was calculated as about 1.58 μm/h. Therefore, in the anodic oxidation, generated alumina layer is dissolved into chromic acid.

(5) Optimum temperature for anodic oxidation

It has been observed in the preceding that equilibrium thickness of alumina layer was decided by temperature of electrolyte bath. This considers that equilibrium thickness was determined by the balance of generation and dissolution rate of alumina layer. To form a thick alumina layer efficiently, temperature at which thickness of alumina layer per unit electricity is maximum is considered to be the optimum temperature. The generation rate of alumina layer at 298 K-303 K was calculated as 1.5 μm/h from figure 2.8. Figure 2.8s shows the thickness of alumina layer per 12 h. From this figure, the generation rate at 298 K or less is calculated as 1.5 μm/h or less. Therefore, optimum temperature, at which generation rate and equilibrium thickness are large, is 298 K.

(6) Current density

The effects of current density on the anodized alumina layer are studied here. Under high current density, burn out of the surface of alumina layer was observed at over 100 V. This burn out was caused by electric discharge. **Figure 2.11** shows photograph and illustration of surface of anodized alumina layers. Number of electric discharge mark increased with current density. **Figure 2.12** shows XRD analysis of surface of anodized alumina layer. Anodized alumina layer which was prepared under normal conditions showed amorphous alumina which was the same as Inoue's report [2]. On the other hand, burned out alumina layer showed γ alumina peak by XRD analysis and the structure was quite different from anodized plate which is prepared under normal conditions. It seems reasonable to suppose that the burn out causes the change of structure of anodized alumina layer.

Figure 2.13 shows how thickness of alumina layer changes with current density up to 1000 A/m2. Change of BET surface area, which is measured after hot water treatment and calcination of the anodized plate, is shown in **figure 2.14**. Thickness of generated alumina layer showed a rapid drop with the current density. Gas which was generated from anode and cathode increased with current density. Thus, it is considered that electric quantity supplied to the anode was consumed for electric discharge and electrolysis of water under high current density.

Ideal catalyst support is porous and thick. Thus, anodic oxidation should be operated at under 100 V with the optimized current density 20 A/m2.

2.3 Hot water treatment and platinum content

Hydration of anodized alumina layer

(1) Roughness factor of alumina layer

BET surface area is increased by hydration of anodized alumina layer and followed by calcination. The BET surface area of the alumina plate prepared by anodic oxidation, hot water treatment and calcination was measured. **Figure 2.15** shows roughness factor which is calculated from BET surface area, and apparent surface area changes with thickness of alumina layer.

(2) XMA analysis of cross section of alumina layer

Figure 2.16 shows EPMA analysis of cross section of catalyst support layer which is prepared by anodic oxidation, hot water treatment and calcination. The X axis shows length from the alumina/aluminum interface and the Y axis shows intensity of X ray of each element. Intensity of aluminum and oxygen were high at the bottom of alumina layer and platinum was not impregnated to the bottom. It seems that the structure of alumina layer is not uniform and the bottom of alumina layer has high density.

Impregnation of platinum into anodized alumina layer

(3) Liquid volume for hot water treatment

Effect of liquid volume for hot water treatment on platinum content is shown in **figure 2.17**. The ratio of liquid volume to surface area of plate (e) was used, and e was changed from 1 to 10. Platinum content increased with e and the rise brings the platinum content to a maximum at e=4. Therefore, e>4 was used for hot water treatment.

(4) Concentration of platinum

Effects of concentration of platinum and time of hot water treatment on platinum content are shown in **figure 2.18**. Thickness of alumina layer was 20 μm. Platinum content increased with time and the increment was large at high concentrations of platinum. After 3 h of hot water treatment, platinum content showed the highest point and this was unrelated to the concentration of platinum.

Figure 2.19 shows EPMA analysis of cross section of prepared catalysts, catalyst (A) and (B) were prepared by 1 h and 4 h of hot water treatment. After 1 h of hot water treatment, platinum was impregnated to the alumina layer uniformly, but the intensity of X ray was small, since platinum content was small.

(5) Thickness of alumina layer

Figure 2.20 shows effect of thickness of alumina layer on platinum content. Thicknesses of alumina layer used were 10 μm, 20 μm and 30 μm. Platinum concentration was 1.0 g-Pt/L and treated time was 2 h. Platinum content increased with thickness of alumina layer and was 2.9 g-Pt/m^2 at 30 μm in thickness.

Figure 2.21 shows EPMA analysis of cross section of prepared catalyst of 20 μm and 30 μm thickness. Platinum was impregnated into the alumina layer uniformly. It was clear that the platinum content increased with thickness of alumina layer. Platinum content per unit BET surface area was about 170 μg-Pt/m^2-BET. Platinum content per unit weight of alumina layer was about 3 wt%.

Assuming that platinum particles were adsorbed to alumina layer by chemical potential (chemisorption), the number of sites which platinum particles were adsorbed to was the same per unit volume of anodized alumina. From this assumption, platinum content per unit surface area could be increased by thickness and BET surface area of alumina layer. There is room for further investigation.

2.4 Catalytic reactivity of plate type catalyst

Prepared catalysts were evaluated by catalytic reactivity of cyclohexane dehydrogenation for endothermic reaction of cyclohexane/ benzene/ hydrogen chemical heat pump. **Figure 2.22** shows catalytic reactivity change with time for 4 catalysts prepared. Catalyst (B) has 20 μm thickness of alumina layer and base aluminum is high purity, 99.99%. Catalyst (A), (C), (D) were prepared using commercial aluminum and have 10 μm, 20 μm and 30 μm thickness respectively. Physical properties of prepared catalysts are shown in **table 2.1**. Platinum content increased with thickness of alumina layer and platinum dispersion was almost the same, i.e. 0.4-0.5. The reaction rate showed dynamic steady state after 20 h of reaction. The constant reaction rate after 20 h of reaction increased with platinum content. The reactivity of (D) was three times as high as that of (A). The steady state was 3.5 mol/(h•m^2) and it continued to 130 h of reaction. It was clear that catalytic reactivity can be raised by preparing thick catalyst.

CONCLUSIONS

A thin-layered catalyst supported on a metal plate is one of the ideal types of catalysts which make it possible to design a compact reactor. A Pt/Al_2O_3/Al plate type catalyst was prepared by anodic oxidation (AO) of a commercial aluminum plate, followed by hot-water treatment (HWT) in chloroplatinic acid solution. In this chapter, preparation conditions of the plate type catalyst were investigated as follows:

(1) Effects of aluminum purity on the physical properties of catalyst and the catalytic reactivity were studied. Purity of aluminum has an effect on the thickness of anodized alumina layer but it has no effect on the catalyst content and the catalytic reactivity.

(2) The conditions for preparing an anodized layer of any thickness under 30 μm were established. The thickness of the alumina film was controlled by anodization conditions such as time and temperature of electrolyte bath.

(3) The Pt content on the catalyst surface was controlled by conditions of HWT and increased with thickness of alumina layer up to 3.5 g-Pt/m^2. The amount of Pt supported per BET surface area of alumina was 170-180 μg/m^2, which corresponds to 3 wt% of alumina, and the dispersion of Pt was around 0.5, regardless of the thickness of the alumina film.

(4) Catalyst with 30 μm of alumina film showed a constant reaction rate per apparent surface area of 3.5 mol/(h·m^2) for cyclohexane dehydrogenation at C_6H_{12}/N_2=1/10, 1 atm and 473 K for 130 hours. It was clear that commercial aluminum can be used as material for plate type catalyst.

References

1) Hashioka,T., S. Kosedo, M. Itoh, K. Yamamoto and H. Kameyama :Chem. Let.,1987,1067 (1987)
2) Inoue, M., Master thesis, (1991)
3) Kameyama, H., M. Yamashita and Y. Saitoh: *Shokubai*, 31,5,285 (1989)
4) Kameyama H.,M. Inoue,R. Yamanaka and K. Murata: Chem. Eng.(JPN),36,2,42(1991)
5) Kameyama, H. and M. Itoh: Chem. Eng.(JPN), 34, 4, 58 (1989)
6) Kei-kinzoku kyokai,(ed): "Aluminum Hand Book", 4th. ed., Shoueisha (1990)
7) Nishimura, S., S. Takeoka and H. Kameyama; *Shokubai*, 32, 7, p.488-489 (1990)
8) Sanshou Shokubai Iinkai:*Shokubai*,31,317 (1989)
9) Yamaseki, K., S. Nakayasu and K. Yamamoto, H. Kameyama : *Kagaku Kogaku Ronbunshu*, 17, 2, 267, (1991)

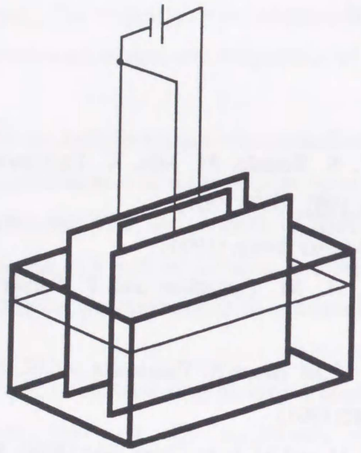

Fig.2.1 Apparatus for anodization

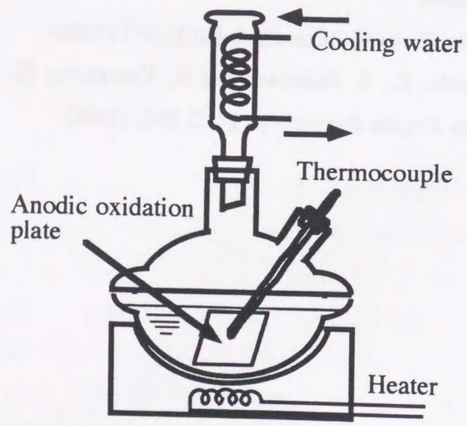

Fig.2.2 Apparatus for hot water treatment

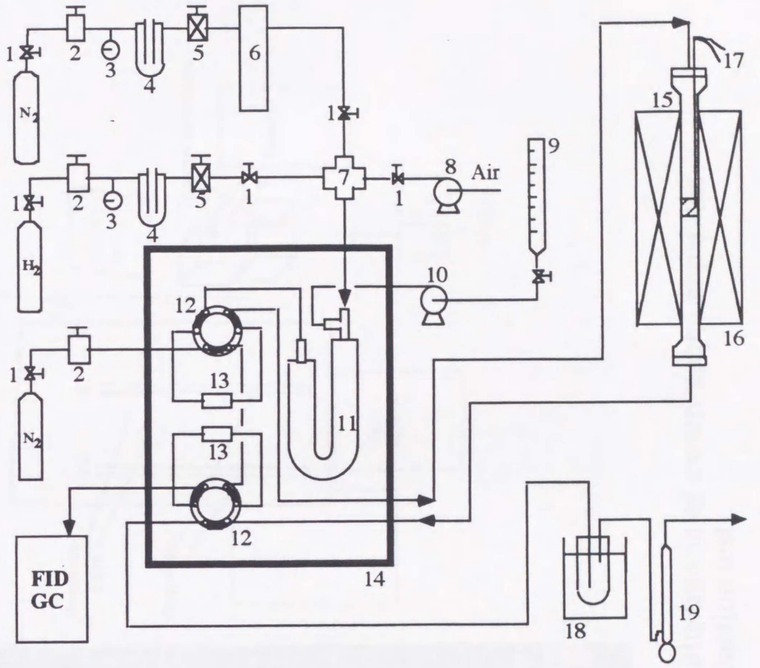

1. Stop valve
2. Pressure regulator
3. Pressure gauge
4. Flow meter
5. Mass flow valve
6. Deoxygen column
7. Cross union
8. Air pump
9. Buret
10. Perista pump
11. Evaporator
12. Six-way cock
13. Sampler
14. Oven
15. Reaction tube
16. Heater
17. C.A. thermocouple
18. Condenser
19. Soapfilm flowmeter

Figure 2. 3 Experimental apparatus for reaction test

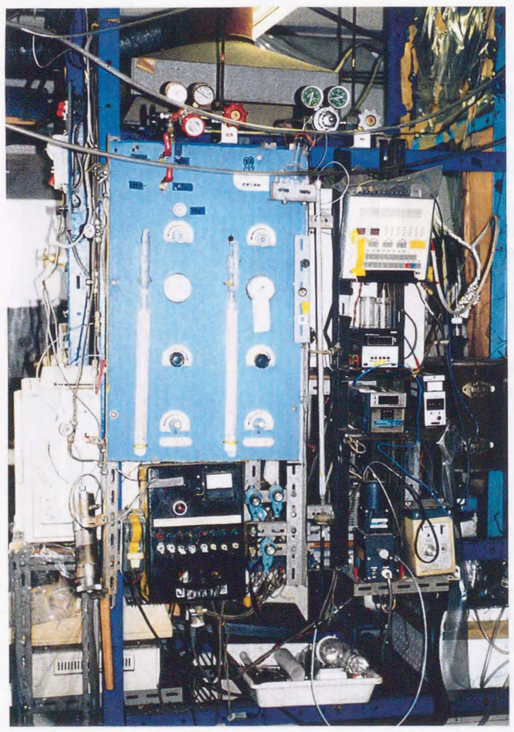

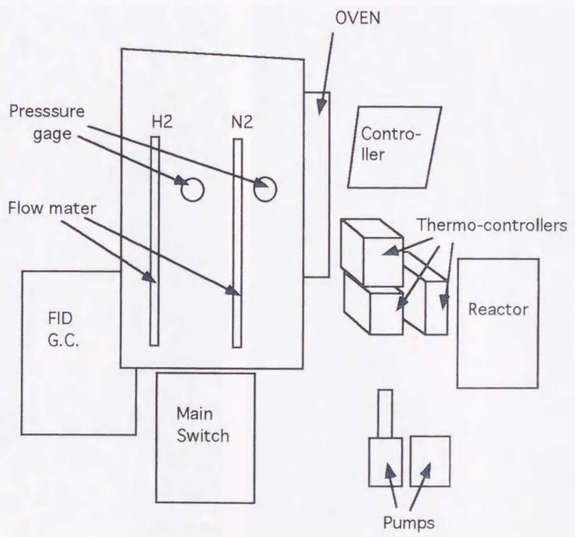

Fig. 2.4 Photograph and illustration of experimental apparatus for reaction test

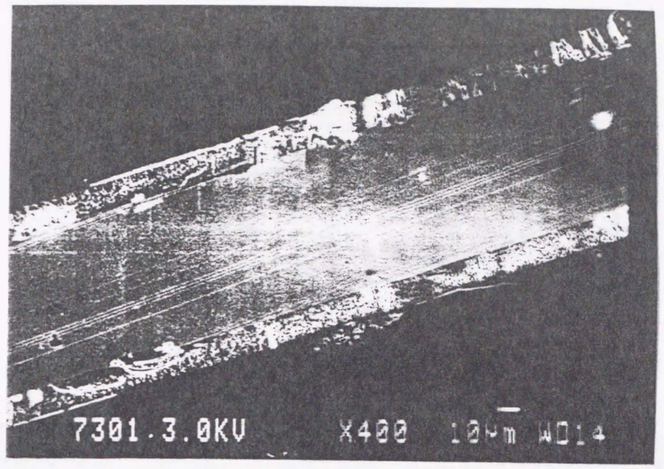

Cross section of anodized alumina layer

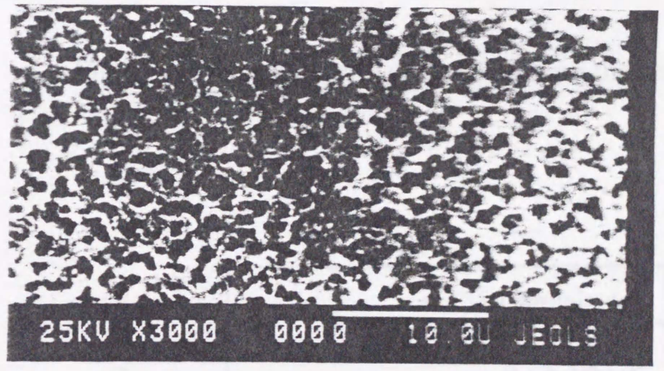

Surface of anodized alumina layer

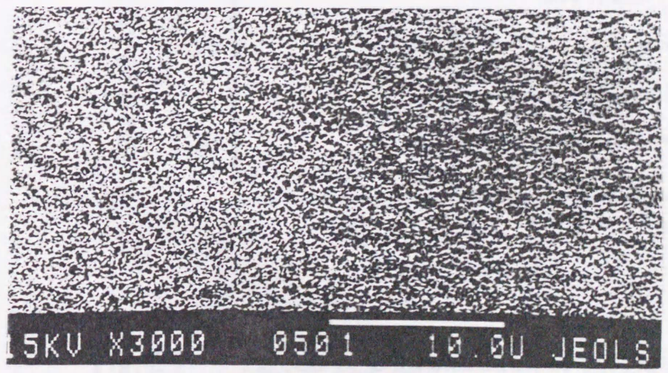

Surface of catalyst layer after hot water treatment and calcination

Figure 2.5 SEM analysis of cross section and surface of anodized alumina layer and following hot water treatment.

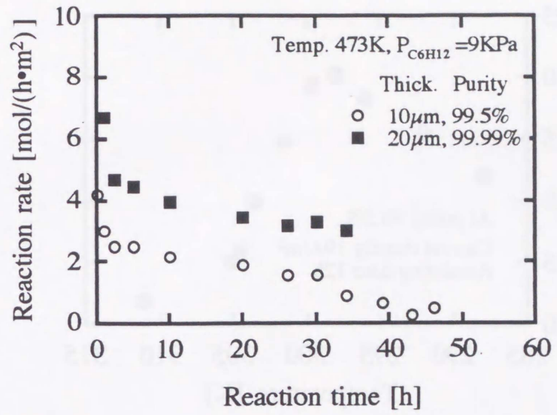

Fig.2.6 Effects of purity of aluminum on the reactivity

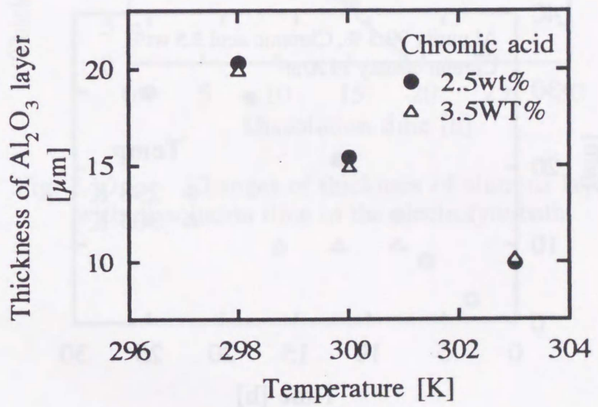

Fig. 2.7 Effects of concentration of chromic acid solution as electrolyte on the thickness of anodized alumina layer

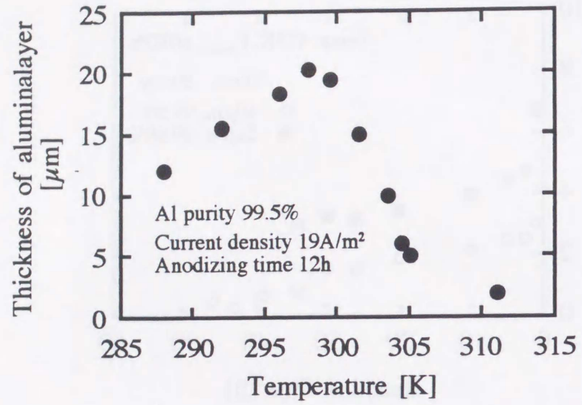

Fig.2.8 Thickness of alumina layer changes with anodized time at each temperature

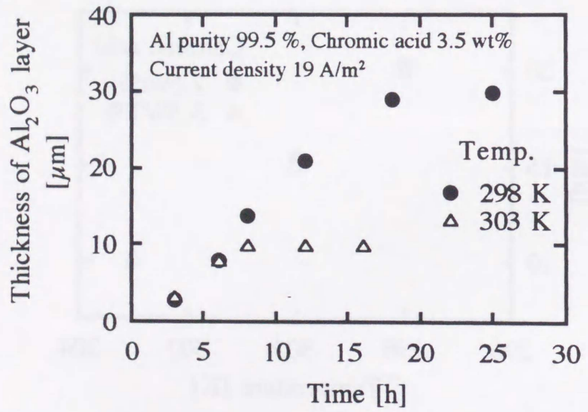

Fig. 2.9 Effect of anodized temperature on the alumina thickness

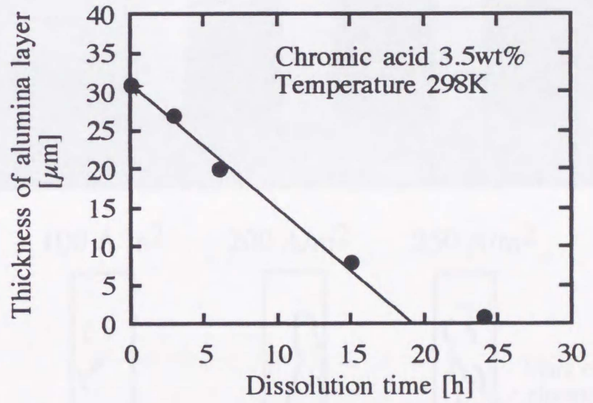

Fig. 2.10 Changes of thickness of alumina layer with dissolution time in the electrolyte bath

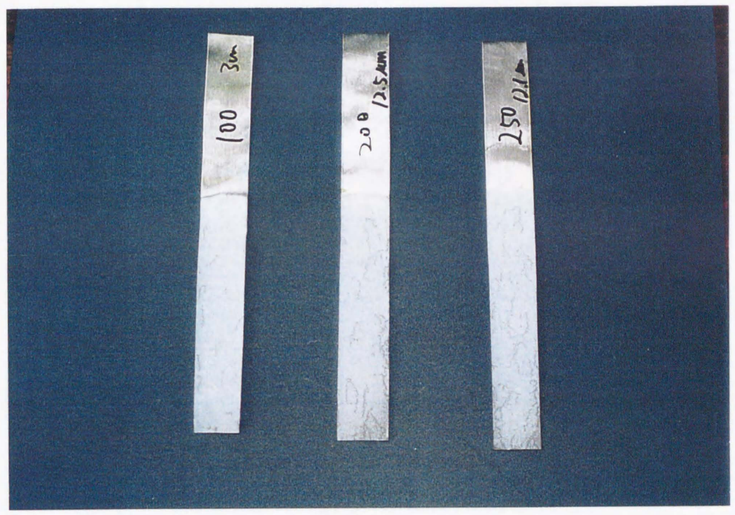

Fig. 2.11 Photograph and illustration of surface of burned our anodized alumina layers

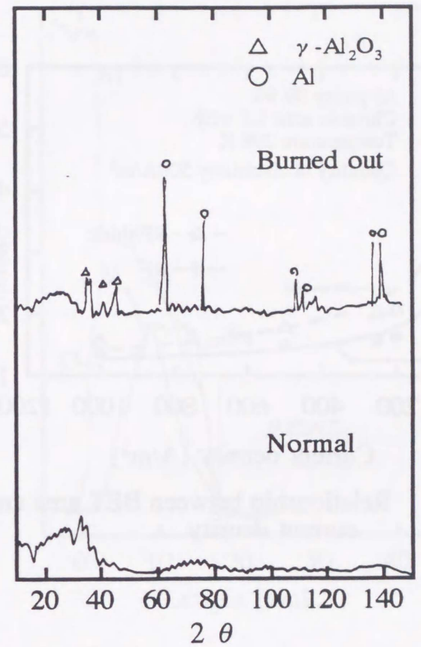

Fig. 2.12 XRD analysis of anodized alumina layer

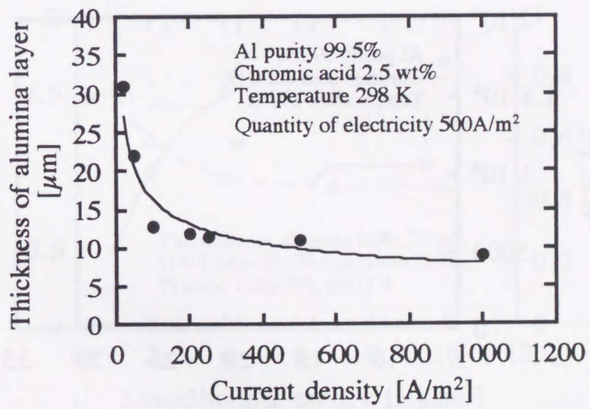

Fig. 2.13 Effect of current density on the thickness of anodized alumina layer

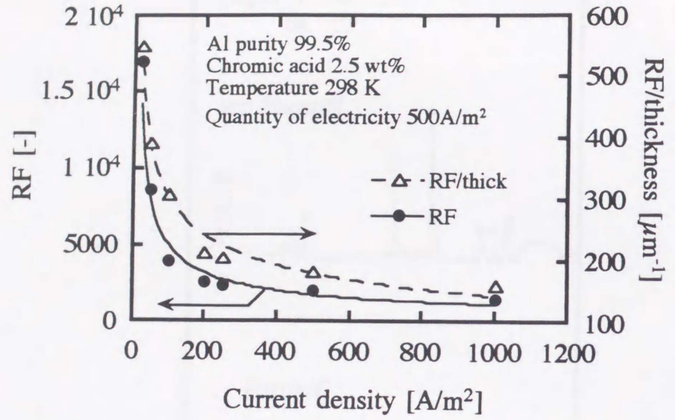

Fig. 2.14 Relationship between BET area and current density

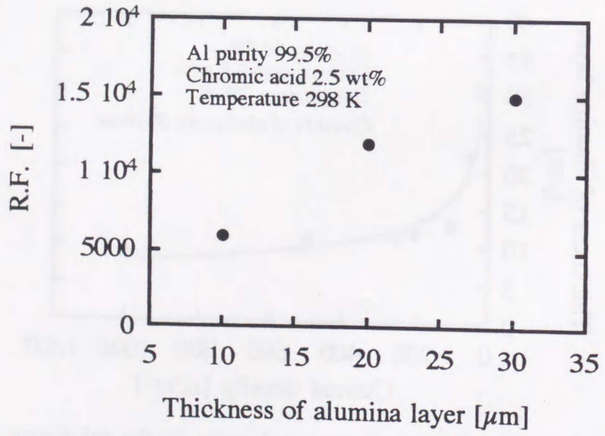

FIg. 2.15 RF changes with the catalyst thickness

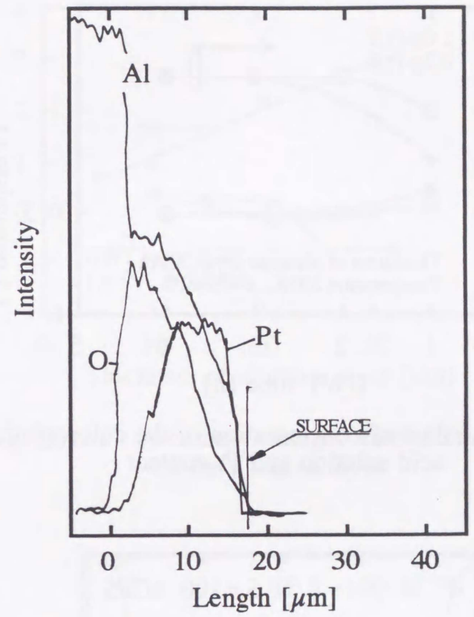

Fig. 2.16 EPMA analysis of prepared catalyst layer

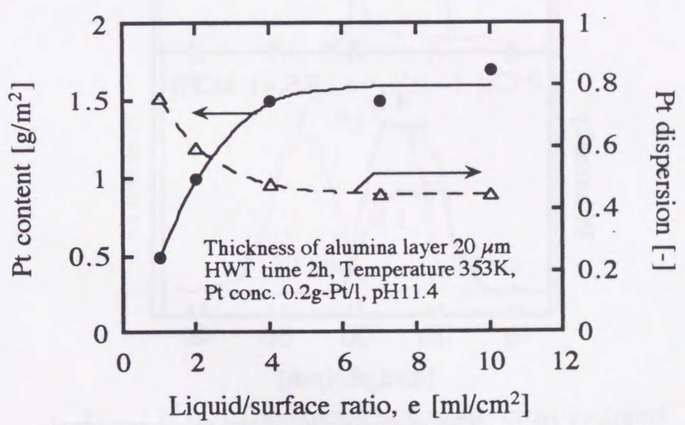

Fig. 2.17 Relationship between e and the Pt content

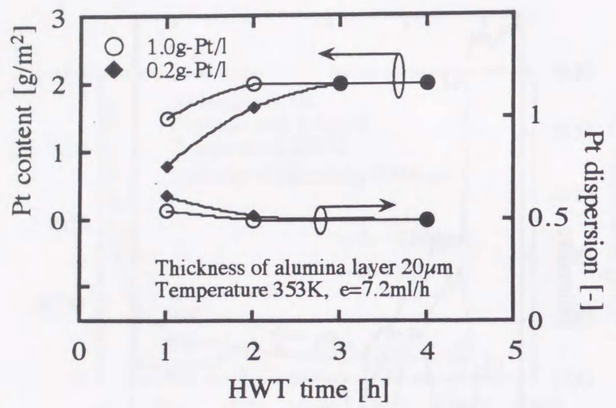

Fig. 2.18 Effect of concentration of the chloroplatinic acid solution and Pt content

Fig. 2.19 The comparison of the cross-sectional EPMA patterns of catalysts prepared with different HWT time

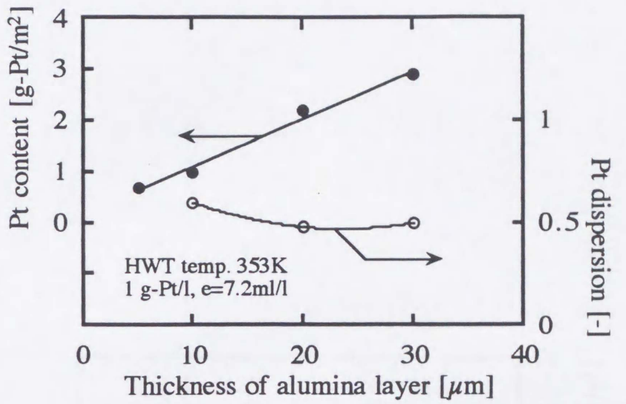

Fig. 2.20 Pt content changes with the thickness of the alumina layer

Fig. 2.21 The comparison of the cross-sectional EPMA patterns of catalysts of 20μm and 30 μm thickness

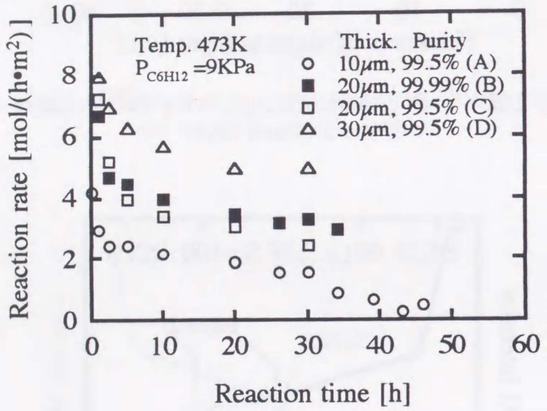

Fig. 2.22 Reactivity changes with time

Chapter

3

Preparation Method Of The Plate Type Catalyst Using Oxalic Acid

INTRODUCTION

In the following sections I shall be examining the design and the performance of tube wall reactors. The catalytic reactivity per apparent surface area is directly related to the reactor volume and this is one of the important factors for reactor size (Chapter 7).

The purpose of this chapter is to improve catalytic reactivity of the plate type catalyst. The effects of thickness and porosity of anodized alumina layer on platinum content and the catalytic reactivity were examined. Oxalic acid solution was used for the anodic oxidation (AO) process for two reasons 4). Firstly, the thick alumina layer can be formed in oxalic acid solution. Secondly, chromic acid causes serious water pollution and its usage is limited.

In AO process, an alumina layer more than 350 μm thick was formed on aluminum plate. Porosity of the anodized alumina plate increased with the time of pore widening and time of AO. Weight of impregnated Platinum per unit volume increased with porosity. The maximum platinum content was 15.8 g-Pt/m^2 and this was 5 times larger than the previous catalyst. Platinum dispersion of each catalyst was about 0.5. The reactivity of cyclohexane dehydrogenation increased with catalyst content. The highest reactivity after 20 h was about 12 mol/(h·m^2) and 3 times as high as the previously reported catalyst. It was clear that the reactivity achieved the target reactivity.

1 EXPERIMENTAL

1.1 Preparation of the plate type catalyst

(1) Anodic Oxidation (AO)

An aluminum plate (JIS-A1050, 99.5 % in purity, 0.3 or 1.0 mm in thickness) was pretreated in 20 wt% NaOH solution for 3 min., and 30 wt%

HNO_3 solution for 3 min., then rinsed with deionized water. Both sides of the plate were anodized in aqueous solution of 4 wt% oxalic acid, at current density (CD) of 20-200 A/m2, at 283-303 K, by electric quantity up to 3550 A·h/m2. An alumina layer was formed on the aluminum body. The anodized plate was rinsed with deionized water, dried at room temperature and calcined in air at 623 K for 1 h. **Table 3.1** shows the AO conditions of the samples, A-N, studied in this chapter.

Table 3. 1 Preparation conditions of the plate type catalysts

Sample	Temp. of AO [K]	CD [A/m2]	Quantity of electricity [Ah/m2]	PW time [h]
A	293	50	750	3
B	293	50	750	8
C	293	50	750	10
D	293	200	800	-
E	293	100	800	-
F	293	30	800	-
G	293	20	800	-
H	283	50	750	-
I	288	50	3550	-
J	293	50	800	-
K	293	50	3400	-
L	298	50	800	-
M	298	50	1208	-
N	303	50	500	-

Note : AO : Anodic Oxidation, CD : Current Density
PW : Pore Widening

(2) Pore Widening (PW)

The anodized plates with 100 μm alumina thickness were soaked in 4 wt% of oxalic acid solution at 293 K for 1-12 h. PW conditions are summarized in Table 3.1 for the samples A-C.

(3) Hot Water Treatment (HWT)

In this process, platinum was impregnated in the alumina layer. The anodized alumina plate was soaked in chloroplatinic acid solution of 1.0 g-Pt/L at pH 11.4 (controlled by ammonia), at 353 K and for 1-6 h. The plate was rinsed with deionized water, soaked in 0.3 wt% KCl solution at room temperature for 20 min and rinsed with deionized water again. Then, the plate was dried at room temperature and calcined in air at 623 K for 1 h.

1.2 Characterization of the catalyst

Pore size distribution of anodized alumina layer was measured with mercury porosimetry. Thickness of alumina layer was measured with a thickness meter (Helmut Fischer ISOSCOPE MP-2). Porosity of the alumina layer was calculated by dividing apparent alumina density by pure alumina density. Platinum distribution in the alumina layer was measured by X-ray microanalyser (XMA). Quantity of platinum content was measured by atomic absorption spectroscopy (Shimazu AA-680). Platinum dispersion was determined by CO pulse method.

1.3 Measurement of catalytic reactivity

The catalytic reactivities of the catalysts were evaluated by cyclohexane dehydrogenation which is used for endothermic reaction of cyclohexane/benzene/hydrogen chemical heat pump (CBH-CHP). The chemical reaction is expressed in equation(3.1).

$$C_6H_{12} + 206\ kJ/mole \overset{473K}{\Leftrightarrow} C_6H_6 + 3H_2 \qquad (3.1)$$

A flow type reactor was used as **a differential reactor**. The plate type catalyst, 5×10 mm² and small aluminum tips, 5×5 mm² as dilutors were packed in pyrex reaction tube of 11 mm in inner diameter. The height of the catalyst bed was 10-15 mm. Activation of the catalyst was performed by oxidation in air (623 K, 12 h) and reduction in a mixture gas (H_2 of 10 l/h and N_2 of 15 l/h) at 623 K for 2 h. In the reaction tests, cyclohexane was diluted with nitrogen, and the dilution ratio was 10. Concentrations at the inlet and outlet gases of the reaction tube were analyzed by FID gas chromatography (Shimazu GC-8A). Changes in dehydrogenation reactivity of cyclohexane with time were measured at 473 K, 0.1 MPa.

2 RESULTS AND DISCUSSION

2.1 Conditions of Anodic Oxidation

(1) Thickness of aluminum plate

Effects of thickness of aluminum plate on thickness of anodized alumina layer were studied. **Figure 3.1** shows thickness of the alumina layer changes with time under different thickness of aluminum plates. The concentration of oxalic acid was 4 wt%, the current density was 50 A/m² and the temperature was 293 K. The thickness of alumina layer on the aluminum plates of thickness 0.3 mm raised to the peak of 100 μm and on those of 1.0 mm increased more than 230 μm. The reason why the thickness of aluminum plate affects on the thickness of anodized alumina layer is considered using a model of heat balance of anodic oxidation as follows.

Figure 3.2 shows the illustration of heat balance of the cross section of

an anodizing alumina/aluminum plate. The anodization occurs at the alumina/aluminum interface. The oxidation of aluminum is an exothermic reaction and the reaction heat (Q_{AO}) is transferred through aluminum plate (Q_{AL}) and electrolyte oxalic acid (Q_{EL}).

$$Q_{AO} = Q_{AL} + Q_{EL} \qquad (3.2)$$

The two patterns of heat transfer were considered as follows:

Case (A) In the first stage of AO, generated alumina layer is thin and the heat transfer coefficient of anodized alumina layer is large, in spite of thermal conductivity 10 times smaller than that of aluminum. In this situation, temperature difference (ΔT) between alumina/aluminum interface and the surface of alumina layer is small.

Case (B) The anodized alumina layer becomes thick and aluminum plate is becoming thinner by anodization, the heat transfer coefficient of anodized alumina layer is small and ΔT between alumina/aluminum interface and alumina surface tends to be large. Then the reaction heat Q_{AO} is mainly removed through the aluminum plate and the temperature of aluminum also rises due to large heat flux Q_{AL}. Therefore, temperature of alumina/aluminum interface is rising higher than in the first stage of AO, case (A) and the dissolution of alumina layer is accelerated. For the reasons mentioned above, thickness of aluminum is one of the important factors in forming a thick alumina layer.

(2) Concentration of oxalic acid solution

The optimum concentration of oxalic acid solution was studied. **Table 3.2** shows solubility of oxalic acid in water. **Figure 3.3** shows effects of concentration of oxalic acid (1-8 wt%) on the thickness of anodized alumina layer under 50 A/m² of current density, at 293 K. The result of the examination is that the mean thickness is almost the same in spite of the concentration of oxalic acid. The purpose of the anodic oxidation is to form

a thick and porous alumina layer on aluminum plate, uniformly. With the concentration of 1, 2 wt%, the thickness was not uniform. The thickness on upper part of the plate was thick, which does not suit catalyst support. In the case of 8 wt% of concentration, lot of oxalic acid was consumed for AO, which causes high cost. Therefore, we took the optimum concentration as 4 wt%.

Table 3. 2 Solubility of oxalic acid in water*

Temperature [K]	Solubility [g/100g-water]
273	3.42
293	8.69
313	17.71
333	30.71

**Kagaku bin-ran kiso-hen* II-188

(3) Generation rate of anodized alumina layer

Anodized alumina layer was dissolved into acid as described later. Initial generation rate of the anodized alumina layer was not affected by the dissolution into electrolyte, since the effect of dissolution increases with AO time. And the real generation rate of the alumina layer could be equal to the initial generation rate. **Figure 3.4** shows effects of anodized temperature and current density (CD) on initial generation rate of alumina layer. Though the rate did not relate to anodized temperature, it increased linearly with CD.

The mechanism of AO process is being continued steadily by many researchers and we do not discuss the mechanism in detail here. Shimura *et al.* [5] have proposed a model. With this model, the amount of anodized alumina was limited to the concentration of aluminum ion which is related to CD. Therefore, the real generation rate would be related to CD.

(4) Dissolution and porosity of the alumina layer

Effect of dissolution of alumina layer on porosity and pore size distribution of the alumina layer is studied in this section. **Figure 3.5** shows changes in thickness and porosity with pore widening (PW) time. The thickness decreased linearly and the porosity increased linearly with the PW time. **Figure 3.6** shows pore side distribution of the alumina layer. Peak pore radius of alumina layer increased from 32 nm to 38 nm with 12 h of PW. Therefore, it shows that alumina dissolves from both inside and outside surfaces of anodized alumina layer.

Two theories about the dissolution of alumina layer have been proposed. One is the pore shortening theory and the other is the pore widening theory. Diggle et. al. [1] advanced the pore shortening theory that only the surface of alumina layer is dissolved into acid solution. Nagayama et. al. propounded the pore widening theory that alumina layer is dissolved into acid solution from inside the alumina layer. Recently, it has been established that the alumina layer is dissolved from inside the anodized alumina layer and these results support a similar view.

This dissolution rate is closely related to temperature, and thickness of alumina layer shows a different peak according to the anodizing temperature.

(5) Effect of current density on the porosity

Figure 3.7 shows the effect of current density on the porosity of alumina layer at the initial stage of anodization (up to 4h of anodization). The result of the experiment was that the porosity of alumina layer declined with the current density. The decrease of number of pores on the alumina layer was observed using SEM analysis and it is likely that the porosity declined with the reduction of number of pores. **Figure 3.8** shows the relationship between current density and voltage of anodization. The voltage increased with the current density. Ebihara et. al. [2] reported that pore radius and number has been affected by voltage of anodization, and further consideration is required as to whether current or voltage affects the number

and the radius of pores on alumina layer.

(6) Effect of current density on the thickness and roughness factor

Figure 3.9 shows changes in thickness with time of anodic oxidation for each current density (CD), 20-200 A/m^2, under 293 K constant. Thickness of the alumina layer showed a maximum at more than 20 h at low CD: the maximum thickness was limited to 30 μm at 20 A/m^2 and limited to 66 μm at 30 A/m^2. The thickness increased with CD. This was because the generation rate changed with the CD in spite of the fact that the dissolution rate was constant.

Figure 3.10 shows that the roughness factor (RF), thickness and porosity change with the current density under 800 Ah/m^2 of electric quantity at 298 K. The RF was measured after hot water treatment and calcination of anodized alumina layer. The RF showed the highest point of 30000 at 50 A/m^2 of CD. As we saw before, the thickness and the porosity were closely related to the current density. The thickness showed a peak at 100 μm over 100 A/m^2 of CD and the porosity decreased with the CD from 0.4 to 0.25. The roughness factor means the ratio of apparent surface area to inside surface area (BET surface area), thus, it is proportional to the BET surface area. High surface area is usually described for high reactivity per unit volume so catalyst should be porous. Therefore the RF is one of the important factors for estimating the catalyst support and 50 A/m^2 of current density is suitable for the catalyst.

(7) Long period of anodic oxidation under constant current density

Figure 3.11 shows changes in alumina thickness with 0-3550 A·h/m^2 of electric quantity, at 283-303 K under 50 A/m^2 constant. Equilibrium thickness increased with a fall in the anodized temperature. This was because dissolution rate decreased with a fall in the anodized temperature in spite of the fact that generation rate was constant. Maximum thickness of alumina layer was more than 350 μm at 283 K, 3550 Ah/m^2. From the data of J-M in

Table 2, it was also shown that the porosity of anodized alumina layer increased with AO time by dissolution.

(8) Long period of anodic oxidation under constant voltage

In this section, long period of anodic oxidation was tried under constant voltage, 40 V. **Figure 3.12** shows the thickness and porosity change with quantity of electricity under constant voltage 40 V. The alumina thickness increased with time and showed a peak of 110 μm at 20 h, after that it decreased with time. The porosity of the alumina layer was almost constant till 20 h of anodization and it increased linearly after 20 h. Current density decreased with the anodizing time while the thickness increased, and after the peak, the current density was the same. The reason for this is not hard to see:

1) Alumina is an insulator but anodized alumina layer has a porous structure and electrical conductivity. The resistance increased with the thickness of alumina layer. Current density was determined by the electrical resistance of the alumina layer under 40 V constant, thus, the current density decreased with the thickness of alumina layer.
2) Generation rate of anodized alumina layer is proportional to current density. Thus, the generation rate is controlled with anodic oxidation time up to 20 h.
3) Dissolution rate of alumina layer into electrolyte is determined by the temperature of electrolyte. And equilibrium thickness of anodized alumina layer is decided by the balance of generation and dissolution rate of alumina layer. Therefore, after 20 h of AO, the thickness of alumina layer is decreased by the dissolution and the porosity is increased by it.

2.2 Conditions of hot water treatment

(1) Hydration of the anodized alumina layer

Inoue [3] studied the phenomena of hydration of the anodized alumina layer which is prepared using chromic acid and is 10-20 μm in thickness, as follows:

1) It takes 6 h at 313 K, 1h at 333 K and 0.5 h at 353 K to hydrate the alumina layer.
2) The alumina layer could be hydrated in the range of pH3-pH11.

In this portion of the study, anodized alumina layer prepared using oxalic acid was used for hydration. Thickness of alumina layer was about 100 μm. **Figure 3.13** shows the weight of hydrated water changes with time of hot water treatment under the ratio of volume of hot water and treated plate, e>4, at 353 K and under pH11.4. A change of weight was not observed after 1h of hot water treatment and it was clear that the alumina layer hydrated in a short time.

(2) Hot water treatment time and Platinum content

Platinum is impregnated into the anodized alumina layer by hot water treatment (HWT). **Figure 3.14** shows the changes of weight of impregnated platinum into the alumina layer with HWT time. Thickness of alumina layer was about 100 μm, concentration of chloroplatinic acid solution was 1g-Pt/L and temperature was 353 K. The platinum content rose to a peak at 6 h of HWT. The time of 6h was longer than that of the alumina layer prepared by AO in chromic acid solution. In chapter 2, it was clear that the alumina is hydrated in a short time but impregnation of platinum within the alumina layer takes a long time. Impregnated platinum is distributed in all over the alumina layer of 30 μm and the platinum content was about 170 μg/BET-m^2. It is thought that the thickness using oxalic acid solution was more than 3 times that using chromic acid solution, and it took a long time for Pt impregnation.

(3) Effect of pore widening on platinum content

Figure 3.15 shows platinum content change with pore widening (PW)

time. The platinum content per unit volume increased with the PW time but thickness of alumina layer decreased with PW time. Thus, platinum content per apparent surface area showed a peak at 3 h of PW time. Further discussion of these phenomena will be presented later.

(4) Platinum content within anodized alumina layer

Figure 3.16 shows changes of platinum content per apparent surface area with electric quantity of anodization under 40V constant. Platinum content per unit volume was 0.04 g-Pt/cm^3-Al_2O_3 constant till 800 Ah/m^2 of anodization. The value increased with further anodization, it seems that this is caused by the increase of porosity. Platinum content per apparent surface area showed a peak at 1050 Ah/m^2 of anodization. The porosity and the thickness of alumina layer are important factors for platinum content per apparent surface area and the details are studied as following.

(5) Porosity of alumina layer and platinum content

Figure 3.17 shows changes in platinum content per unit volume with porosity of anodized alumina layer. The platinum content per unit volume increased with the porosity up to 9 wt%. **Figure 3.18** shows XMA analysis of the cross section of the plate type catalysts, samples M and J. X-axis shows depth of alumina layer. Impregnated platinum of the high porosity anodized alumina, sample M, is distributed further in depth.

Koda *et. al.* [6] have clarified the mechanism of hydration of anodized thin alumina layer. When anodized alumina is soaked into hot water, the alumina is hydrated and the volume is increased. Then, the pores of alumina layer are filled with the hydrated alumina in a short time. In chapter 2, it has been shown that the alumina is hydrated in a short time but impregnation of platinum within the alumina layer takes a long time.

These results indicate that much more anodized alumina of high porosity would be hydrated and platinum could be impregnated deeply, since it would take much more time for hydrated alumina to block the pores. Illustration of

this mechanism is shown in **figure 3.19**. On the other hand, if the alumina layer is dissolved further by extended pore widening, the porosity is large but the thickness of alumina layer decreases to hold less platinum. The point which we especially emphasize is that balance of the thickness and the porosity is the important factor in designing plate type catalyst.

Table 3.2 shows that platinum content per apparent surface area of sample I was the largest. The platinum content was 15.8 g-Pt/m^2 which was 5 times larger than that using chromic acid. Platinum dispersion of every catalyst was about 0.5. The mean of platinum content per BET area was about 160 μg/BET-m^2 which was almost the same as that using chromic acid.

2.3 Catalytic reactivity

(1) Electrolyte and reactivity

Inoue reported that chromium was impregnated into catalyst layer by anodic oxidation of chromic acid solution. Thus, it is considered that some kind of electrolyte affects the catalytic reactivity. Turn over frequency (TOF) of catalysts prepared using chromic acid and oxalic acid are compared in **figure 3.20** and **table 3.3**. TOF means generation rate of molecular benzene per catalyst site and per unit time. Both TOF are almost the same and the reactivity of cyclohexane dehydrogenation was not affected by this kind of electrolyte.

(2) Catalytic reactivity of plate type catalyst

Figure 3.21 shows changes in cyclohexane dehydrogenation reactivity of samples B, M, K, I and reported catalyst with reaction time. Each catalyst showed highest reactivity at initial reaction time and the reactivity decreased with time and showed a steady state after 20 h of reaction time. The steady reactivity increased with catalyst content and the reactivity of sample K was about 3 times as high as the catalyst reported in **chapter 2**. The highest

reactivity reached the target reactivity, which is discussed in **chapter 7**.

Table3. 3 Physical properties of plate type catalysts

Sample	Thickness of alumina layer [μm]	Poro-sity [-]	Pt content [wt%]	Pt content [g/m^2]	Pt dispersion [-]
A	89	0.55	4.5	4.74	0.56
B	74	0.63	6.6	4.55	0.56
C	70	0.71	6.3	3.86	0.57
D	100	0.29	2.4	3.0	0.45
E	100	0.37	3.0	3.8	0.47
F	66	0.58	5.1	3.39	0.50
G	37	0.70	7.5	2.89	0.53
H	98	0.49	2.1	2.67	0.48
I	327	0.59	3.98	15.84	0.47
J	100	0.49	2.96	4.12	0.42
K	270	0.62	3.95	13.41	0.59
L	79	0.48	3.27	3.88	0.51
M	86	0.70	9.23	11.01	0.48
N	29	0.52	4.12	2.99	0.49

CONCLUSIONS

This chapter covers preparation method by using oxalic acid for anodic oxidation, and the following conclusions are drawn from the present investigation.

(1) In AO process, alumina layer more than 350 μm thick was prepared. Porosity of the alumina layer was increased by pore widening (PW) and more than 0.79 in porosity was formed. Thickness and porosity of anodized alumina layer were determined by balance of generation rate and dissolution rate.

(2) Impregnated platinum content per apparent surface area increased with thickness and porosity of the anodized alumina layer. The maximum content was 15.8 g-Pt/m^2. Platinum dispersion of each catalyst was about 0.5.

(3) Reactivity of cyclohexane dehydrogenation increased with platinum content. The highest reactivity was about 3 times as high as the previous catalyst. The reactivity reached the target reactivity.

References

1) Diggle, J. W., T. C. Downie and C. W. Goulding: J. Electrochem. Soc., 116, 10, 1347(1969)

2) Ebihara, K., H. Takahashi and S. Nagayama: *Kinzoku hyoumen gijutu*, 34, 11,548 (1983)

3) Inoue, M., Master Thesis,1991

4) Keikinnzoku Kyoukai, (ed): "Aluminum Hand book", 4 th. ed., Shoueisha (1990)

5) Shimura, M. and T. Fukushima: *Kinzoku Hyoumen Gijutu*, 27, 10, 480(1976)

6) Koda M., H. Takahashi and S. Nagayama, *Kinzoku Hyoumen Gijutsu*, 27, p.480 (1976)

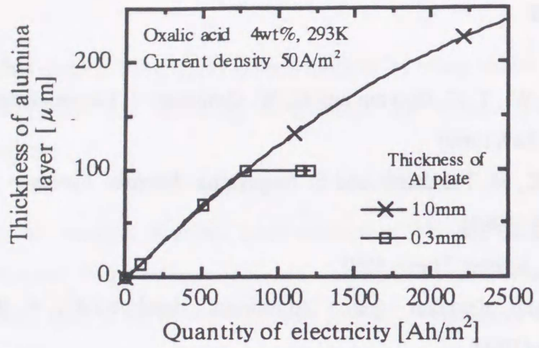

Fig.3.1 Effect of thickness of aluminum on the thickness of the anodized alumina layer

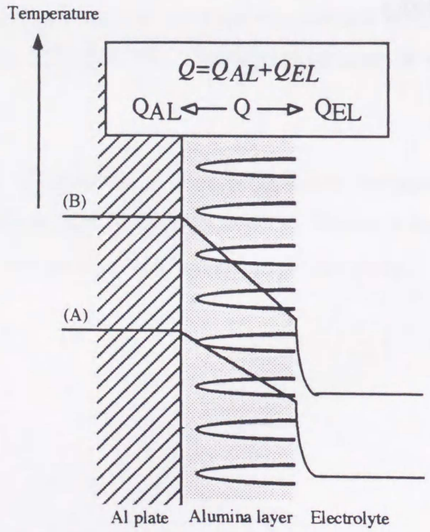

Fig. 3.2 Illustration of the heat transfer of the anodized aluminum plate

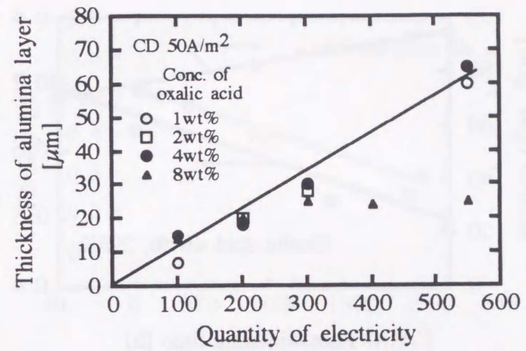

Fig.3.3 Effect of concentration of oxalic acid on the thickness of the alumina layer

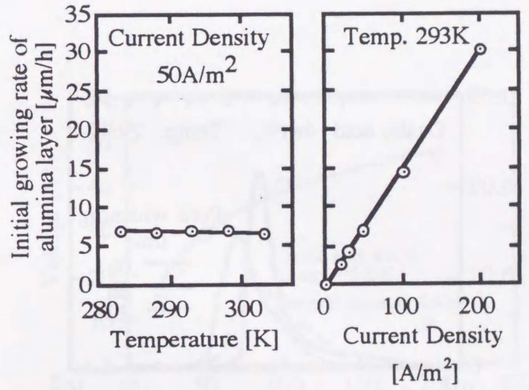

Fig.3.4 Initial anodized alumina layer generation rate with temperature or current density

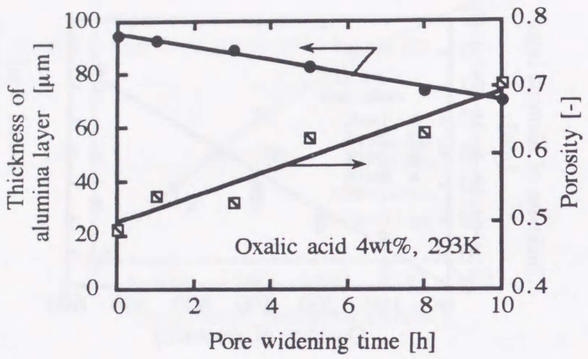

Fig. 3.5 Porosity of alumina layer changes with the pore widening time

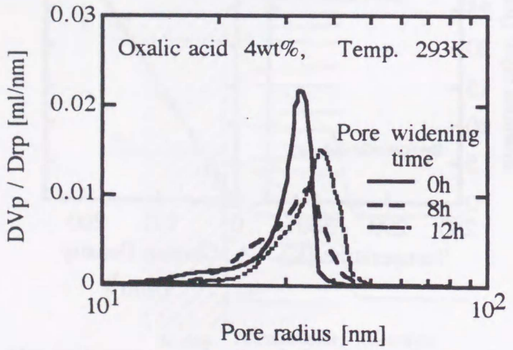

Fig. 3.6 Effect of the pore widening time on the pore size distributions of anodized alumina layer

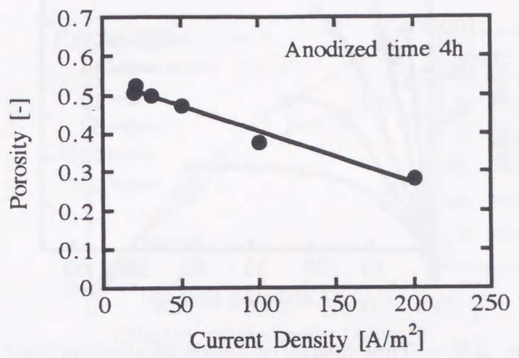

Fig. 3.7 Porosity of alumina layer changes with the density

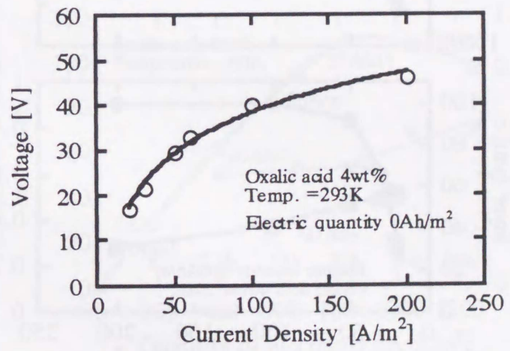

Fig. 3.8 Anodized voltage changes with each current density

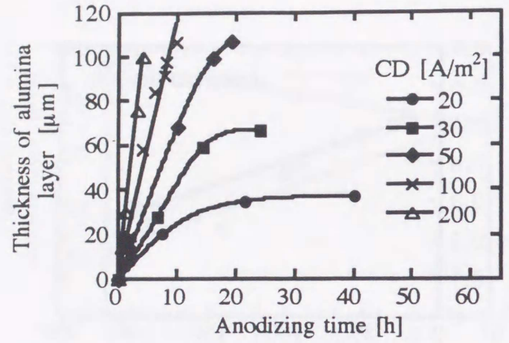

Fig. 3.9 Time history of anodized alumina layer of each current density: Oxalic acid 4wt%, 293K

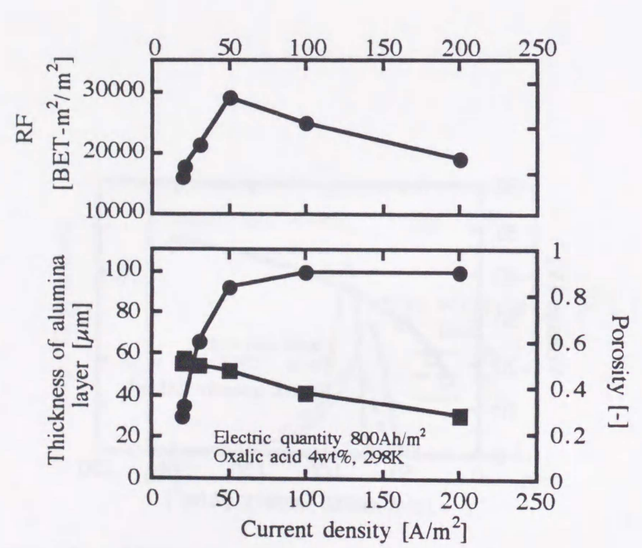

Fig. 3.10 Thickness, porosity and RF changes with current density on anodic oxidation

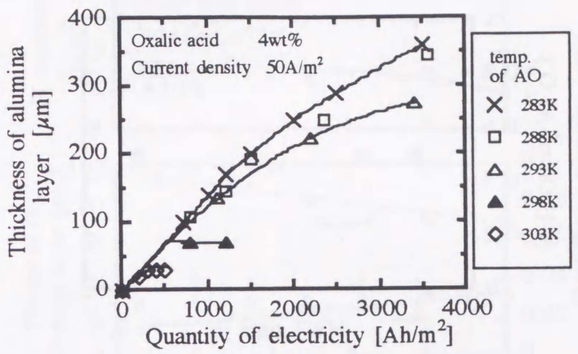

Fig. 3.11 Relationship between thickness of anodized alumina layer and electric quantity: CD=50 A•h/m²

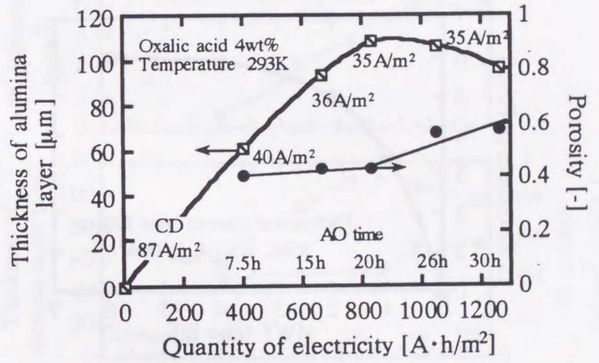

Fig. 3.12 Changes of anodized alumina layer with electrical quantity under anodized voltage constnat, 40V

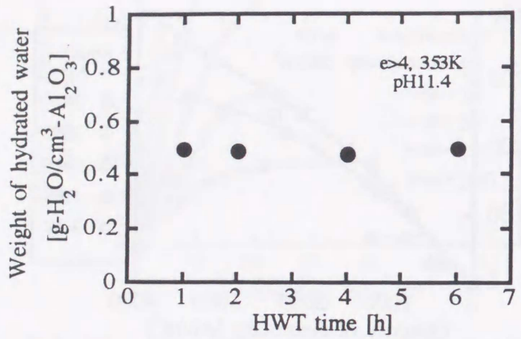

Fig. 3.13 Hydrated water into the anodized alumina changes with hot water treatment time

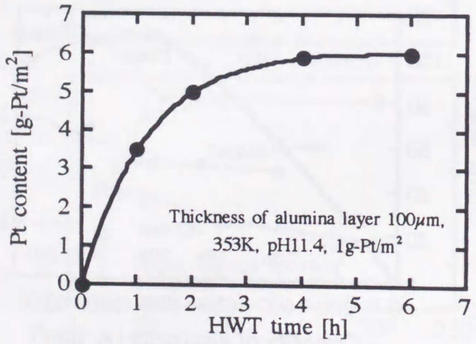

Fig. 3.14 Pt content changes with hot water treatment time

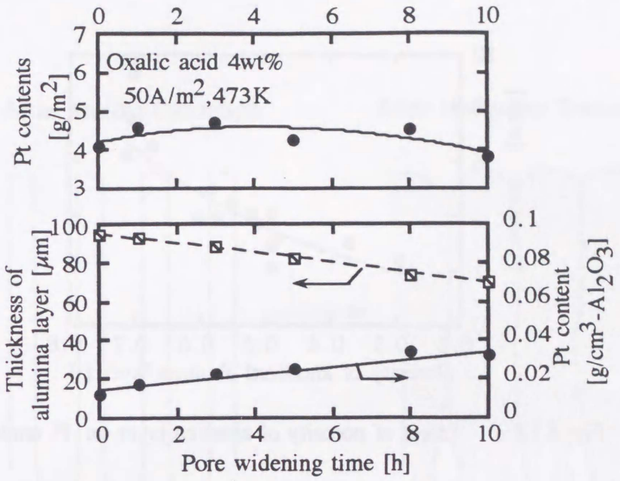

Fig.3.15 Effects of pore widening on the Pt content

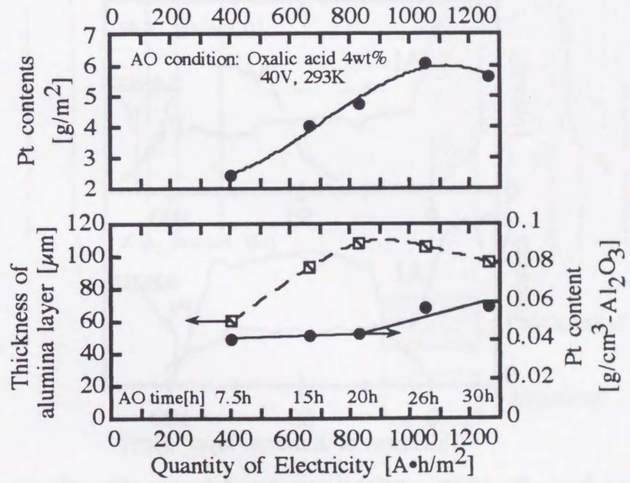

Fig. 3.16 Pt content changes with the anodized time under anodized voltage constant, 40V

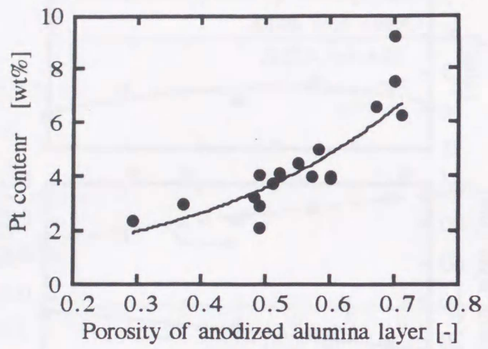

Fig. 3.17 Effect of porosity of alumina layer on Pt content

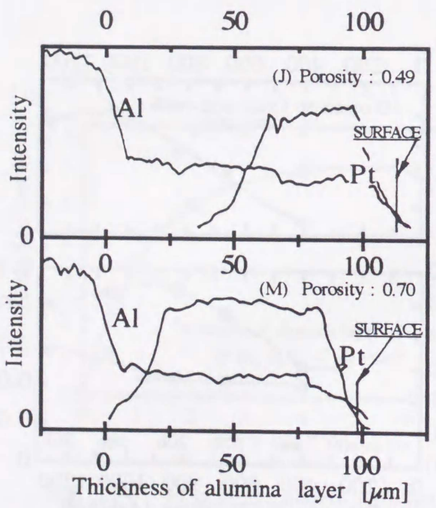

Fig. 3.18 EPMA patterns of cross section of the plate catalysts, sample M and J

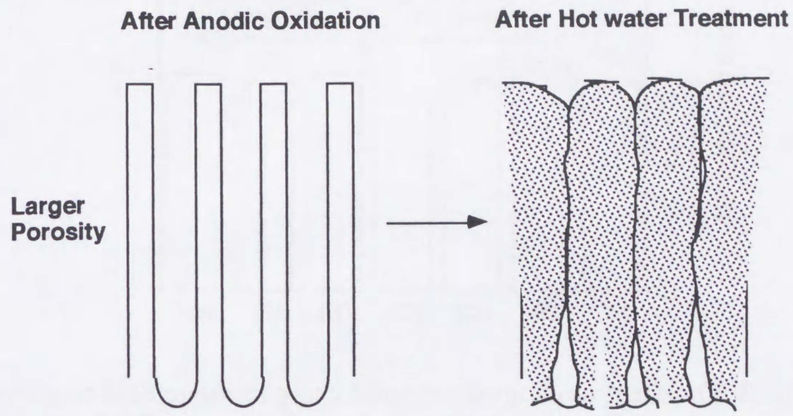

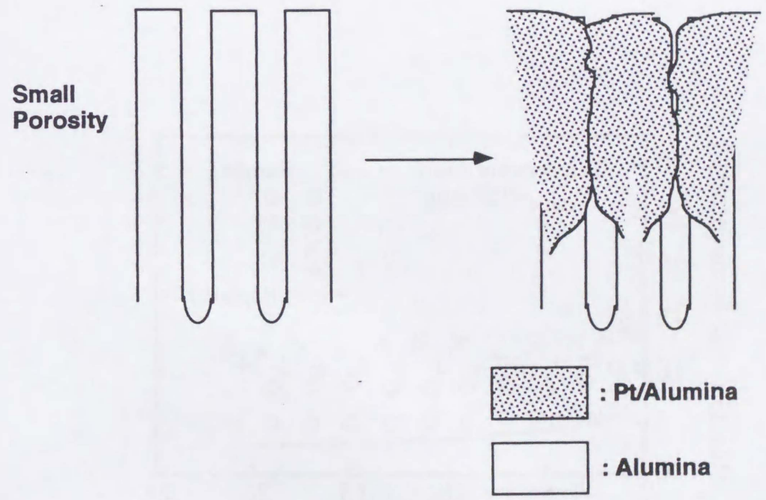

Fig. 3.19 Illustration of cross section of hydrated anodized alumina layer with porosity

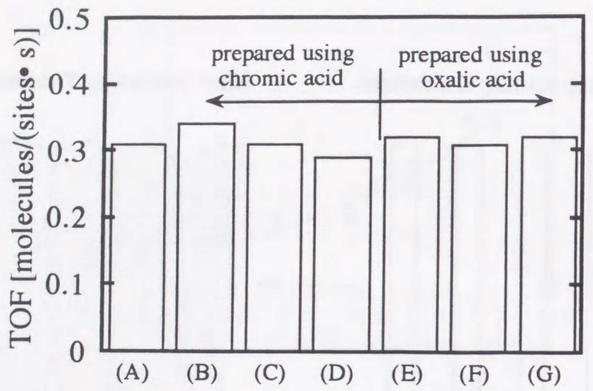

Fig. 3.20 Effect of catalyst prepared using chromic acid solution or oxalic acid solution as electrolyte on the TOF of cyclohexane dehydrogenation

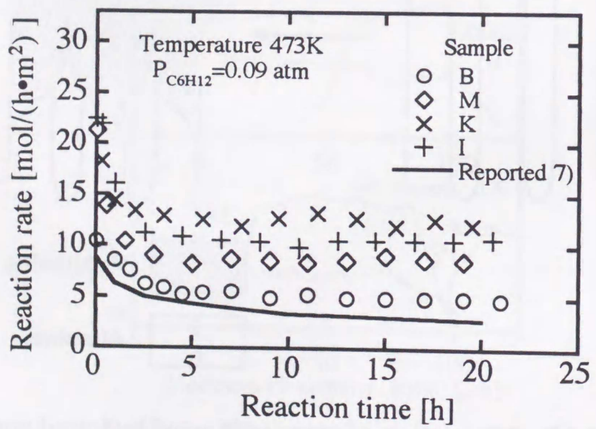

Fig. 3.21 Changes in ractivity of cyclohexane dehydrogenation with time

Chapter

4

EFFECTIVENESS FACTOR OF THE PLATE TYPE CATALYST

INTRODUCTION

During the cyclohexane dehydrogenation, the reactant must diffuse first from the fluid to the outside surface of the catalyst and then through minute and irregularly shaped pores to the interior. Chemical potential decreases in the direction of diffusion through the porous structure, so the catalyst surface in the interior is in contact with a fluid of lower reactant concentration and higher product concentration than the external fluid. Thus, the internal surface is not as effective as it would be if it were all exposed to contact with the external fluid. The degree of diffusion limitation is characterized by the effectiveness factor η, defined as the ratio of the observed rate of reaction to that which would occur in the absence of diffusion effects within the pores of the catalyst.

Though the effectiveness factor has been one of the important factors to design conventional pellet type catalysts, the optimization of a plate type catalyst has never been studied. In this chapter, the effectiveness factor of the plate type catalyst was investigated. The following items have been studied.

(1) Analysis of the structure of the catalyst layer
(2) Experimental determination of the effectiveness factor
(3) Design of the catalyst to improve the reactivity

1 THEORETICAL MODEL OF EFFECTIVENESS FACTOR OF PLATE TYPE CATALYST

1.1 Effectiveness factor of plate type catalyst

A mathematical model of effectiveness factor is described in the following. The change of the concentration of cyclohexane (Cc) with time (t) at the depth (l) from catalyst surface can be given as follows:

$$\frac{\partial C_c}{\partial t} = D\left(\frac{\partial^2 C_c}{\partial l^2}\right) - r_V \qquad (4.1)$$

Temperature gradients in the catalyst layer have been calculated within 0.1 K [5]. Therefore, the temperature in the catalyst layer was assumed to be isothermal. The reaction rate of the cyclohexane dehydrogenation (r_V) is proportional to concentration of cyclohexane [5], then we have:

$$r_V = k \cdot C_c \qquad (4.2)$$

In the steady state, the cyclohexane concentration is constant with time, and the left-hand of Eq.(4.1) is zero. The combination of Eq.(4.1) and Eq.(4.2) gives the differential equation:

$$D\left(\frac{\partial^2 C_c}{\partial l^2}\right) = k \cdot C_c \qquad (4.3)$$

with the boundary conditions:

$$l = 0 : C_c = C_c^\circ \qquad (4.4)$$

$$l = L : \frac{dC_c}{dL} = 0 \qquad (4.5)$$

here, L is thickness of Pt/Al_2O_3 catalyst layer. the solution to Eq.(4.3) is:

$$\frac{C_c}{C_c^\circ} = \frac{cosh\phi(1 - l/L)}{cosh\phi} \qquad (4.6)$$

$$\because \ \phi = L\sqrt{\frac{k}{D}} \qquad (4.7)$$

where ϕ is the Thiele number. The concentration gradient of reactant in the

catalyst increases with the value of ϕ, and the effectiveness factor η approaches zero.

If the thickness of the catalyst layer is very thin, all catalyst particles are exposed to contact with the external fluid and used for reaction, regardless of the effective diffusion coefficient. Then, this catalyst shows the maximum reaction rate r_{smax}. The maximum reaction rate per catalyst surface area can be given as:

$$r_{smax} = k \cdot C_c^\circ \cdot L \qquad (4.8)$$

Under steady state conditions, the observed reaction rate per catalyst surface area is equal to diffusion rate at catalyst surface:

$$r_s = -D \cdot \left(\frac{\partial C_c}{\partial l}\right)_{l=0} \qquad (4.9)$$

using Eq.(4.6), the solution is:

$$r_s = D \cdot C_c^\circ \cdot \sqrt{\frac{k}{D}} \cdot tanh\phi \qquad (4.10)$$

The effectiveness factor (η) of the plate type catalyst can be expressed by dividing Eq.(4.10) by Eq.(4.8):

$$\eta = \frac{r_s}{r_{smax}} = \frac{tanh\phi}{\phi} \qquad (4.11)$$

1.2 Calculation of effectiveness factor from experimental results

The observed reaction rate by experiment includes the diffusion effects and it is expressed as $\eta \cdot k$. The Weisz number, which is one of the dimensionless numbers, was used to calculate the effectiveness factor from

the experimental result [8].

The Weisz number is expressed in the following equations:

$$W_S = \Phi^2 \cdot \eta = \left(L \cdot \sqrt{\frac{k}{D}}\right) \cdot \eta = (\eta \cdot k)\frac{L^2}{D} \quad (4.12)$$

$$W_S = \Phi^2 \cdot \eta = \Phi \cdot tanh\Phi \quad (4.13)$$

We can calculate the Weisz number from experimental result by using Eq.(4.12) andϕ can be calculated using Eq.(4.13), then, the effectiveness factors are determined by Eq.(4.11).

2 EXPERIMENTAL

2.1 Preparation of the plate type catalyst

The catalyst support was prepared by anodic oxidation. The platinum catalyst particles are impregnated within the alumina layer by hot water treatment [4)9)]. The preparation conditions of the catalyst have been reported in chapter 3. Alumina layers up to 320 μm in thickness have been used in this study.

2.2 Characterization of the catalyst

The pore size distribution of the catalyst layer was calculated from nitrogen adsorption data by the Dollimore method [1)]. The thickness of the Pt/Al_2O_3 catalyst layer was measured by X-ray microanalyser (XMA). The platinum content of the catalyst layer was measured by atomic absorption spectroscopy (Shimazu AA-680). The platinum dispersion in the catalyst layer was evaluated by CO pulse method [6)]. The physical properties of the plate type catalysts are shown in **Table 4.1**.

Table 4.1 Physical properties of prepared catalysts

Sample	Thickness of catalyst layer [μm]	Pt contents		Pt dispersion [-]
		[g/m2]	[wt%]	
A	9	1.1	-	0.51
B	15	1.9	-	0.44
C	27	2.9	7.2	0.47
D	50	5.7	8.9	0.53
E	80	11.1	10.2	0.48
F	175	13.41	7.9	0.59
G	195	15.84	8.0	0.47

2.3 Measurement of catalytic reactivity

Cyclohexane dehydrogenation was used as the test reaction to estimate the effectiveness factor of the plate type catalyst [3)]. The reaction conditions are already reported in a former study [9)]. Cyclohexane was diluted with nitrogen at a ratio of 1:10. Concentrations at the inlet and outlet gas of the reaction tube were analyzed by FID gas chromatography (Shimazu GC-8A). Under stable conditions, changes in the dehydrogenation reactivity of cyclohexane with the catalyst thickness were measured at 473 K, 0.1 MPa [4)].

3 RESULTS AND DISCUSSION

3.1 Effective diffusion coefficient of the plate type catalyst

To calculate the effectiveness factor of the plate type catalyst, first it was necessary to estimate the effective diffusion coefficient. The effective diffusion coefficient (D) is given by the peak pore radius and the porosity of the catalyst layer.

(1) Pore size distribution of the plate type catalyst

Measurement of the amount of adsorbed gas as a function of the relative pressure is used for determining the pore size distribution. **Figure 4.1** shows the calculated pore size distribution of a plate type catalyst. This catalyst had a narrow pore size distribution. The peak pore radius was about 2 nm. This was unrelated to the preparation conditions.

(2) Diffusion coefficient in the pores

Pore diffusion may occur either by bulk or Knudsen diffusion. In this study, cyclohexane was assumed to be diffused into the pores mainly by Knudsen diffusion, because the partial pressure of cyclohexane was low (9 kPa) and the pores were quite small (2 nm in radius) [7]. Therefore, the diffusion coefficient into the pores (D_N) is given by:

$$D_N = 3.067 \cdot r_e \cdot \sqrt{\frac{T}{M}} = 4.60 \times 10^{-7}\ m^2/s \qquad (4.14)$$

$$\because T = 473K,\ M = 0.084kg/mol,\ r_e = 20 \times 10^{-10} m$$

(3) Effective diffusion coefficient

The effective diffusion coefficient of the catalyst layer was estimated by the parallel path model [2]. The model assumes the pore structure as comprising an array of parallel cylindrical pores having the same pore size distribution. The effective diffusion coefficient is calculated by using the diffusion coefficient into pores, the porosity of catalyst layer ε, and the tortuosity factor τ. The tortuosity factor is expressed as follows:

$$\tau = (Le/L)^2 \qquad (4.15)$$

where *Le* is length of the tortuous diffusion path. Though the tortuosity

factor τ is independent of pore size, diffusion mode and diffusion species, a factor of 2 to 4 is predicted in many cases [7]. And for diffusion through a randomly oriented system of cylindrical pores τ=3. Thus, in this study, the tortuosity factor was assumed to be 3. The porosity of the catalyst varied from 0.4 to 0.6 (Chapter 3). In this study, the porosity was assumed to be 0.5. The effective diffusion coefficient was mathematically expressed as follows:

$$D = \frac{\varepsilon}{\tau} \cdot D_N = 7.67 \cdot 10^{-8} m^2/s \qquad (4.16)$$

$$\because\ \varepsilon = 0.5,\ \tau = 3$$

3.2 Changes in reaction rate with thickness of catalyst layer

(1) Thickness of catalyst layer

Figure 4.2 shows the XMA analysis of the cross section of the plate type catalysts, samples C, E and F. The X-axis shows the depth of the alumina layer from the surface and the Y-axis shows the intensity of the X rays of each element. The area in which both platinum and aluminum show a peak is Pt/Al_2O_3 catalyst layer. The thickness could be measured from this XMA pattern and **table 4.1** shows the thickness of catalysts prepared. In each catalyst, X-ray intensity of platinum from the surface to bottom of the catalyst layer was almost the same, thus the platinum was dispersing uniformly within the alumina support layer.

(2) Platinum content per alumina weight

The platinum content per alumina weight was calculated from the thickness of the Pt/Al_2O_3 catalyst layer, the density of the alumina layer and the platinum content of the catalyst. **Table 4.1** shows these results. The platinum content of each catalyst was about 7-10 wt%.

(3) Catalytic reactivity with thickness of catalyst layer

Figure 4.3 shows the relationship between thickness of Pt/Al_2O_3 catalyst layer and reaction rate of cyclohexane dehydrogenation in steady state. Up to 80 μm, the reaction rate was proportional to the thickness. There is a slight increase of the reaction rate to 150 μm and then no further improvement was observed, even at a thickness of 150 μm.

3.3 Effectiveness factor of the plate type catalyst

The Weisz number of each catalyst was calculated from the experimental results using eq.(4.12). And then, Thiele number, ϕ was calculated using eq.(4.13). The reaction rate constant, k was also calculated using eq.(4.7). **Table 4.2** shows k', Ws, ϕ, k and η of each catalyst. The mean value of k was about 18 s^{-1} and unrelated to the thickness of the catalyst layer. This seems to be natural because the Pt content and dispersion of each catalyst were 7-10 wt% and 0.4-0.6.

Table 4.2 The k, k', Ws, ϕ and η of each prepared catalyst

Sample	$k'(=\eta \cdot k)$ [1/s]	Ws [-]	ϕ [−]	k [1/s]	η [-]
A	16.15	0.05	0.23	16.5	0.98
B	12.80	0.06	0.24	14.2	0.90
C	12.77	0.13	0.36	14.8	0.86
D	12.59	0.69	0.94	16.1	0.78
E	14.40	1.05	1.24	21.2	0.68
F	7.78	3.04	3.05	23.6	0.33
G	5.92	2.55	2.59	19.7	0.30

Figure 4.4 shows the effectiveness factor of the plate type catalyst which is calculated using eq.(4.11). The ratio and effectiveness factor decreased to 0.3 and 0.7 respectively at 80 μm thickness. **Figure 4.5** shows the variation of the cyclohexane concentration with the depth of the catalyst layer. The diffusion of cyclohexane into the catalyst layer was a serious problem at thicker catalyst layers.

3.4 Improvement of the catalytic reactivity

The observed reaction rate can be calculated using eq.(4.10). The observed reaction rate increases with the thickness of catalyst layer but it reaches the highest point, since the effectiveness factor decreases with the thickness. The highest reaction rate can be expressed as follows:

$$L \to \infty,\ r_s \to C_C^{\circ} \cdot \sqrt{D \times k} \qquad (4.17)$$

The highest reaction rate is determined by the effective diffusion coefficient and the reaction rate constant. Therefore, the reactivity can be improved by increments of the two parameters.

(1) Reaction rate constant and reactivity

Figure 4.6 shows the reaction rate changes with the catalyst thickness for different rate constants. The effective diffusion coefficient was assumed to be the same as experimental results. The reaction rate improves with the reaction rate constant but the thickness in which the highest reaction rate showed is small. Therefore, there is no need to prepare a thick catalyst layer when the reaction rate constant is high. To improve the reaction rate constant, the following should be done in future catalyst preparation:

1) Augmentation of Pt contents and dispersion
2) Research of another catalyst species which shows high reactivity

(2) Effective diffusion coefficient and reactivity

The small pore causes a diffusive resistance and this affects the easy access of reactants to catalyst sites and removal of products.

Figure 4.7 shows the reaction rate changes with the thickness assuming different effective diffusion coefficients. The reaction rate constant k was taken from the experimental results. The reaction rate improves with the effective diffusion coefficient which could be increased by expansion of the peak pore radius. However, by this method, BET surface area would be decreased and this causes low reaction rate constant due to low Pt content, and finally, the highest reaction rate would be decreased. Therefore, the pore structure of the catalyst must be changed to improve the diffusion coefficient while keeping the reaction rate constant high.

A bimodal pore size distribution is one solution. The large pores are used for diffusion of reactant and small pores are used for reaction. If the reaction rate constant per unit volume would be kept the same by the small pores, the final reaction rate could be large, as shown in **figure 4.7**. In the future, further experiments will be carried out to prepare a catalyst with a bimodal pore structure. **Figure 4.8** shows pore size distributions of the anodized alumina layer and the prepared catalyst. Anodized alumina layer has a narrow pore distribution with 50 nm radius in spite of the pore size distribution of the catalyst being 2 nm radius. Therefore, it is possible to prepare a catalyst with bimodal pore structure which has pore peaks at 50 nm and 2 nm radius by optimizing the conditions of hot water treatment.

CONCLUSIONS

In this study, the effectiveness factor of the plate type catalyst was studied theoretically and experimentally. The following conclusions are drawn from the present investigation.

(1) The $Pt/Al_2O_3/Al$ plate type catalyst prepared by anodic oxidation and hot water treatment had a porous structure with a narrow pore size distribution. Most of the pores were about 2 nm in radius.

(2) Though reaction rate of cyclohexane dehydrogenation was proportional to the catalyst thickness up to 80 μm, it reached the highest point. In thick catalyst of 195 μm, the effectiveness factor was decreased to 0.3

(3) The highest reaction rate was decided by the effective diffusion coefficient and the reaction rate constant.

(4) Reaction rate constant could be improved by increasing the Pt content per alumina weight and the dispersion of impregnated platinum.

(5) A large effective diffusion coefficient would improve the reaction rate in thick catalyst layers. A bimodal pore structure is one solution to keep reaction rate constant high with a large effective diffusion coefficient.

NOMENCLATURE

C_C	:	Concentration of cyclohexane	[mol/m^3]
D	:	Effective diffusion coefficient	[m^2/s]
D_N	:	Diffusion coefficient into pore	[m^2/s]
k	:	Reaction rate constant	[1/s]
l	:	Depth of the catalyst	[μm]
L	:	Length of catalyst layer	[μm]
Le	:	Length of the tortuous diffusion path	[μm]
M	:	Mole weight of cyclohexane	[Kg/mol]
r_S	:	Reaction rate of cyclohexane dehydrogenation per apparent surface area	[mol/(h·m^2)]
r_V	:	Reaction rate of cyclohexane dehydrogenation per catalyst volume	[mol/(h·m^3)]
r_e	:	Average pore radius of catalyst layer	[nm]
t	:	time	[sec], [h]
T	:	Reaction temperature	[K]
Ws	:	Weisz number	[-]
ε	:	Porosity of catalyst layer	[-]
η	:	Effectiveness factor of catalyst	[-]
ϕ	:	Thiele number	[-]
τ	:	Tortuosity factor	[-]

Superscript

$^\circ$: Initial

Subscript

max : Maximum

References

1) Dollimore, D., G. R. Heal : J. Appl. Chem.,14, 3, p.109, 1964
2) Johnson, M. F. L. and W. E. Stewart: J of Catal., 4, p.248(1965)
3) Kameyama, H., M. Yamashita, K. Yamamoto and T. Kabe: Proc. World Congress III of Chemical Engineering, Tokyo, p.649(1986)
4) Murata K., K. Yamamoto and H. Kameyama: *Kagaku Kogaku Ronbunshu*, 19, 1, p.41(1993)
5) Murata, K., K. Yamamoto and H. Kameyama: *Kagaku Kogaku Ronbunshu*, 19, 5, p.849(1993)
6) Sanshou Shokubai Iinkai, (ed): *Shokubai*, 31, 317 (1989)
7) Satterfield, C. N. "Heterogeneous Catalysis in Industrial Practice" , McGraw-Hill (1991)
8) Weisz, P. B.: Z. Phys. Chem. Neue. Folge, 11, 1(1957)
9) Yamaseki, K., S. Nakayashu, K. Yamamoto and H.Kameyama: *Kagaku Kogaku Ronbunshu*, 17, 267(1991)

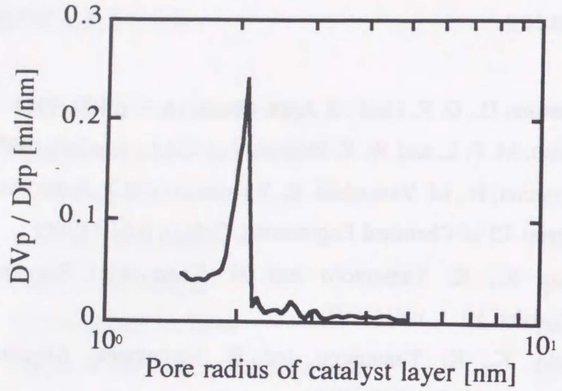

Fig. 4.1 Pore size distribution of the plate type catalyst

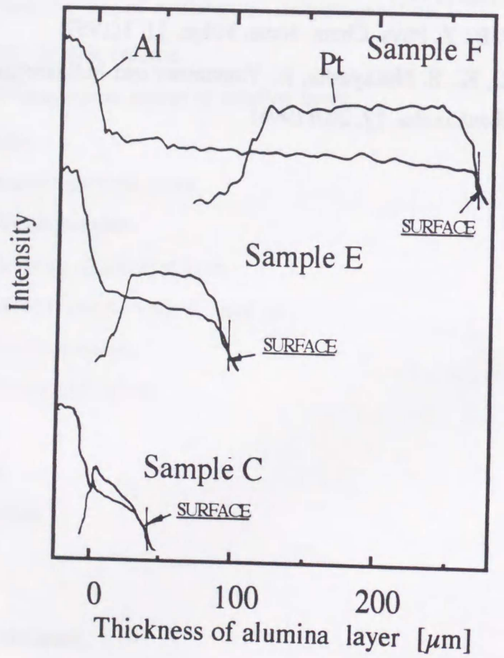

Fig. 4.2 EPMA patterns of cross section of the plate type catalysts, Sample C, E and F

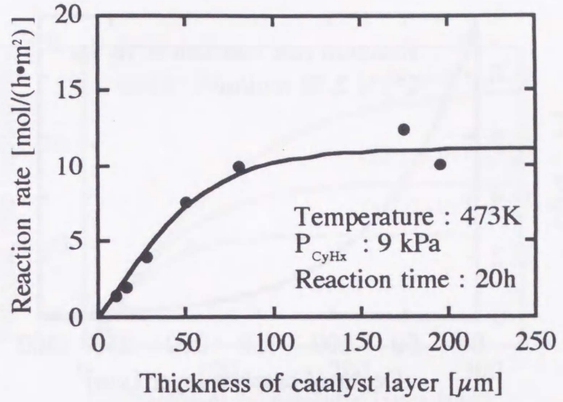

Fig.4.3 Effect of thickness of catalytic layer on catalytic reactivity

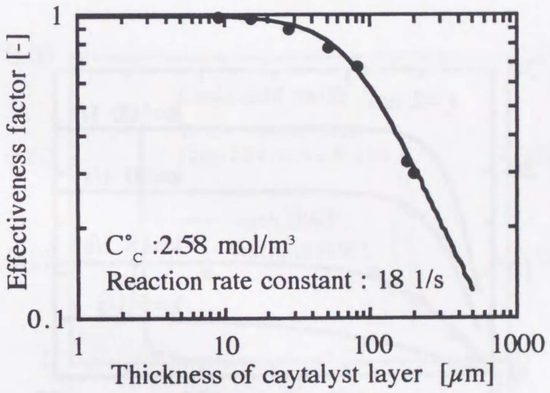

Fig. 4.4 Relationship between thickness of catalyst layer and effectiveness factor

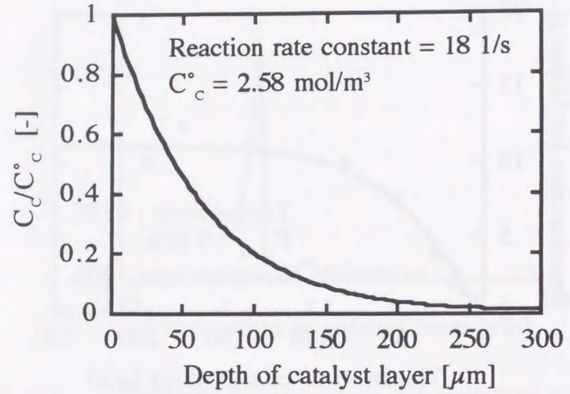

Fig. 4.5 Relationship between depth of catalyst layer and concentration ratio of cyclohexane

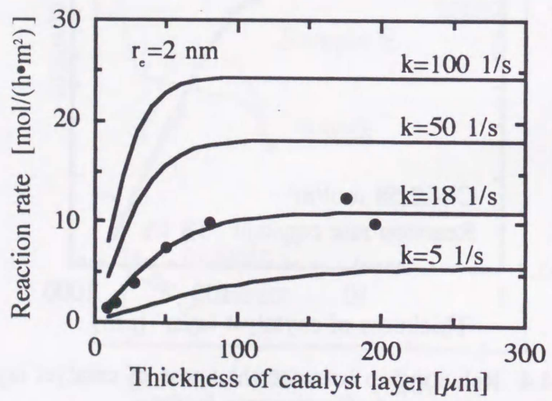

Fig. 4.6 Effect of reaction rate constant (k) on reaction rate with thickness of catalyst layer

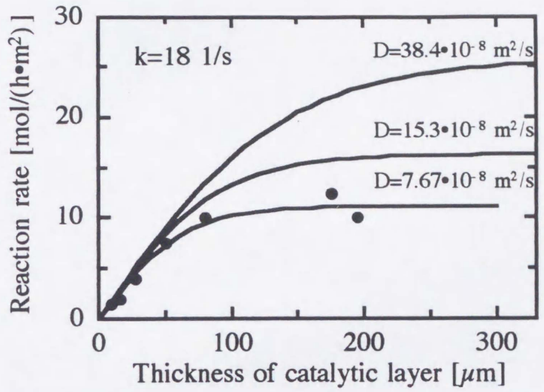

Fig. 4.7 Reaction rate changes in catalyst thickness per each diffusion coefficient, where k is constant

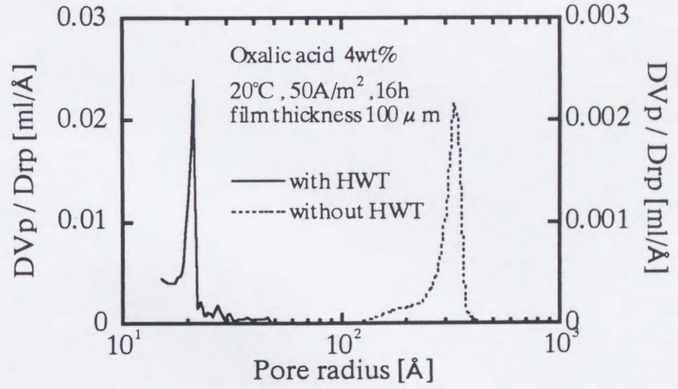

Fig. 4.8 Pore size distributions of the anodized alumina layer and the Pt/alumina catalyst layer

Chapter

5

Deactivation And Durability Of The Plate Type Catalyst

INTRODUCTION

In this chapter, durability and lifetime of plate type catalysts in dehydrogenation of cyclohexane were studied. In industrial processes, pressure of hydrogen is high to control carbon deposit and deactivation of catalyst but the pressure causes low conversion of dehydrogenation. In the case of chemical heat pumps, the dehydrogenation conversion influences total system performance, thermal efficiency and coefficient of performance. Therefore, deactivation of catalyst is a problem.

A catalyst loses its reactivity for various reasons :

1, Poisoning
2, Fouling
3, Reduction of active area by sintering or migration
4, Loss of active species

A catalyst poison is an impurity present in the feed stream that reduces catalyst reactivity. The poison in the case of plate type catalyst for cyclohexane dehydrogenation has been reported as sulfur compounds in the feed. This poisoning can be controlled by purification of cyclohexane using Raney nickel [6].

Carbonaceous deposits (coke) is a kind of fouling. The reactivity of fresh catalyst drops rapidly during the first few hours of reaction time and then more slowly thereafter. It has been reported that the coking occurs on the plate type catalyst when using purified cyclohexane [8].

Figure 5.1 shows typical change of reactivity of plate type catalyst on cyclohexane dehydrogenation. Thickness of catalyst layer was 20 μm. This change is almost same as typical change of catalytic reactivity [2]. The reactivity can be classified into three areas as classifications of conventional catalyst, as follows:

[A] The reaction when that the reactivity of fresh catalyst drops rapidly in a few hours of reaction.

[B] The reaction time when the reactivity drops slowly.

[C] The reaction time when the reactivity drops rapidly after the slow deactivation .

For industrial purposes, reaction rate during [B] has been used, since the reactivity is almost steady. Therefore, the time when the catalyst shows steady reactivity is important. In this chapter, the deactivation of the plate type catalyst was studied experimentally and theoretically and models of deactivation were proposed.

1 MODEL OF DEACTIVATION AND CATALYTIC REACTIVITY

A model of deactivation was proposed, using the model of effectiveness factor of plate type catalyst. The reaction rate r_S which is observed by experiment was expressed as Eq.(5.1) [6]. Here, D is the effective diffusion coefficient into the pores, the concentration of cyclohexane on the catalyst surface is C°_C , k is reaction rate constant ϕ is Thiele number and L is thickness of alumina layer. The ratio of concentration of cyclohexane at a depth l to that on the surface is expressed as Eq.(5.2).

$$r_S = D \cdot C^{\circ}_C \cdot \sqrt{\frac{k}{D}} \cdot tanh\phi \qquad (5.1)$$

$$\because \ \phi = L\sqrt{\frac{k}{D}}$$

$$\frac{C_C}{C^{\circ}_C} = \frac{cosh\phi(1 - l/L)}{cosh\phi} \qquad (5.2)$$

Figure 5.2 shows distributions of cyclohexane concentration ratio through the depth, which is calculated using eq.(5.2). The reaction rate on the surface is the highest regardless of coefficient of diffusion and reaction rate constant. Generally, as the volume of carbonaceous deposits increases with volume of generated product, coking may mainly occur on the catalyst surface as per **figure 5.3**. Therefore, I have varied two of the important parameters, reaction rate constant and coefficient of diffusion, and discussed the catalyst deactivation.

2 EXPERIMENTAL

2.1 Preparation of the plate type catalyst

Alumina catalyst support layer was formed by anodic oxidation of commercial aluminum. Platinum particles as catalyst were impregnated by hot water treatment. After the hot water treatment, potassium was impregnated and the effect of potassium on the reaction rate change was discussed. The detailed preparation conditions were shown in chapters 2 and 3 [3].

Physical properties of prepared catalyst were as follows. The thickness of Pt/Al_2O_3 catalyst was up to 150 μm, the porosity was 0.5, mean pore radius in the catalyst layer was 2 nm, platinum dispersion was 0.5 and the impregnated platinum particles were distributed uniformly in the alumina catalyst support layer.

2.2 Characterization of prepared catalyst

The pore size distribution of the catalyst layer was calculated from nitrogen adsorption data by the Dollimore method [1]. The thickness of the

Pt/Al_2O_3 catalyst layer was measured by X-ray microanalyser (XMA). The platinum content of the catalyst layer was measured by atomic absorption spectroscopy (Shimazu AA-680). The number of catalyst sites was measured by CO pulse method.

2.3 Measurement of catalytic reactivity

The catalytic reactivities of the catalysts were evaluated by cyclohexane dehydrogenation, which is used for endothermic reaction of cyclohexane/benzene/hydrogen chemical heat pump (CBH-CHP) [4)5)]. The chemical reaction is expressed in equation (5.3).

$$C_6H_{12} + 206\ kJ/mole \overset{473K}{\Leftrightarrow} C_6H_6 + 3H_2 \qquad (5.3)$$

A flow type reactor was used as a differential reactor [7)]. The plate type catalyst, 5×10 mm^2 and small aluminum tips, 5×5 mm^2, as dilutors, were packed in pyrex reaction tube of 11 mm inner diameter. The height of the catalyst bed was 10-15 mm. Activation of the catalyst was performed by oxidation in air (623 K, 12 h) and reduction in a mixture gas (H_2 of 10 L/h and N_2 of 15 L/h) at 623 K for 2 h. In the reaction tests, cyclohexane was diluted with nitrogen, and the dilution ratio was 1:10. Concentrations at the inlet and outlet gases of the reaction tube were analyzed by FID gas chromatography (Shimazu GC-8A). Changes in dehydrogenation reactivity of cyclohexane with time were measured at 473 K and 0.1 MPa total pressure.

Deactivated catalyst was reactivated by oxidation by air at 623 K, 12 h and 2 L/h of air and followed by hydrogen reduction at 623 K, 2 h and 25 L/h (diluted by nitrogen, the concentration of hydrogen was 60 mol%).

Catalytic reactivity of the tube wall type reactor was measured using the same flow type reactor as an integral reactor. Tube type catalyst was inserted

into the reaction tube. The length of tube wall reactor was 8.5 cm. Changes of conversion of cyclohexane dehydrogenation with time were measured.

3 RESULTS AND DISCUSSION

3.1 Analysis of deactivated catalysts

(1) The CO adsorption to the catalyst and reactivity

The quantity of CO adsorbed to the catalysts, which show several different reactivities with time, as per figure 5.1, were analyzed. The absolute quantities of the following samples were measured by the CO pulse method; Al_2O_3 catalyst support layer, fresh catalysts with different thickness, catalyst showing steady state, deactivated catalyst and refresh catalyst.

Before measuring the quantity of CO adsorption to the catalyst, standard pretreatment of air oxidation and hydrogen reduction is conducted to clean the catalyst. In steady state of catalytic reactivity, reactants such as cyclohexane, benzene and hydrogen are adsorbed on the platinum and the remaining exposed platinum is used for the reaction. Therefore, in another sample, no pretreatment to remove the adsorbed reactants was conducted. **Figure 5.4** shows relationship between the quantity of adsorbed CO and catalytic reactivity.

1) Alumina catalyst support showed no reactivity and adsorbed quantity was also zero. The reactivity of fresh catalysts increased linearly with the amount of CO adsorbed.
2) Quantity of CO adsorbed to used catalysts before pretreatment (no pretreatment) matched well with the plot of fresh catalyst, and the quantity of CO adsorption shows catalytic reactivity.
3) Adsorbed quantity of CO to used catalysts after pretreatment is greater than the value with no pretreatment and less than the value of fresh

catalyst. Some reactants, like carbonaceous deposits, would still be adsorbed on the catalyst after the pretreatment.

4) Quantity of CO adsorbed to refreshed catalyst showed the same as fresh catalyst and sintering and migration did not occur.

5) In the area [B], the area of platinum exposed would be the same, since the reactivity was the same. In the area [C], there is a sudden dip in the reactivity, and this would be caused by the decrease in exposed platinum area.

(2) Pore size distribution of the deactivated catalyst

To discuss the deactivation of catalyst, pore size distribution of deactivated catalyst was measured. **Figure 5.5** shows the results. The peak pore radius was same but the peak was lower than that of fresh catalyst. Before measuring the pore size distribution, standard pretreatment of calcination under vacuum was conducted and some carbonaceous material would be removed. Then, this distribution would not be the same as that under deactivation. Further study must be undertaken to measure the deactivated catalyst.

3.2 Reactivity change with time and the deactivated model

Model of catalyst deactivation was discussed using reactivity change with time. Actually, both reaction rate constant k and effective diffusion coefficient D would change with time. In this study both factors were treated separately and sensitive parameters are considered.

(1) Effects of the reaction rate constant

Potassium has been reported to control carbonaceous deposits. Pt/Al_2O_3/Al catalyst with no potassium was prepared and the reactivity change with time is shown in **figure 5.6**. The reactivity showed rapid drop and decreased linearly. In this case, the following model would be applied.

Figure 5.7 shows pore blockade model. The carbonaceous deposits are

supposed to blockade the micro pores in the catalyst immediately, and platinum particles inside of the pores could not be used for reaction. The remaining pores are supposed to be used for the reaction under the same reaction rate constant and effective diffusion coefficient. The volume of deposits increases with time. In this case, reaction rate constant per unit volume would decrease with the deposits.

Figure 5.8 shows reactivity changes with reaction rate constant, and the changes were calculated using Eq.(5.1). The reaction rate decreased linearly with decrease of reaction rate constant, regardless of thickness of catalyst layer. As the reaction rate constant would decrease with reaction time due to carbon deposits, X-axis of reaction rate constant corresponds to reaction time. The relationship between reaction time and reaction rate constant remains for further investigation. Since the characteristics of changes of reaction rate are almost the same as in the examination, this model can be applied for catalyst on which carbonaceous materials deposit easily.

(2) Effects of the effective diffusion coefficient

Figure 5.9 shows reaction rate changes with reaction time for two thicknesses of catalyst layer, 30 μm and 80 μm. In these catalysts, potassium was impregnated after hot water treatment. Though the catalyst with 30 μm thickness showed a stable reaction rate after rapid drop, in the case of 80 μm thickness, there was no stable reaction rate and it decreased linearly. For the catalyst with 30 μm thickness, after the stable reaction rate, there is a sudden drop in reaction rate. Those characteristics are discussed as follows.

Figure 5.10 shows the pore narrowed model. In the model, the carbonaceous deposits narrow the micro pores and the mass transfer of the reactants into the catalyst pores becomes rate controlling. Then, the reaction rate decreases with the reaction time. The volume of deposits increases with time.

Figure 5.11 shows reactivity changes with pore radius and the changes were calculated into using Eq.(5.1). The changes of reaction rate with pore

radius is classified into three patterns, according to thickness of catalyst layer:

1) In the case of thickness of 10 μm, the reaction rate was stable regardless of pore radius.
2) In the catalyst with 30 μm thickness, the reaction rate was steady till 0.5 nm pore radius, and showed rapid drop with decrease of pore radius.
3) More than 30 μm in thickness, reaction rate gradually declines with decrease this decline accelerates.

These phenomena are caused by the effectiveness factor of the catalysts. The value of the thick catalyst is small and the reaction rate is sensitive to the effectiveness diffusion coefficient which is decided by pore radius. Then, the reaction rate decreased gradually with decrease of pore radius. In the case of 30 μm, effectiveness factor is high (0.86) and mass transfer is not rate controlling for the reaction. But if the rate controlling step is changed to mass transfer from reaction, the reaction rate decreased with pore radius.

As the pore radius would be narrowed by carbon deposits with reaction time, X-axis of reaction rate constant corresponds to reaction time. The relationship between reaction time and pore radius remains for further investigation. If rate of carbonaceous deposits is clarified, it would be possible to predict the catalyst life by using these models. Since the characteristics of changes of reaction rate are almost the same as in these examinations, this model can be applied for catalyst which controls carbonaceous deposits.

3.3 Durability of the tube wall catalyst

In this part, reactivity change with time of tube wall reactor was studied. Inside of the tube, a Pt/Al_2O_3 catalyst layer 150 μm in thickness was formed, and the length, L_C was 8.5 cm. In this catalyst, potassium was impregnated. The apparatus was used as an integral reactor and the reaction was conducted for 1000 h.

Figure 5.12 shows changes in conversion of cyclohexane with reaction

time. In this condition, equilibrium conversion is 33 % of cyclohexane. Initial reaction rate was about 33 % and it decreased rapidly and showed a constant value after 50 h of reaction. The stable value 25 % continued to 200 h, and then decreased gradually to 1000 h of reaction. The reaction rate after 1000 h was about 60 % of the steady value.

We can think of a catalyst in the shape of a thin ring whose thickness is ΔL, then the tube catalyst consists of many units of these ring catalysts. Each ring catalyst from end to end shows a reaction rate which is decided by the composition of the reactant. The conversion of the tube catalyst is calculated as an integration of reaction rate of each ring catalyst. The reactivity changes with the time of ring catalyst is allowed by the pore narrowed model, and the following are considered:

1) In initial reaction, all parts of the catalyst are fresh and show high reactivity. The reactivity decreases rapidly, like that of a differential reactor.
2) The conversion showed constant till 200 h. All parts of the catalyst were considered to show a constant reaction rate, like area [B] above.
3) Since a sudden dip of reactivity is caused by carbon deposits in the reaction, the reactivity of small parts of the catalyst decreased, from the entrance of the tube catalyst. Thus the conversion which is calculated by integration of the reactivity decreased gradually.

If quantity of carbonaceous deposits on the catalyst is known, the durability of the tube catalyst can be determined.

CONCLUSIONS

The deactivation mechanism and durability of the tube wall catalyst during dehydrogenation of cyclohexane was studied.

1) Deactivation of this tube wall catalyst caused by carbon deposits. Sintering, migration and loss of active species were not observed. The reactivity of a refreshed catalyst was as high as for fresh catalysts.

2) Reaction rate increased linearly with quantity of CO adsorbed.

3) A deactivation model was proposed by using the model of effectiveness factor of plate type catalyst. The reaction rate r_c which is observed in terms of experiment was expressed by effective diffusion coefficient and reaction rate constant.

4) Experimental results on reaction rate changes of the potassium free catalyst showed that reaction rate decreased linearly with time and these results matched the pore blockade model.

5) With potassium in the catalyst, the pore narrowed model matched the experimental results well. In the model, the carbonaceous deposits narrow the micro pores, and the mass transfer of the reactants into the catalyst pores becomes rate controlling. Thus, the reaction rate decreases with the reaction time.

6) In the long-life test of a tube type catalyst, the catalyst showed a steady reactivity in the reaction time from 50 h to 200 h, but deactivation gradually proceeded to reach the value of 60 % of steady reactivity after the reaction time of 1000 h. This phenomenon is expressed by the pore narrowed model.

NOMENCLATURE

C_c	:	Concentration of cyclohexane	[mol/m3]
D	:	Effective diffusion coefficient	[m2/s]
k	:	Reaction rate constant	[s-1]
l	:	Depth of the catalyst	[μ m]
L	:	Thickness of the catalyst layer	[μ m]
L_C	:	Length of the tube wall catalyst	[cm]
r_S	:	Reaction rate of cyclohexane dehydrogenation per surface area	[mol/(h・m2)]
ϕ	:	Thiele number	[-]

Superscript

° : Initial

References

1) Dollimore, D., G. R. Heal; J. appl. Chem., 14, 3,p.109-114 (1964)
2) Furuoya, I. ; *Shokubai*, 18, 3, p.60-66,1976
3) Murata K., K. Yamamoto and H. Kameyama; *Kagaku Kogaku Ronbunshu*, 19, 1, p.41-47 (1993)
4) Muata, K. and H. Kameyama; ALUTOPIA, 23, 10, p.9-15, 1993
5) Murata, K. and H. Kameyama; Proceeding of Int. Hydrogen and Clean Energy Symposium '95, Japan, Tokyo, p.313-316, 1995
6) Nishimura S., S. Takeoka and H. Kameyama;*Shokubai*, 32, 7, p.488-489 (1990)
7) Sanshou Shokubai Iinkai, (ed), *Shokubai*, 31, p.317 (1989)
8) Yamaseki K., S. Nakayashu, K. Yamamoto and H.Kameyama; *Kagaku Kogaku Ronbunshu*, 17, p.267-272 (1991)

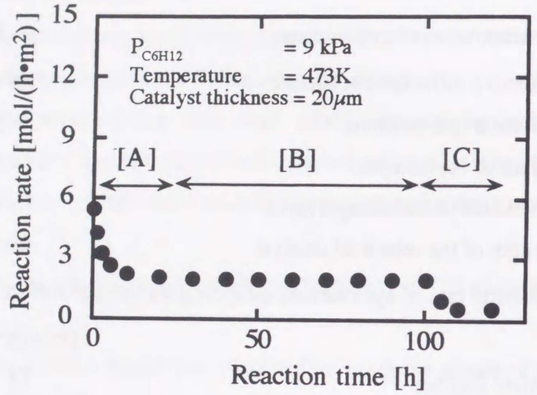

Fig.5.1 Changes in catalytic reactivity with time

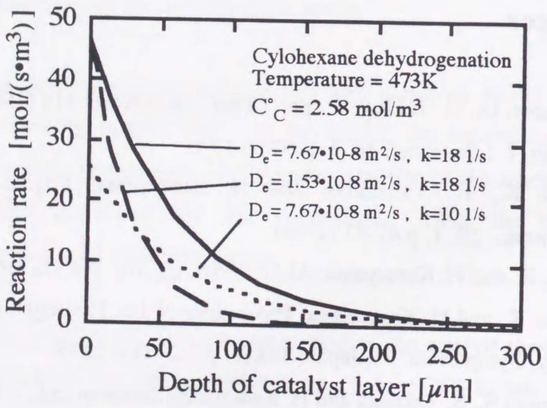

Fig. 5.2. Changes in the reaction rate with the depth of the catalyst

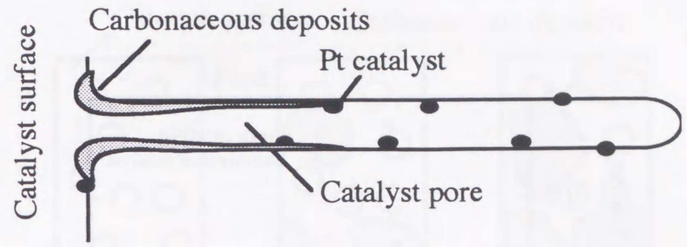

Fig. 5.3 Illustration of the carbonaceous deposits in the catalyst layer

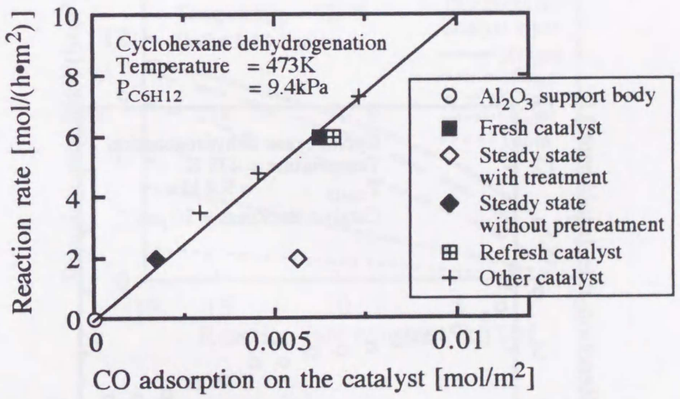

Fig. 5.4 Relationship between CO adsorption on the catalyst and the reaction rate

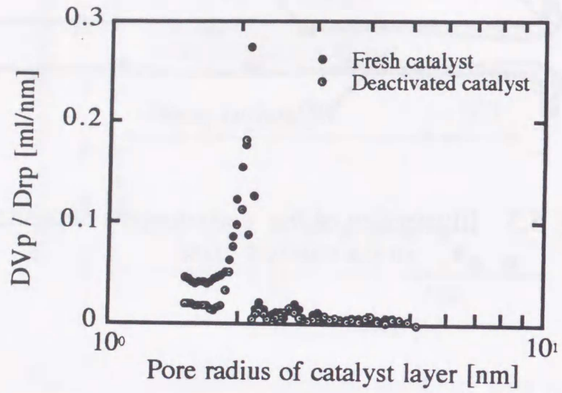

Fig. 5.5 Pore size distribution of a fresh catalyst and the deactivated catalyst

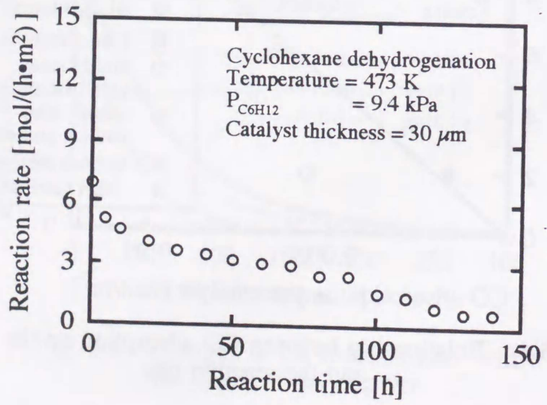

Fig. 5.6 Reactivity changes of the catalyst without potassium addition

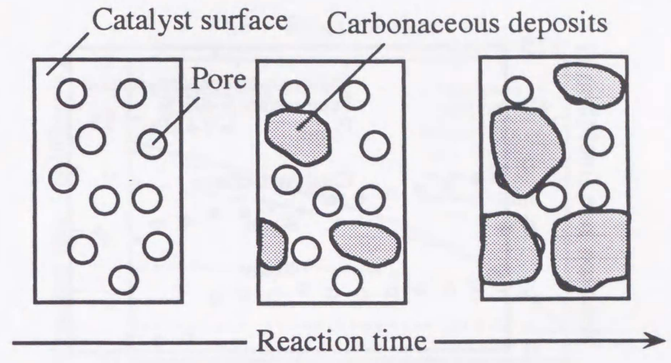

Fig. 5.7 Illustration of the deactivation model of blockading of the pores in the catalyst layer

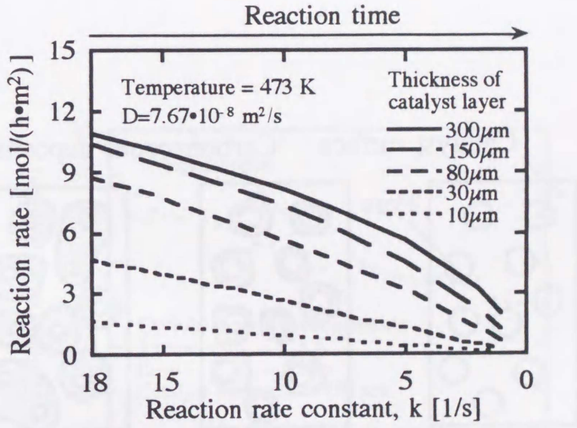

Fig. 5.8 Changes in the reaction rate of cyclohexane dehydrogenation in relation to the k for different thicknesses

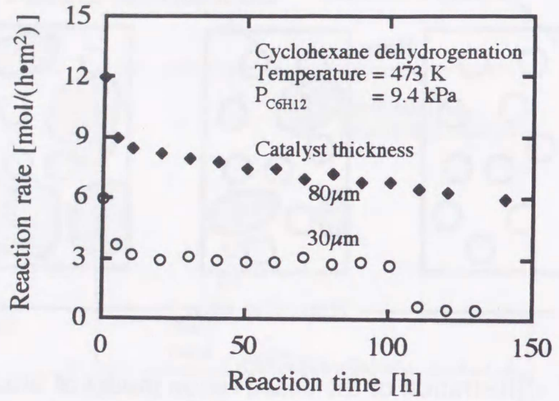

Fig. 5.9 Reaction rate changes with time, for thick and thin catalyst

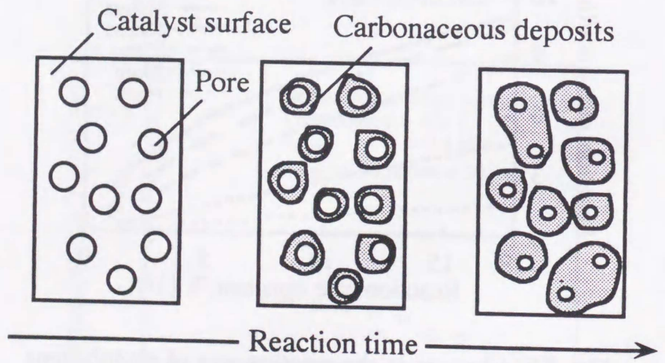

Fig. 5.10 Illustration of the deactivation model of narrowing the pores in the catalyst layer

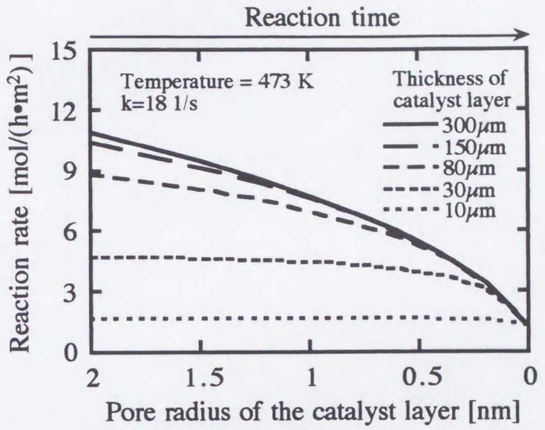

Fig. 5.11 Reaction rate changes according to the pore radius of the catalyst, for different thickness

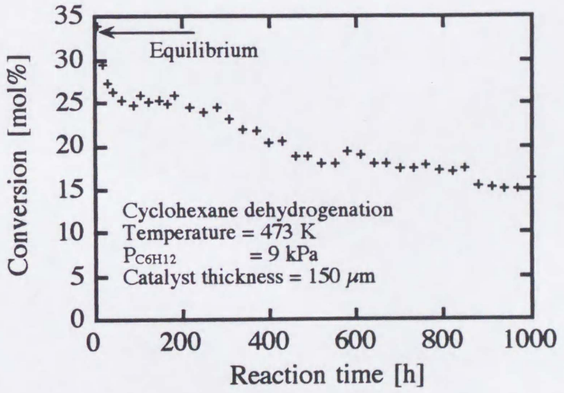

Fig. 5.12 Conversion changes of the tube wall type catalyst with reaction time

Chapter

6

Mass Transfer In Tube Wall Reactor Developing Laminar Flow

INTRODUCTION

In the wall type reactor, the catalyst layers are only formed on the surface of the reactor walls and size of tube wall reactor tends to be larger than that of conventional fixed bed reactor. This is caused by two reasons as follows:

1) Volume of catalyst supported is smaller than that of fixed bed reactor.
2) Mass transfer in the radial tends to control the total reaction rate.

These two elements would be breakthrough points for design of tube wall reactors.

In recent years, there has been some interest in the theoretical analysis of radial mass transfer in tubular reactors. In these analysis, the flow has been supposed to be fully developed laminar or turbulent flow [1-10].

In developed laminar flow, velocity difference between center and wall is large, and mass transfer controls the total reaction rate. To escape this controlling step, some researchers packed inert material in the catalyst tube. But this causes large pressure loss in the reactor.

The dehydrogenation of cyclohexane at 0.1 MPa and 473 K is gas phase reaction. Reynolds number is about 2 and the flow is laminar. In these conditions, while a fully developed laminar flow, it is likely that radial mass transfer controls the reaction.

On the other hand, while laminar flow is still developing, it has been reported that radial mass transfer was different from that of fully developed laminar. The value is larger than that of developed laminar flow and near that of turbulent flow [1)2)].

In this chapter I focus on developing laminar flow. The radial mass transfer under developing laminar flow was studied. Reaction conditions, in which reaction rate is controlling, was proposed using static mixer.

1 THEORETICAL MODEL OF RADIAL MASS TRANSFER IN THE TUBE WALL REACTOR

1.1 Mass transfer of reactant in the tube wall reactor

Figure 6.1 shows illustration of the reactor wall. The reactant, cyclohexane molecules diffuse to the catalytic reactor wall and they are dehydrogenated on the catalyst wall. In developing laminar flow, it has been reported that radial gas flow velocity distribution is almost same as a plug flow [1)2)]. Near catalyst wall, the velocity is decreased by friction to the wall and the boundary layer is formed on the catalyst wall.

In the boundary layer, the reactant moved to catalyst wall at mass transfer coefficient k_M. The total reaction rate constant k_T is determined by reaction rate constant k_R ($k_R=r_S/C_{CS}$) and mass transfer coefficient in the boundary layer k_M. The total reaction constant k_T is expressed as follows:

$$\frac{1}{k_T}=\frac{1}{k_M}+\frac{1}{k_R} \qquad (6.1)$$

Figure 6.2 shows the ratio of total reaction rate k_T and reaction rate constant k_R (k_T/k_R) changes with the ratio of mass transfer coefficient k_M and reaction rate constant k_R (k_M/k_R). The k_T/k_R increases with the k_M/k_R and the value rises to 1. This means that if the k_M is 20 times larger than the k_R ($k_M/k_R > 20$), k_T is almost same as k_R ($k_T/k_R \fallingdotseq 1$). In this condition, the cyclohexane concentration on the catalyst surface C_{CS} is almost same as the cyclohexane concentration of bulk C_{C0} ($C_{C0}=C_{CS}$). Then, the mass transfer coefficient in the boundary layer can be neglected for the reaction. Therefore, the ratio of mass transfer coefficient and reaction rate constant

k_M/k_R is one of the important parameter to evaluate the condition of reaction in the tube wall reactor. In this chapter, the value of this ratio is thought as key parameter and the ideal ratio is assumed to be 20 [-].

1.2 Ideal conversion changes with gas velocity

Conversion changes of the tube wall reactor with gas velocity for each reaction rate constant was calculated using a simulator (see next **chapter 7**). In this calculation, k_M/k_R was supposed to be larger than 20, then, C_{CS} is same as C_{C0}. **Figure 6.3** shows the calculated conversion changes with SV. This conversion changes with space velocity SV are ideal condition of reaction. And the reaction rate is controlling the total reaction of this tube wall reactor.

In the following, the experimental results were compared to the calculated results.

2 EXPERIMENTAL

2.1 Preparation of the tube wall catalyst

The commercial **aluminum tube** (JIS A-1050, 11 mm in diameter, 2-12.5 cm in length and 99.5 % in purity) was used to prepare tube wall catalyst. Inside the aluminum tube was anodized by oxalic acid and followed by hot water treatment in chroloplatinic acid solution. Experimental apparatus for anodic oxidation was shown in **figure 6.4**. The conditions were same as reported paper and chapters 2,3. Pt/Al_2O_3 catalyst layer 270 μm in thickness was formed inside surface of aluminum tube. **Figure 6.5** is a photograph of the prepared tube wall catalyst. Platinum content was about 10 wt% per alumina weight and about 10 g/m^2 per apparent surface area. Platinum dispersion was about 0.5.

2.2 Reactivity of the tube wall reactor

Catalytic reactivity of prepared tube catalyst was estimated by cyclohexane dehydrogenation, 473 K, 0.1 MPa. Reaction conditions were same as those in chapters 2-5. Surface temperature of the catalyst was controlled at 472-474 K. **Figure 6.6** shows illustration of reactor with tube wall catalyst. Tube wall catalyst was inserted into reaction Pyrex tube. Length of the catalyst was changed from 2 cm to 12.5 cm. Spiral plate that plate was spiraling 180 degree in 4 cm, or flat aluminum plate was inserted into tube wall catalyst to promote the radial mass transfer.

3 RESULTS AND DISCUSSION

3.1 Thickness of boundary layer

Under developing laminar flow, thickness of boundary layer is increasing with the distance from the entrance of the catalyst tube. It would be considered that the boundary layer thickness at the entrance and the exit are not same. This may cause the change of mass transfer coefficient.

Thickness of boundary layer is proportional to the square root of the distance from entrance of tube. The distance to fully develop the boundary layer is calculated as 10 times longer than the tube wall catalyst used in this experimental.

Figure 6.7 shows conversion changes with catalyst length under same gas velocity. The experimental results were matched well to the calculated results. These results show that mass transfer coefficient in the boundary layer through the tube wall catalyst is quite larger than the reaction rate constant. Therefore, effect of catalyst length on mass transfer coefficient can be neglected.

3.2 Mass transfer coefficient in the boundary layer

Figure 6.8 shows comparison of experimental and calculated results for conversion changes with gas velocity. The experimental results are lower than that of calculated at low gas velocity. This means that mass transfer through the boundary layer controls overall reaction at low gas velocity and thickness of boundary layer increased with decrement space velocity.

Using experimental results, total reaction rate constant k_T was calculated (See **chapter 7**). The reaction rate has been proposed to proportion to pressure of cyclohexane as follows:

$$r_S = k_T \times C_{C0} \qquad (6.2)$$

Figure 6.9 shows total reaction rate constant k_T changes with space velocity with each reactivity. It is cleat that decrement of total reaction rate constant is large at high reactivity catalyst.

Mass transfer coefficient was calculated from overall reaction rate and reaction rate constant measured by differential reactor (see **chapter 5**) by using eq.(6.1). The results are shown in **Figure 6.10.** Mass transfer coefficient was proportional to the 2 power of the space velocity regardless of reactivity. This is because the thickness of boundary layer is also proportional to the square root of gas velocity. To satisfy the key parameter, the ratio of mass transfer coefficient and reaction rate constant, space velocity SV more than 3000 is needed.

3.3 Effects of static mixer on controlling step

It has been clear that boundary layer thickness is important for reaction of tube wall catalyst. Static mixer was inserted into tube and this effect was considered.

Figure 6.11 shows effect of static mixer on conversion changes with time under space velocity 1700 h^{-1}. At first only tube catalyst was used for reaction. After the catalyst showed steady state, reactor temperature was dropped to room temperature and a spiral was inserted. Then the reaction

test restarted.

During the insertion of spiral, nitrogen gas was used for purge. After the insertion of the spiral, reaction rate showed high. This is because that the surface of catalyst was cleaned by purge of nitrogen. After 10 h of further reaction, the catalyst showed steady state again. The steady state reaction rate was 3 points higher than that of tube catalyst without static mixer.

3.4 Effects of spiral shape on conversion

Figure 6.12 shows effect of shape of static mixer on conversion changes with space velocity. In this study, the effects of flat plate and spiral plate were compared. By using static mixer, conversion at low space velocity was increased and the value was matched to the calculated result. This results show that static mixer accelerates the mass transfer in boundary layer. The different of shape of static mixer on conversion was not observed. **Figure 6.13** shows that effects of static mixer on conversion changes for each reactivity. Every reactivity matched well to calculated result.

Effects of static mixer was considered that the reactant gas was mixed mechanically by mixer. Pressure drop of static mixer was negligible under Raynolds number of about 10.

CONCLUSIONS

In this chapter, mass transfer in the tube wall reactor developing laminar flow was studied. The following conclusions are drawn from the present investigation:

1) Mass transfer coefficient more than 20 times larger than reaction rate constant was needed for reaction controlling step. Ideal conversion

changes under reaction controlling was calculated.

2) In developing laminar flow, thickness of boundary layer is increasing with the distance from entrance of catalyst tube. Experimental results show that mass transfer coefficient in the boundary layer through the catalyst is quite larger than the reaction rate constant. Therefore, effect of catalyst length on mass transfer coefficient is neglected.

3) The conversion by experimental were lower than calculated results at low gas velocity. Mass transfer through the boundary layer is controlling overall reaction under 3000 h^{-1} of space velocity.

4) Using spiral or plate in the tube catalyst increased conversion at low space velocity. This results show that static mixer accelerate the mass transfer in boundary layer by mixing.

Nomenclature

C_C	:	Concentration of cyclohexane	[mol/m3]
k_M	:	Mass transfer coefficient in boudary layer	[m/s]
k_T	:	Total reaction rate constant	[m/s]
k_R	:	Reaction rate constant	[m/s]
r_S	:	Reaction rate of cyclohexane dehydrogenation per apparent surface area	[mol/(s·m2)]
SV	:	Space velocity	[h-1]

<Subscript>

0	:	initial
S	:	surface

References

1) ARASHI, N. : *Kagaku Kogaku Ronbunshu*, 6, 5, 476(1980)
2) ARASHI, N. : *Kagaku Kogaku Ronbunshu*, 10, 3, 359(1984)
3) FIELD, J. H. : I&EC Prod. Res. Dev., 3, 150(1964)
4) INOUE, H. : *Kagaku Kogaku Ronbunshu*, 5, 6, 609(1979)
5) INOUE, H. : *Kagaku Kogaku Ronbunshu*, 6, 1, 98(1980)
6) JOHNSTONE, H. F. : I & EC, 46, 4, 702(1954)
7) KASAOKA, S. : *Kagaku Kogaku Ronbunshu*, 33, 6, 69(1969)
8) KATZ, S. : Chem. Engng Sci., 10, 202(1959)
9) SMITH, T. G. : Chem. Eng. Sci., 30, 2-E, 221(1975)
10) SMITH, T. G. : Chem. Eng. Sci., 31, 1071(1976)

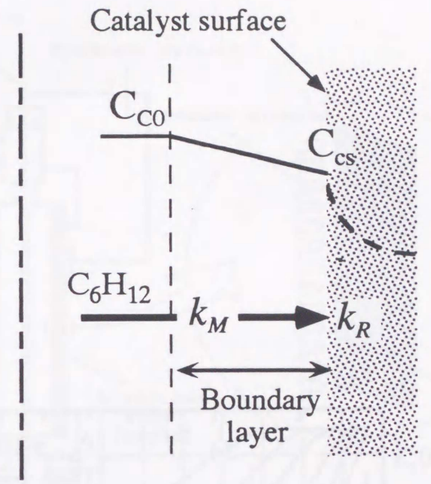

Fig. 6.1 Illustration of mass transfer in the wall type reactor

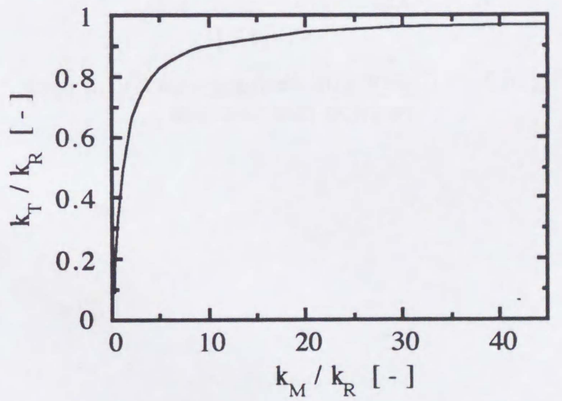

Fig. 6.2 Total reaction constant change with mass transfer coefficient

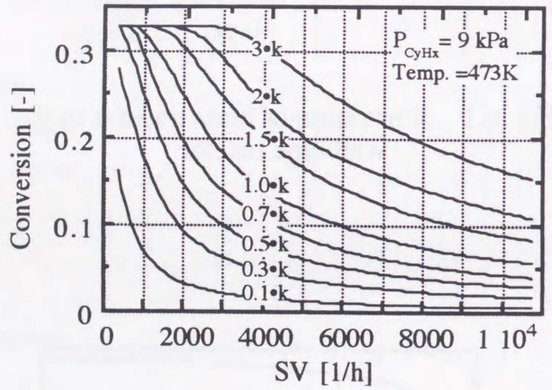

Fig. 6.3 Conversion changes with SV in each reaction rate constant

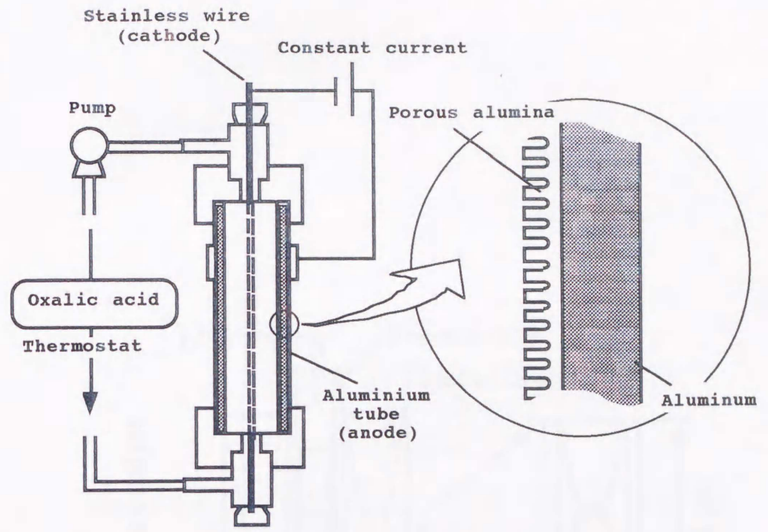

Fig. 6.4 Experimental apparatus for anodic oxidation of tube

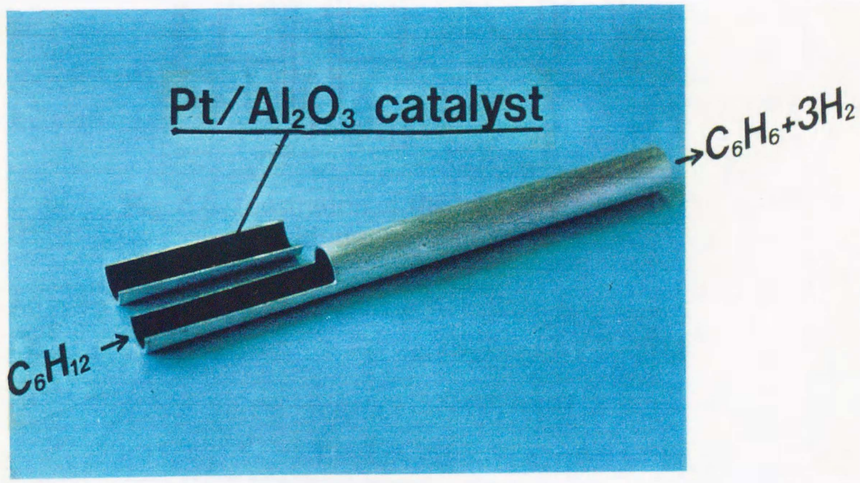

Figure 6.5 Photograph of tube wall catalyst inside surface was catalyzed by Platinum/ alumina

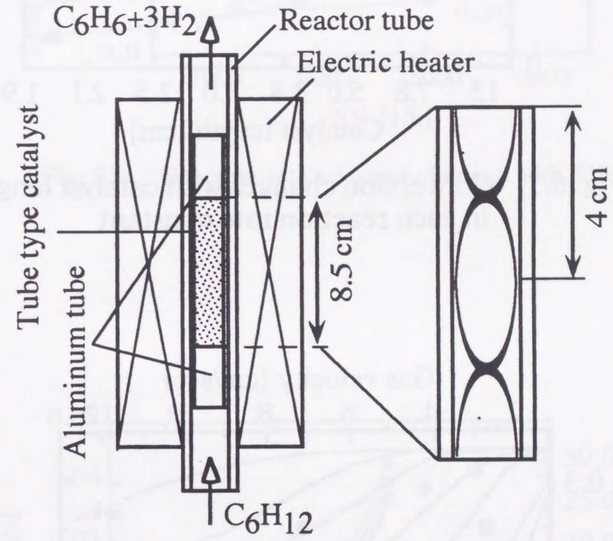

Fig. 6.6 Illustration of the tube wall reactor with the static mixer

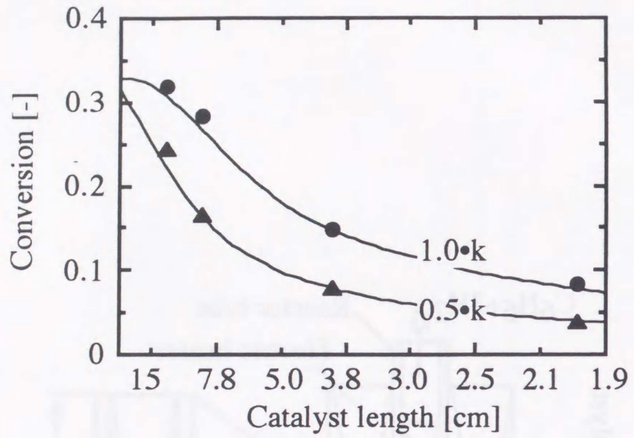

Fig. 6.7 Conversion changes with catalyst length in each reaction rate constant

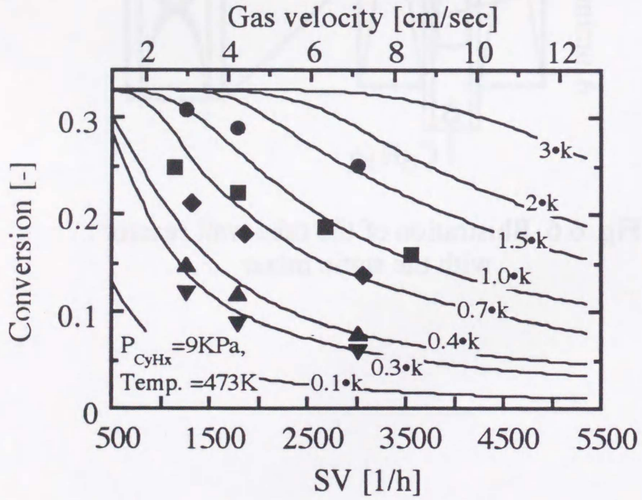

Fig. 6.8 Conversion changes with SV

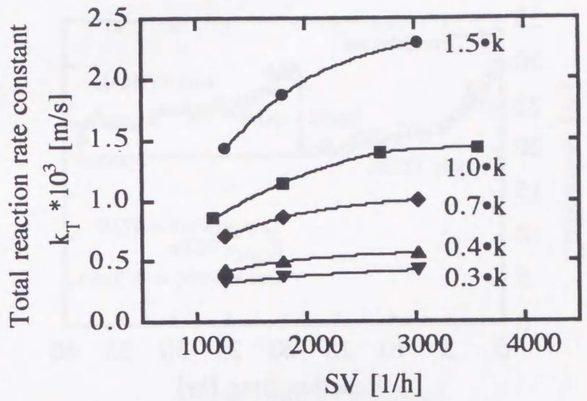

Fig. 6.9 Reaction rate constant changes with SV

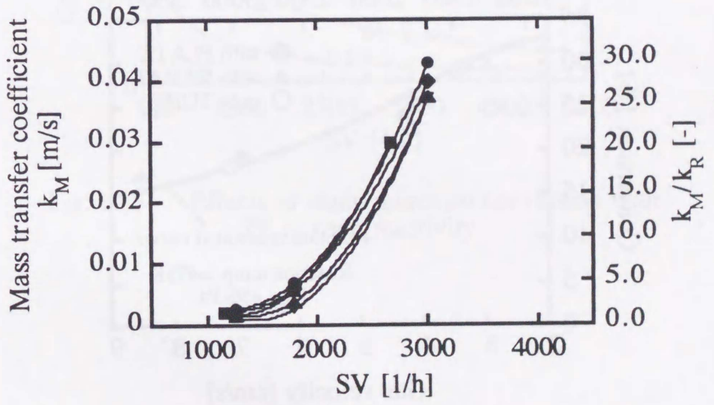

Fig. 6.10 Mass transfer coefficient changes with SV

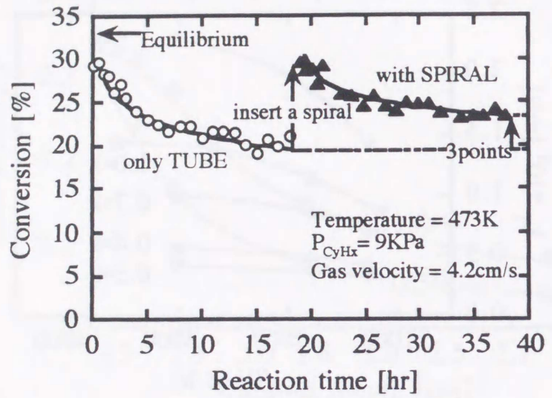

Fig. 6.11 Conversion changes with time before and after using the static mixer

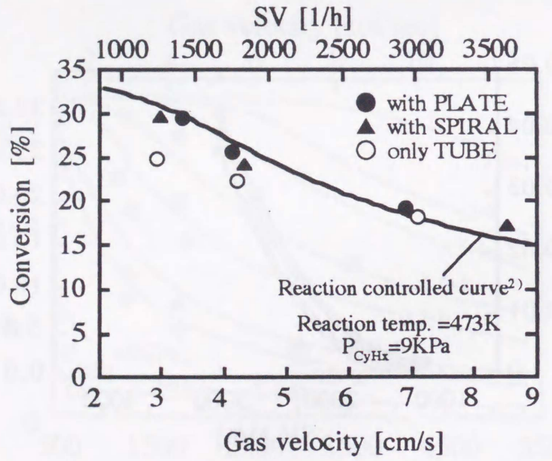

Fig. 6.12 Effects of static mixer and plate on conversion

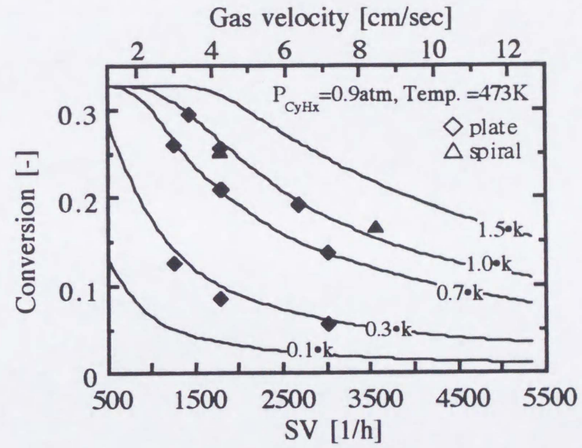

Fig. 6.13 Effects of static mixer on conversion with SV in each reactivity

Chapter

7

Simulation Of Tube Wall Reactors

INTRODUCTION

Chemical heat pumps with various kinds of reaction have been proposed and studied. Tube wall reactors which easily transform thermal energy into chemical energy are needed for CHPs to reduce exergy loss. A thin layer catalyst supported on a metal has high thermal conductivity and well suits the wall type reactor [2].

In this section, feasibility study of tube wall reactor was investigated by using a simulator. The reactor wall is assumed to be made of $Pt/Al_2O_3/Al$ plate type catalyst with high thermal conductivity.

At first, reaction mechanism and equation of reaction rate of cyclohexane dehydrogenation around 9 kPa and 473 K was decided. Adsorption of cyclohexane molecules to the catalyst site is the controlling step under 10 kPa of partial pressure of cyclohexane. The rate of cyclohexane dehydrogenation was controlled by adsorption rate of cyclohexane molecule to the catalyst surface.

Conversion and temperature distributions in tube wall reactor and fixed bed reactor were studied. The temperature and conversion distributions are narrower in radius than those of the fixed bed reactor, and the wall type reactor was preferable for use in CHPs.

Propriety of this simulation model was shown. Tube wall reactors of 2-12.5 cm length and with 300 μm thickness of catalyst layer inside the tube were prepared. Calculation results matched experimental results well.

Design for a compact tube wall reactor was proposed. It has been shown that compact tube wall reactor could be designed by reducing diameter of reactor tube and by increasing catalyst thickness.

Process design for tube wall reactor was also proposed. In some cases, there is no need for a feed preheater for tube wall reactor. This causes cost down and flexibility for process design.

1 DETERMINATION OF EQUATION OF CYCLOHEXANE DEHYDROGENATION

To estimate the performance of tube wall reactor, equation of reaction rate must be determined. In this study, target reaction is cyclohexane dehydrogenation. Langmuir-Hinshelwood model was assumed to determine the equation. The chemical reaction is expressed in equation(7.1).

$$C_6H_{12} + 206\ kJ/mole \overset{473K}{\Leftrightarrow} C_6H_6 + 3H_2 \qquad (7.1)$$

$Pt/Al_2O_3/Al$ catalyst with 30 μm thickness was used [7]. Differential reactor, the same apparatus as in chapter 2, was used.

Before the reaction test, reactivation of the catalyst was done by oxidation in air at 623 K for 12 h and reduction in hydrogen stream at 623 K for 2 h . Cyclohexane diluted by nitrogen (dilution ratio was 10) flowed at a rate of 7.5 ml-cyclohexane/h and the concentrations at inlet and outlet gases of the reaction tube were determined with GC equipped with FID (Shimazu GC-8A).

2 MATHEMATICAL MODEL OF TUBE WALL REACTOR

2.1 Model of tube wall reactor

Model of tube wall reactor is shown in **figure 7.1**. Inside diameter was 2 mm - 10 mm, thickness of catalyst layer was 30 μm - 300 μm. Though platinum particles are distributed within actual catalyst layer, the particles were supposed to exist on inside surface of the catalyst layer and the reaction

was assumed to occur on inside surface area.

As reactant gas flows inside tube, cyclohexane diffuses to inside surface of the catalyst and dehydrogenation occurs on inside surface. The reaction temperature is the same as inside surface temperature and the reaction heat is supplied from outside tube and inside gas.

Boundary layer exists on inside surface. This causes resistance to heat and mass transfer, between reactant gas and inside catalyst wall. The following was shown in previous chapter 6:

1) Under high gas velocity the resistance to mass transfer in the boundary layer has been negligible.
2) While developing laminar flow, gas flow can be supposed to be plug flow.

Based on these results the following assumptions were made:

1) Temperature of outside surface is same as that of heat media.
2) Axial diffusion may be negligible.
3) Physical properties such as reaction heat and heat capacity are assumed to be the same.

Under these conditions, heat balance and material balance of the system is as follows:

i) Heat balance

$$-\frac{\partial T}{\partial z} + \frac{k_e}{G \cdot C_p}\left(\frac{\partial^2 T}{\partial R^2} + \frac{1}{R}\cdot\frac{\partial T}{\partial R}\right) = 0 \qquad (7.1)$$

ii) Material balance

$$-\frac{\partial X}{\partial z} + \frac{D}{u}\left(\frac{\partial^2 X}{\partial R^2} + \frac{1}{R}\cdot\frac{\partial X}{\partial R}\right) = 0 \qquad (7.2)$$

The boundary conditions are:

1) $z=0$: $X=0,\ T=T_0$ (7.3)

2) $R=0$: $\partial T/\partial R=0,\ \partial X/\partial R=0$ (7.4)

3) R=Riw : $\partial X/\partial R=-r_W \cdot M(G \cdot u \cdot D \cdot Y_0)$ (7.5)

$$-ke \cdot \partial T/\partial R =$$
$$h_W \cdot (T_{iw}-T) = (-H) \cdot (-r_W)+(kc/d) \cdot (T_{iw}-T_w) \quad (7.6)$$

2.2 Model of fixed bed reactor

Reactor tube is 25 mm in diameter. Catalyst particles 3 mm in diameter are packed in the reactor tube, with porosity 0.51. Reaction heat is supplied from heat medium outside tube and inside wall temperature is assumed to be same as that of outside wall.

i) Heat balance

$$-\frac{\partial T}{\partial z}+\frac{k_e}{G \cdot C_P}\left(\frac{\partial^2 T}{\partial R^2}+\frac{1}{R}\cdot\frac{\partial T}{\partial R}\right)+\frac{-H \cdot (-r_F)}{G \cdot C_P}=0 \quad (7.7)$$

ii) Material balance

$$-\frac{\partial X}{\partial z}+\frac{D}{u}\left(\frac{\partial^2 X}{\partial R^2}+\frac{1}{R}\cdot\frac{\partial X}{\partial R}\right)+\frac{-M \cdot (-r_F)}{G \cdot Y_0}=0 \quad (7.8)$$

The boundary conditions are:

1) z=0 : $X=0\ ,\ T=T_0$ (7.9)

2) R=0 : $\partial T/\partial R=0,\ \partial X/\partial R=0$ (7.10)

3) R=Rw : $\partial X/\partial R=0$ (7.11)

$$-ke \cdot \partial T/\partial R=h_W \cdot (T_{iw}-T) \quad (7.12)$$

2.3 Physical properties

Table 7.1 shows physical properties. These properties are referred to *Kagaku Kogaku Binran* [5]) and calculated using equations arranged by Sato [8]). It should be noted that the diffusion coefficient of cyclohexane and thermal efficiency in fixed bed reactor are quite different from those of tube wall reactor.

Thermal conductivity of $Pt/Al_2O_3/Al$ catalyst was calculated using series model. **Figure 7.2** shows changes of thermal conductivity of alumina layer. The thermal conductivity drops rapidly with alumina thickness.

Thermal conductivity of anodized aluminum plate was measured as 105 kcal/(m•h•k). The thickness of alumina layer on both sides was 10 μm and aluminum thickness was 3 mm. The calculated value at 20 μm of alumina layer was almost the same as the measured value, so this model was

appropriate. On the other hand, thermal conductivity of fixed bed reactor wall was assumed to be very large.

2.4 Calculation

The solution of Eqs.(7.1)-(7.12) was solved using the conventional method on a using personal computer [1)6)]. Reaction rate which is determined by experimental was used. Parameters using this simulation are shown in **Table 7.2**.

Table 7.1 Physical properties

	Tube wall reactor	Fixed bed reactor
Diffusion coefficient of feed gas, D [m²/h]	0.731	0.183
Heat capacity of feed gas, Cp [J/(kg•K)]	$2.13 \cdot 10^3$	$2.13 \cdot 10^3$
Thermal conductivity ke [W/(m•K)]	0.03 (Gas phase)	0.115
Film coefficient of heat transfer, hw [W/(m²·K)]	30 ~130	130
Reaction enthalpy H [kJ/mol]	206	206

Table 7.2 Reaction conditions

Temperature of inlet gas, [K]	473
Temperature of heat medium, [K]	473
Feed gas flow rate, G [kg/(m•s)]	$8.83 \cdot 10^{-3}$
Diameter of reactor, [mm]	Tube wall reactor, 2 ~10 / Fixed bed reactor, 25
Conversion of inlet gas [-]	0
Conversion of outlet gas [-]	0.3
Average catalyst particle size, [mmϕ]	3 (Fixed bed reactor)
Thickness of catalyst layer, [μm]	30 ~300 (Tube wall reactor)

3 RESULTS AND DISCUSSION

3.1 Reaction kinetics

Eq.(7.13) shows reaction equation of cyclohexane dehydrogenation.

$$C_6H_{12} + 206\ kJ/mole \Leftrightarrow C_6H_6 + 3H_2 \quad (7.13)$$

Many kinetics have been reported concerning this reaction, using the Langmuir-Hinshelwood model:

1) Cyclohexane adsorption to the catalyst is controlling step under 10 kPa of cyclohexane pressure using Ni catalyst [3)9)].
2) Desorption of generated benzene is controlling step over 10 kPa [4)].

In this study, reaction pressure is less than 10 kPa, the same as 1) and adsorption controlling model was assumed, and the reaction rate is shown in Eq.(7.14).

$$r = k_W \cdot \frac{P_C - P_B \cdot P_H^3 \cdot K_P^{-1}}{1 + K_C \cdot P_B \cdot P_H^3 \cdot K_P^{-1} + K_B \cdot P_B + K_H \cdot P_H} \quad (7.14)$$

In this condition, since partial pressure of every element is low and equilibrium conversion is 0.3 shown in Eq.(7.15), a simpler kinetic expression is given as Eq.(7.16).

$$1 >> K_C \cdot P_B \cdot P_H^3 \cdot K_P^{-1},\ K_B \cdot P_B,\ K_H \cdot P_H \quad (7.15)$$

$$r = k_W \cdot (P_C - P_B \cdot P_H^3 K_P^{-1}) \quad (7.16)$$

Initial reaction rate is given as follows:

$$r_0 = k_W \cdot P_C \quad (7.17)$$

Then, reaction rate constant is,

$$k_W = r_0 / P_c \quad (7.18)$$

3.2 Experimental results and kinetic model

Figure 7.3 shows initial reaction rate changes with partial pressure of cyclohexane. The initial reaction rate increased linearly with the pressure of cyclohexane. The experimental results matched the kinetic model well .

Figure 7.4 shows r_0/P_c changes with P_C. Reaction rate constant was measured by arrhenius. The activation energy of this reaction is 91.5 kJ/mol (**Figure 7.5**). This value is almost the same as that in a previous paper [9)].

Equation of cyclohexane dehydrogenation could be written as follows.

$$r = k_W \cdot (P_C - P_B \cdot P_H{}^3 K_P{}^{-1}) \quad (7.19)$$

$$k_W = 3.46 \cdot 10^{11} \cdot exp(-11000/T) \quad (7.20)$$

$$K_P = exp(-26400/T + 47.6) \quad (7.21)$$

3.3 Calculated results of tube wall reactor and fixed bed reactor

Figure 7.6 shows calculated results of temperature and conversion distribution with catalyst length in tube wall reactor. Reactor diameter is 10 mm and velocity of cyclohexane is 0.04 m/s. Temperature drop on the

surface of catalytic wall is about 0.15 K. This shows tube wall reactor has high thermal conductivity. Radial temperature and conversion distribution is almost zero.

Figure 7.7 shows calculated results of temperature and conversion distribution with reactor tube length in fixed bed reactor. Reactor diameter is 25 mm and cyclohexane gas velocity is 0.04 m/s.

Maximum temperature drop is 40 K and it appears at some distance below the inlet. Conversion difference between wall and center is large.

In the center, cyclohexane dehydrogenation is stopped by low temperature. Conversion change in this part is caused by diffusion of generated benzene and hydrogen from the wall. Thus, it is clear that heat transfer from wall to center is the controlling step in the fixed bed reactor.

The length of tube wall reactor showing conversion 0.3 is 2 m and this is 10 times longer than that of the fixed bed reactor. But the catalyst volume of tube wall reactor showing conversion 0.3 is 1/4 of that of fixed bed reactor. Therefore, tube wall reactor tends to be larger but the catalyst volume is small and the catalyst is used effectively for reaction.

3.4 Effect of tube diameter on conversion

The catalyst tube diameter was changed from 10 mm to 2 mm. Conversion and temperature changes with tube catalyst length was shown in **figure 7.8**.

By reducing the reactor tube size, number of catalyst tubes is 25 times larger and the catalyst volume per unit volume is 5 times larger than the previous tube 10 mm in diameter. The reactor volume could be decreased to 1/5 of the previous tube wall reactor.

3.5 Effect of thickness of catalyst layer on conversion

It has been reported that the catalytic reactivity increased with thickness of alumina layer. Effect of the thickness on the conversion is shown in **figure 7.9**. The thickness was assumed to be 300 μm. Catalyst tube diameter was 10 μm.

Catalyst tube length showing conversion of 0.3 is 0.2 m which was the same as that of fixed bed reactor. Inside surface temperature decreases about 1 K by dehydrogenation reaction and heat transfer to the catalyst is not controlling in spite of the fixed bed reactor. By increasing the reactivity per unit area, catalyst length could be shortened and reactor volume decreases.

3.6 Effect of inlet gas temperature on conversion

Usually, reaction gas is preheated and supplied to reactor. Effect of omission of this preheat on conversion is calculated, and these results are shown in **figures 7.10, 7.11**. Inlet gas temperature was supposed to be 373 K.

In the fixed bed reactor, the conversion of outlet gas decreased by omission of preheat. This is because thermal conductivity inside the reactor is low and heat for reaction could not be supplied.

On the other hand, in the tube wall reactor, the thermal conductivity is high and heat for reaction is supplied from reactor wall, and the reaction can proceed. The gas temperature increases to the wall temperature at some distance from the inlet but surface temperature is almost the same as in the case of preheating. This is because heat capacity of gas is smaller than reaction heat. Therefore, preheater of reaction gas can be omitted for tube wall reactor. This gives cost down for construction and flexibility for process design.

3.7 Evaluation of Simulation results

Propriety of the simulator of tube wall reactor was investigated. Tube wall reactor with Pt/Al_2O_3 catalyst layer on inside surface was prepared by the same method as previously reported in chapter 3. The catalyst thickness was about 300 μm. Catalyst length using this examination was 2-12.5 cm.

Conversion changes with catalyst length are shown in figure **7.12**. The calculated conversion changes with thickness match the experimental results well. Therefore, this simulation is a reasonable model.

CONCLUSIONS

In this chapter, reaction kinetics of cyclohexane dehydrogenation are studied. Using the results, simulation of tube wall reactor was investigated and compared with fixed bed reactor. The following are examined.

1) Kinetics of cyclohexane dehydrogenation were studied. Cyclohexane adsorption to the catalyst site is controlling step under 10 kPa of cyclohexane pressure. Equation of cyclohexane dehydrogenation was determined.

2) Conversion and temperature distributions in tube wall reactor and fixed bed reactor were studied. This simulation model matched experimental results well.

3) In the fix bed reactor, temperature difference between center and wall of reactor is large and heat transfer from the wall to the center is the controlling step.

4) In the tube wall reactor, thermal conductivity is large and reaction is the controlling step. The catalyst volume is small but the reactor volume is larger than a fixed bed reactor.

5) Volume of tube wall reactor reduces by increasing high catalyst volume per unit. Small catalyst tube diameter, decreased from 10 mm to 2 mm, or increase of catalyst thickness from 30 μm to 300 μm, reduce reactor volume.

6) There is no need for feed preheater for tube wall reactor. This gives cost down and flexibility for process design.

Nomenclature

Cp	: heat capacity of feed gas	[J•kg-1•K-1]
D	: diffusion coefficient of feed gas	[m2•h-1]
d	: thickness of the $Pt/Al_2O_3/Al$ catalyst	[m]
G	: feed gas flow rate	[kg•m-2•s-1]
H	: reaction enthalpy	[J•mol-1]
hw	: film coefficient of heat transfer	[W•m-2•K-1]
K	: adsorption equilibrium constant	[atm-1]
K_P	: equilibrium constant in equation (13)	[atm3]
kc	: thermal conductivity of the $Pt/Al_2O_3/Al$ catalyst	[W•m-1•K-1]
ke	: thermal conductivity in the reactor	[W•m-1•K-1]
k_F	: reaction rate constant of the catalyst in the fixed-bed reactor	[mol•h-1•m-3•atm-1]
k_W	: reaction rate constant of the Pt/Al2O3/Al catalyst	[mol•h-1•m-2•atm-1]
M	: average molecular weight of the reactant	[kg•mol-1]
P	: partial pressure	[atm]
R	: radial coordinate of the reactor	[m]
r_F	: reaction rate of the catalyst in the fixed-bed reactor	[mol•h-1•m-3],[mol•s-1•m-3]
r_W	: reaction rate of the Pt/Al2O3/Al catalyst	[mol•h-1•m-2],[mol•s-1•m-2]
T	: temperature	[K]
u	: reactant gas velocity	[m•h-1]
X	: conversion	[-]
Y	: mole fraction	[-]
z	: axial coordinate of reactor	[m]
ε	: porosity	[-]

<Subscripts>

B : benzene

C : cyclohexane

H : hydrogen

iw : inside surface of the wall

w : outside surface of the wall

0 : initial

References

1) Hashimoto,K.:"*Han-nou Kogaku*",p.209,Baifukan (1979)

2) Hashioka,T.,S.Kosedo,M.Itoh,K.Yamamoto,H.Kameyama and T.Kabe: Chem.Lett.,1987,1067(1987)

3) Ishikawa,K.,H.Nagamoto and H.Inoue:Preprnts of the 15th Autumn Meeting of The Soc.of Chem. Engrs, Japan,Kanazawa,p.261(1981)

4) Itoh,N.,H.Tanabe,Y.Shindoh and T.Hakuta :*Sekiyu Gakkaishi*,28,323(1985)

5) Kagaku Kogaku Kyoukai,(ed): "*Kagaku Kogaku Binran*" ,5th. ed., Maruzen,Tokyo(1988)

6) Kagaku Kogaku Kyoukai(ed):"BASIC *niyoru Kagakukogaku* programing",p.172,Baifukan(1985)

7) Murata,K.,K.Yamamoto and H.kameyama:*Kagaku kogaku Ronbunshu*, 19,1,41(1993)

8) Sato,K.:"*Bussei teisu suisanho*",Maruzen(1954)

9) Toyoda,K. and E.Echigoya:*Kagaku Kogaku Ronbunshu*,32,1005(1968)

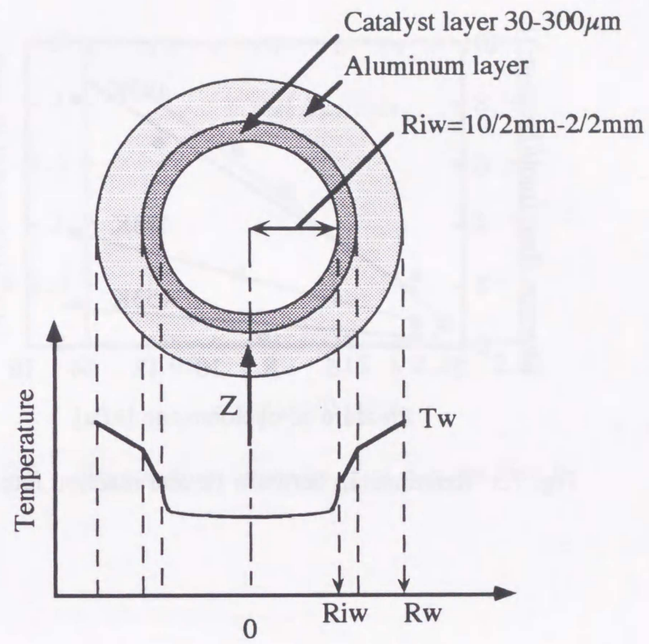

Fig. 7.1 The model of tube wall reactor for thermal transfer

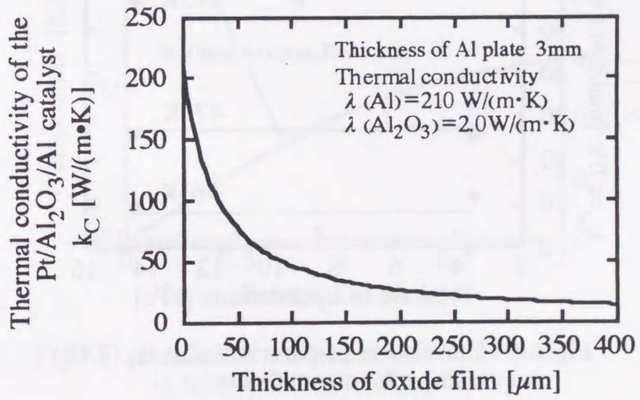

Fig. 7.2 Thermal conductivity of plate type catalyst

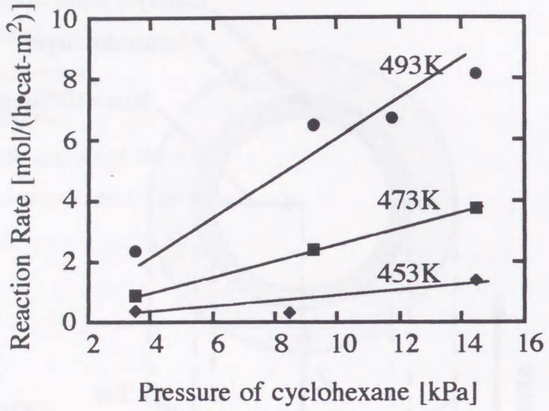

Fig. 7.3 Relationship between Pc and reaction rate

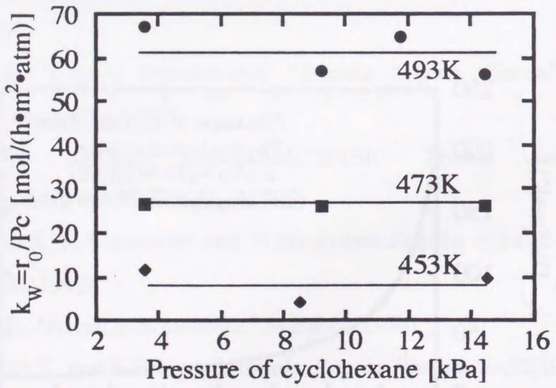

Fig.7.4 Correlation of parameters in Eq.(7.18) using experimental data

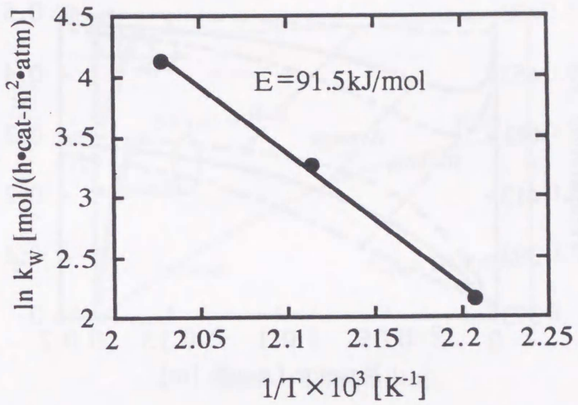

Fig.7.5 Temperature dependency of rate constant k

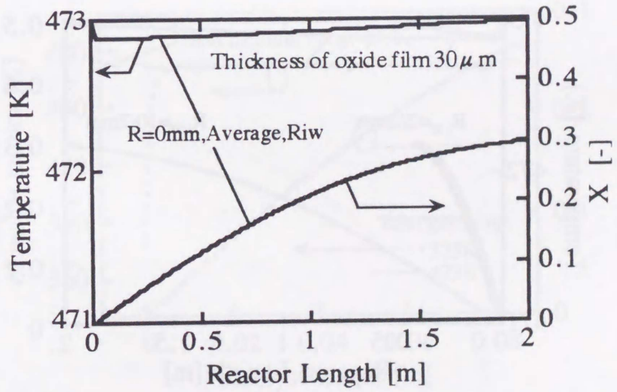

Fig.7.6 Profiles of conversion and temperature in tube wall reactor (R_{iW}=10/2mm)

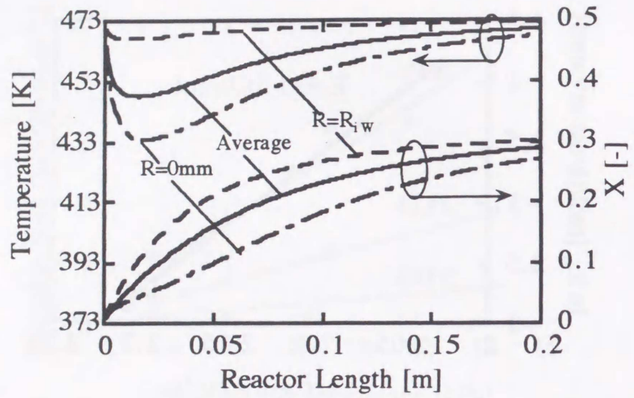

Fig.7.7 Profiles of conversion and temperature in fixed bed reactor (Rw=25mm/2)

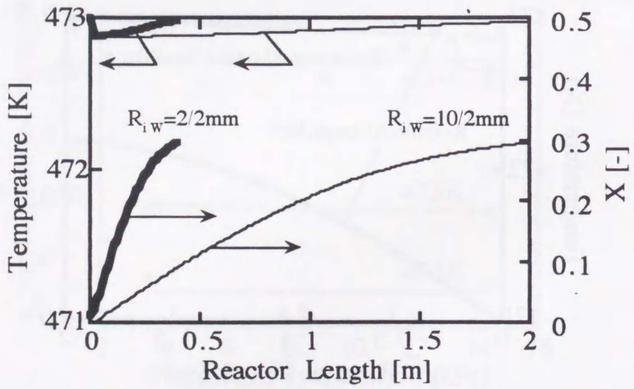

Fig.7.8 Effect of diameter of the tube wall reactor (2 mm and 10 mm) on plofiles of conversion and temperature

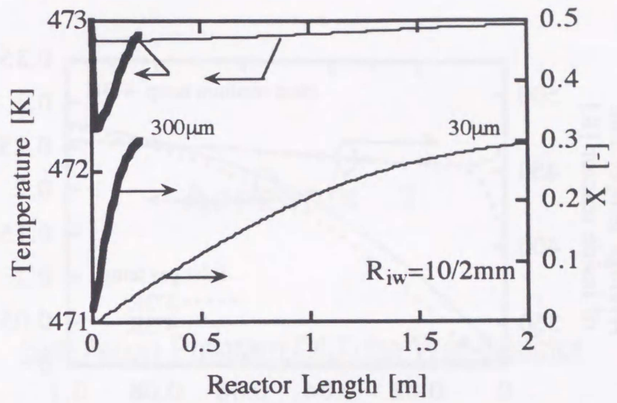

Fig.7.9 Effect of thickness of catalyst layer on profiles of conversion and temperature

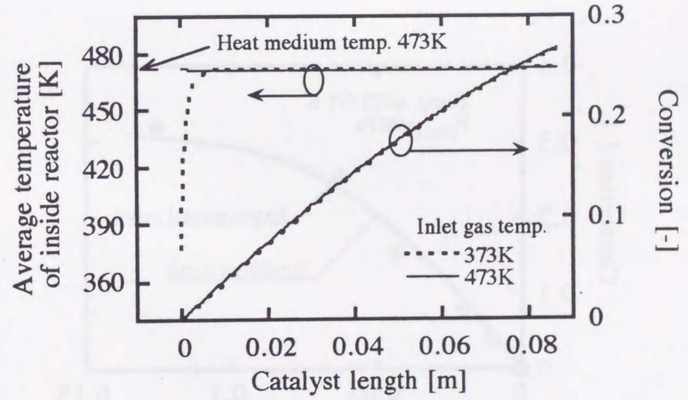

Fig. 7.10 Plofiles of conversion and temperature in tube wall reactor, inlet gas temperature=373K

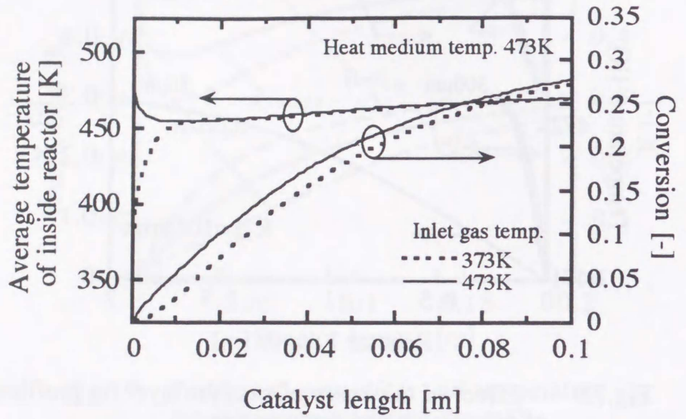

Fig. 7.11 Plofiles of conversion and temperature in fixed bed reactor, inlet gas temperature=373K

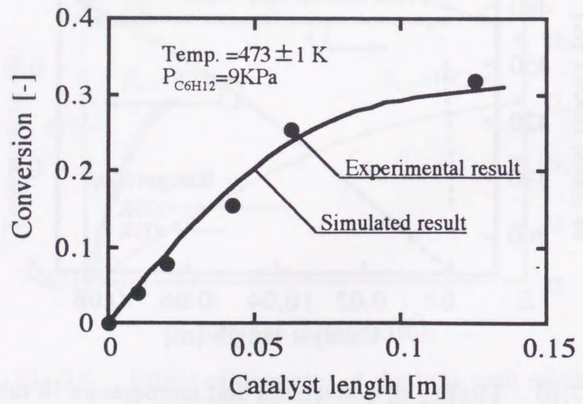

Fig.7.12 Comparison of calculated results with experimental results

APPENDIX 1

Simulation Program Of Tube Wall Reactor

Temperature and conversion distributions in radius of tube wall reactors were calculated by this program. This simulation program was written by N88BASIC.

PROGRAM LIST

```
5   'file name "SIMQ" 92/6/24  ,GE=50,300μ=G*10,LMAX=2m,RW=1mm(半径
    )"624R2T.PRN
10  '      プレート型触媒反応器の設計
20  '      陽解法による２次元的解法
21  '
30  DEFINT I,J,M,N
35   M=10            'M:半径方向の分割数10
40  DIM T0(M),T1(M),F0(M),F1(M),R0(M),R1(M),S(M)'
46  RW=1/1000iii) : LMAX=2iii)
52  Q$="624R2T"'Q$ : ファイルネーム
57  Q$=Q$+".PRN" :OPEN Q$ FOR OUTPUT AS #1
       'データを書き込むファイルをオープンする
70  '  データの入力部分
151  DE=0.73    : GE=50iii)   'DE : ガス有効拡散係数[cm/s]
152  G=.00882*GE : AMAV=.084  : Y0=1    : TW=200iii) : TINI=200iii)  : FINI=0
153       CPM=2130! : DHR=206000! : KE=.03  :  HW=130 'ke,HW
154  FMO=.25    :  PT=1iii)  : TH=10iii) :  EPSI=.05              ': KC=40700!
155   KC=1/(300ii)e-6/2+3e-3/210)*3e-3/3e-3
160  '  パラメータ
165  U=(G*1000/84)*(.0224*(473/298)*(1+TH))*100 '線速度[cm/s]
170  ALP=(-DHR)/G/CPM  : BET=AMAV/G/Y0
180  KAPA=(KE)/G/CPM/RW    : DELT=DE/(U*(RW*100))  :
     TMO=FMO/DELT*KAPA
182  PRINT "FMO ";FMO;" , TMO";TMO
183  PRINT "KC ";KC,"  U=";U
185  IF TMO>.5 THEN TMO=.25 : FMO=TMO*DELT/KAPA
190  AM=M : DY=1/AM      : DX#=DY*DY*TMO/KAPA
200  DL#=RW*DX#/2 : N#=LMAX/DL# : HK=HW*(KC/(KC+HW))*RW/KE
                              'HK:総括伝熱
201  NPRINT#=N#/200 :PRINT "NPRINT# ";NPRINT#
202  NPRINT=INT(NPRINT#)
205  PRINT   "DELT=";DELT;":DX   =";DX#;":DL=";DL#;":FMO=";FMO;":      TMO=";
     TMO
206  PRINT
210  ' 入り口温度と反応率の分布
220  FOR I=0 TO M-1 : T0(I)=TINI : NEXT I
230  FOR I=0 TO M   : F0(I)=FINI : NEXT I
240  T0(M)=(T0(M-1)+HK*DY*TW)/(1+HK*DY)
250  '  パラメータとデータの表示
260  A$="  ##.####^^^^" : C$=A$+"  T:"+A$+A$+A$+A$
270  B$="                F:"+A$+A$+A$+A$
280  D$="##.####^^^^"
290  PRINT " ****DATA****"
300  PRINT USING"  M =###   N =####";M;N#
```



```
410  PRINT"AX.INC    AX.LENGTH        Y=0.0        Y=0.5"                  +"
     Y=1.0      AVE.":PRINT
420  IS=M/2
430  '  反応器入り口の条件
440  FOR I=0 TO M :S(I)=T0(I) : NEXT I
450  GOSUB 1000 : TMIN0=SAV
460  L=0 : J=0
470  PRINT USING"#####"+C$;J;L;T0(0);T0(IS);T0(M);TMIN0;
480  FOR I=0 TO M : S(I)=F0(I) : NEXT I
490  GOSUB 1000 : FMIN0=SAV
500  PRINT USING B$;F0(0);F0(IS);F0(M);FMIN0 :PRINT
505  PRINT #1,L,T0(0),T0(M),TMIN0,F0(0),F0(M),FMIN0
510  FOR I=0 TO M
520    T=T0(I)+273.15 : F=F0(I)
530    GOSUB 1500 : R0(I)=RATE
540  NEXT I
550  '  計算開始
560  ALPDX=ALP*DX# : BETDX=BET*DX#
570  HKDY=HK*DY   : HKDYTW=HKDY*TW
575  N!=INT(N#)
580  WHILE L<LMAX
585    J=J+1
590    L=L+DL#
600    FOR I=0 TO M
610        RASM=R0(I)
620        RAV=.5*(R0(I)+RASM)
630        IF I=0 THEN 640 ELSE 670
640        T1(0)=T0(0)+4*TMO*(T0(1)-T0(0))      '中心部
650        F1(0)=F0(0)+4*FMO*(F0(1)-F0(0))       '
660        GOTO 770
670        IF I<>M THEN 680 ELSE 710
680            T1(I)=T0(I)+TMO*((1+.5/I)*T0(I+1)-2*T0(I)+(1-.5/I)*T0(I-1))   '
               中間部
690        F1(I)=F0(I)+FMO*((1+.5/I)*F0(I+1)-2*F0(I)+(1-.5/I)*F0(I-1))
700        GOTO 770
710        T1(M)=(T1(M-1)+HKDYTW)/(1+HKDY)+ALPDX*RAV
720        F1(M)=F0(M)+2*FMO*(F0(M-1)-F0(M))+BETDX*RAV
730        T=T1(I)+273.15 : F=F1(I)
740        GOSUB 1500 : R1(I)=RATE
750        IF ABS((R1(I)-RASM)/RASM)<=EPSI THEN 770
760        RASM=R1(I) : GOTO 620
770    NEXT I
780  '  結果の表示
790    IF J <> NPRINT  THEN 860
800    FOR I=0 TO M : S(I)=T1(I) : NEXT I
810    GOSUB 1000 : TM1=SAV
820    FOR I=0 TO M : S(I)=F1(I) : NEXT I
830    GOSUB 1000 : FM1=SAV
840    PRINT USING"#####"+C$;J;L;T1(0);T1(IS);T1(M);TM1;
850    PRINT USING B$;F1(0);F1(IS);F1(M);FM1 : PRINT
855        GOSUB 2000
857    J=0
860  '  次のステップの準備
870    FOR I=0 TO M
880        T0(I)=T1(I) : F0(I)=F1(I) : R0(I)=R1(I)
890    NEXT I
```

```
910 WEND
915 CLOSE #1
920 END
1000 '
1001 '  シンプソン法による断面平均値の計算
1010 MM=M/2-1 : SUM=0
1020 FOR JJ=1 TO MM
1030   X2=(2*JJ-1)*DY : Y2=X2*S(2*JJ-1)
1040   X3=X2+DY : Y3=X3*S(2*JJ)
1050   SUM=SUM+4*Y2+2*Y3
1060   NEXT JJ
1070 SAV=2*DY/3*(SUM+4*S(M-1)*(M-1)*DY+S(M)*M*DY)
1080 RETURN
1490 '
1500 '  反応速度の計算
1605 K=3.46E+11*EXP(-11000/T)
1610 KP=EXP(-26490/T+47.6)
1630 A=PT/(1+TH+3*F) : PB=F*A : PC=(1-F)*A : PH=(3*F)*A ':PT=PB+PC+
     PH
1640 RATE=K*(PC-PB*PH^3/KP)/3600*10i     '[mol/(h·m2)]
1650 RETURN
1990 '
2000 '  データの保存
2010 PRINT #1,L,T1(0),T1(M),TM1,F1(0),F1(M),FM1
2020 RETURN
```

PARAMETERS

Following parameters were used in this thesis.

(1) Reaction rate constant

Reaction rate constant of catalyst layer with 30 μm in thick was used as standard. In this program, the reactivity was assumed to be 10 times larger than the standard reactivity.

(2) Thickness of catalyst layer

Standard thickness of catalyst layer was 30 μm. Thermal conductivity of catalyst decreased with thickness of catalyst layer. In this program, the thickness was assumed to be 300 μm.

(3) Another parameters

Following parameters were changed to calculate performance of tube wall reactor. Reactor length (LMAX), Temperature of heat medium of out side of tube wall reactor (TW), Inlet gas temperature (TINI), Mass flow of reactant (GE), Total pressure (PT), Dilution rate (TH).

Chapter

8

DESIGN AND PERFORMANCE OF TUBE WALL REACTORS

INTRODUCTION

Chemical heat pump (CHP) processes utilize endothermic chemical reactions and their exothermic reactions to upgrade industrial waste heat or solar energy by raising temperature [1]. The processes enable energy to be used with high efficiency, to control working temperatures easily and to store and transport energy in the form of stable chemical substances without energy loss. Therefore, an early realization of CHP systems for a practical application is expected in various fields of industry and in wide areas of energy usage. Recently the CHP system, using the reaction couple of cyclohexane dehydrogenation at 473 K, under 0.1 MPa, and benzene hydrogenation at 623 K, 2.0 MPa (**Figure 1.3**) driven by compression work has been proposed [2]. The system is an interesting way to back up the UT-3 cycle for heat and hydrogen storage [3]. Furthermore, this CHP can be tied up in the world energy network (WE-NET) system, which has been proposed for the international transport of thermal energy in the form of hydrogen [4].

In this chemical heat pump, it is important that the mutual transformation between thermal energy and chemical energy is easily done. Therefore a tube wall type reactor (TWR), which has layered catalyst on the inside surface of the metal tube body has been proposed as a heat exchanger in order to have a high heat conduction rate [5][6][7]. The reactor wall can be made of $Pt/Al_2O_3/Al$ plate type catalyst which has high thermal conductivity.

The $Pt/Al_2O_3/Al$ plate type catalyst is prepared by anodic oxidation of a commercial aluminum plate to produce alumina film as a catalyst support, following by hot water treatment in chloroplatinic acid solution to increase BET surface area of the alumina film and simultaneously to impregnate platinum as a catalyst species [6][8]. The conditions for preparing a catalyst film of any thickness under 300 μm was established [7].

In the TWR, the endothermic or the exothermic reaction takes place on

the reactor wall. Simultaneously, also the heat of the reaction is recovered or supplied through the same reactor wall. The present study deals with the performance of a TWR which transforms thermal energy into chemical energy efficiently by endothermic reaction of cyclohexane dehydrogenation. The chemical reaction is expressed in equation(8.1).

$$C_6H_{12}+206\ kJ/mole \Leftrightarrow C_6H_6 + 3H_2 \qquad (8.1)$$

The following parameters have been studied in the present investigation:

(1) Calculation of the TWR and comparison with the performance of a classical FBR by simulation

(2) Development of catalysts in shape of tube wall, fin-tube and fin-plate

1 DESCRIPTION

1.1 Temperature and conversion distribution in the reactors

In this paper, conversion means convert ratio of cyclohexane into benzene and hydrogen. To estimate the performance of a TWR and to compare it with the performance of a FBR, conversion and temperature distributions in the reactor tube are calculated in a simulative study. Radial and longitudinal distributions of temperature and conversion in both types of reactor are calculated by using the rate equation for cyclohexane dehydrogenation determined from experiments **9)10)**. The outside wall of both reactors is assumed to be in contact with pressurized liquid water of 473 K (**Figure 8.1**). The reactor volumes are compared at the conversion of 0.3 (90 % of the equilibrium conversion). The pressure drop in the TWR is calculated by FANNING's equation and in the case of the FBR the ERGUN's equation is used. Physical properties and reaction conditions are listed in **table 8.1**.

Table 8.1 Physical properties and reaction conditions

	TWR	FBR
Diffusion coefficient of feed D [m^2/h]	0.731	0.183
Heat capacity of gas C_p [$J/(Kg \times K)$]	2.13×10^3	2.13×10^3
Thermal conductivity k_e [$W/(m \times K)$]	0.03	0.115
Film coefficient of heat transfer hw[$W/(m^2 \times K)$]	30-130	130
Reaction enthalpy ΔH [KJ/mol]	206	206
Temperature of inlet gas [K]	473	
Temperature of heat medium [K]	473	
Feed rate G [$kg/(m^2 \times s)$]	44.2×10^{-3}	
Diameter of reactor [mm]	10 (TWR), 25 (FBR)	
Conversion of inlet [-]	0	
Conversion of outlet gas [-]	0.3	
Catalyst particle [mm ϕ]	3(FBR)	
Catalyst layer [μm]	270(TWR)	

1.2 Variation of the heat input capacity with reactor scale

The heat input capacity of the endothermic reactor was calculated as a function of the size of the reactor. **Figure 8.2** shows a unit of the model reactor used for the simulation. In the case of the TWR, the catalyst layer is formed on the inside walls of the double-pipe heat exchanger tubes (10 mm in diameter, Radius of reactor tube, R_W=10/2). The thickness of the catalyst layer is 270 μm. In the FBR the reactor tube is filled up with the catalyst. The diameter of the reactor tube and of the Pt/Al_2O_3 catalyst particles are 25 mm (R_W=25/2) and 3 mm, respectively. The arrangement of the reactor tubes within the reactor unit and the tube pitch are also shown in **figure 8.3**. One basic reactor unit is 0.6 m in width, 1.2 m in height and 3 m in length.

The heat input capacity of one unit is 42 kW. The complete endothermic model reactor contains several of these units in order to obtain the heat input capacity required.

2 RESULTS AND DISCUSSION

2.1 Pressure drop for the reactor

The pressure drop for both reactor types is shown in **figure 8.4**. In the FBR, the pressure drop is about 100 times larger than that in the TWR, since the reactor tubes are filled up with the catalyst particles. Therefore, the pressure drop in the FBR should be a serious problem when the reactor scales up.

2.2 Variation of the reactor size

In order to realize the CHP system in an industrial size it is necessary to scale up the endothermic reactor. In this context the heat input capacity of both reactor types is compared at a different reactor size.

(1) Variation of the reactor volume at different heat input capacities

The variation of the reactor volume with the heat input capacity are shown in **figure 8.5**. While the reactor volume in the TWR is always proportional to the capacity, the increment of the reactor volume in the FBR increases with the capacity. When the input capacity is more than 42 kW, the TWR becomes smaller than the FBR at the same capacity. The reason for this behavior is the pressure drop which increases in the FBR rapidly with the reactor volume. This pressure drop restrains the chemical equilibrium and thus diminishes the conversion. Therefore, in a large system the TWR is much more favorable than the FBR.

(2) Variation of the heat input capacity with catalytic reactivity

A large heat input capacity per reactor volume (heat input capacity ratio) reduces the size of the endothermic reactor. The variation of the heat input capacity with the reactivity is shown in **figure 8.6**. The heat input capacity ratio of the TWR is proportional to the reactivity, and the compact reactor could be designed by increasing the reactivity. On the other hand, the increment of the capacity of the FBR remains small in spite of an improved reactivity. This can be explained by the reason that the heat conduction from the wall to the center of the reactor tube is the rate controlling step in cyclohexane dehydrogenation.

2.3 Applications of wall type reactor with heat exchanger function

The fin-tube catalyst whose fin surface has been modified into Pt catalyst by anodization and hot water treatment is shown in **figure 8.7**. Originally the fin tube has been designed for the use in a commercial heat exchanger, whose inner diameter and the length are 25 mm and 100 mm respectively. The spirally attached fin plate was 11 mm in width and 2 mm in pitch. The total apparent surface area of the fin was 0.5 m^2. When the surface is modified by the catalyst, it becomes the most reactive at this point. A tube of this size is expected to be an endothermic reactor of about 720 W for cyclohexane dehydrogenation. **Figure 8.8** shows a conceptional model of the fin-tube reactor. Equipped with the catalyst shown in figure 8, the reactor serves simultaneously as a heat exchanger.

An attempt has been made to design and fabricate a corrugated aluminum plate to increase surface area is shown in **figure 8.9**, whose surface has been modified into Pt catalyst as the former fin-tube surface. The plate is expected to be a part of a many layered plate-fin reactor of any size. Furthermore, when some kinds of separator films are installed together as a unit, it is possible to design a reactor with a function as shown in **figure 8.10**.

CONCLUSIONS

The following conclusions are drawn from the present investigation:

1) The performance of up-scaled reactors was calculated. For heat input capacities over 42 kW the volume of the TWR is smaller than the volume of the FBR.

2) Thermal conductivity must be improved in the FBR to make the endothermic reactor more compact. On the other hand, a compact reactor can be designed by use of a highly reactive catalyst in the TWR. For this reactor type the heat input capacity is proportional to the reactivity.

3) The catalyst layers have been formed on the surfaces of fin-tube and fin-plate type heat exchangers. The fin-tube reactor was expected to be an endothermic reactor of 720 W for cyclohexane dehydrogenation.

NOMENCLATURE

R_W = Radius of reactor tube [m]

References

1) S. Fujii, H. Kameyama, K. Yoshida and D. Kunii : Journal of Chemical Engineering Japan, 10, 3, pp.224-228, 1977
2) H. Kameyama, M. Yamashita, K. Yamamoto and T. Kabe: Proc.: World Congress III of Chemical Engineering, Tokyo, pp.649-652 (1986)
3) H. Kameyama: Proc. Science and Technology for Energy Conversion, pp.261-264 (1990)
4) K. Fukuda: *Sun Shine Journal*, 14, 1, pp.8-10(1993)
5) T. Hashioka, S. Kosedo, M. Itoh, K. Yamamoto, H. Kameyama and T. Kabe :Chemistry Letters, pp.1067-1070(1987)
6) *Ronbunshu*, Vol.19, No.1, pp.41-47 (1993).
7) K. Murata, K. Yamamoto and H. Kameyama : *Hyoumen Gijutu*, in press
8) H. Kameyama, M. Inoue, R. Yamanaka, K. Murata and K. Yamamoto, Chemical Engineering, Vol.36, No.2, pp.42-47(1991).
9) K. Murata, K. Yamamoto and H. Kameyama, *Kagaku Kogaku Ronbunshu*, Vol.19, No.5, pp.849-855 (1993)
10) K. Yamaseki, K. Yamamoto and H. Kameyama, *Kagaku Kougaku Ronbunshu*, Vol.17, pp.267-272 (1991).

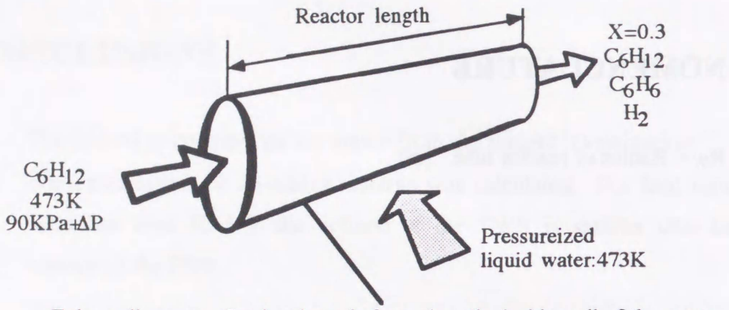

Tube wall reactor: Catalyst layer is formed on the inside wall of the reactor
Fixed bed reactor: Catalyst particles filled up the reactor

Fig. 8.1 Illustration of the reactor tube

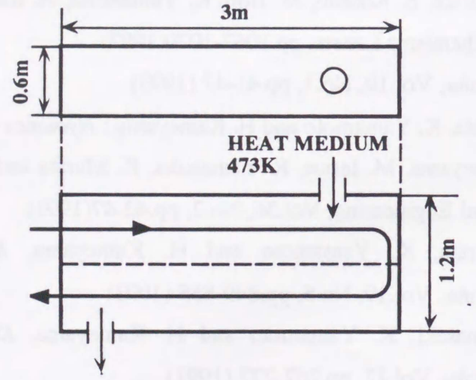

Fig. 8.2 Diagram of reactor unit with heat exchanger function

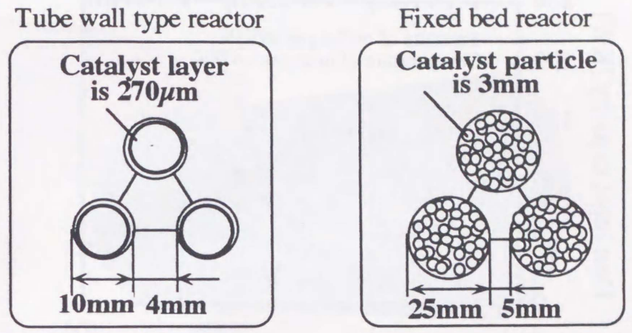

Fig. 8.3 Tube layout and tube pitch in the reactor unit

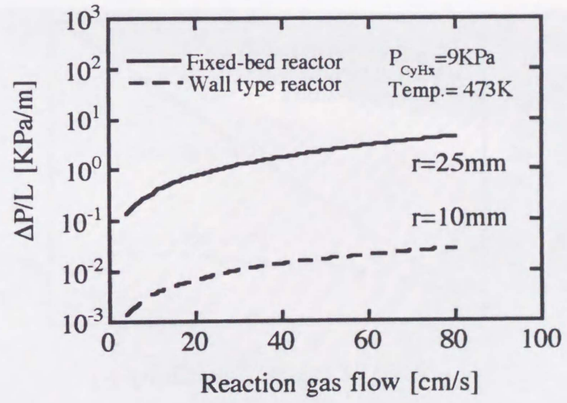

Fig. 8.4 Pressure drop in the tube wall reactor and fixed bed reactor

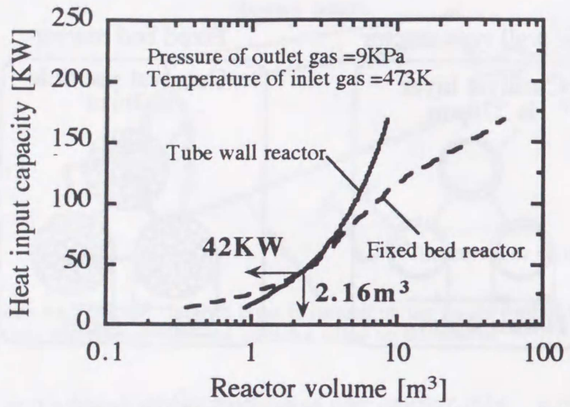

Fig. 8.5 Variation of the reactor volume with the heat input capacity

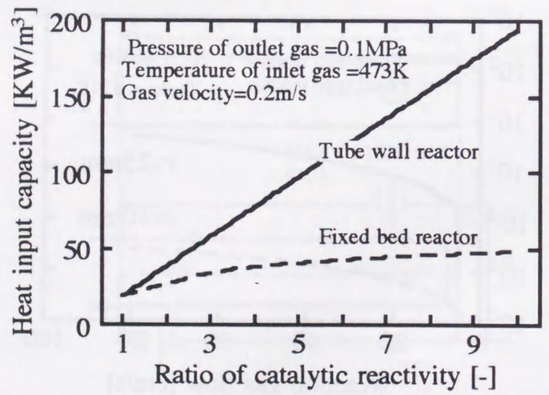

Fig. 8.6 Variation of the reactor volume with the reactivity

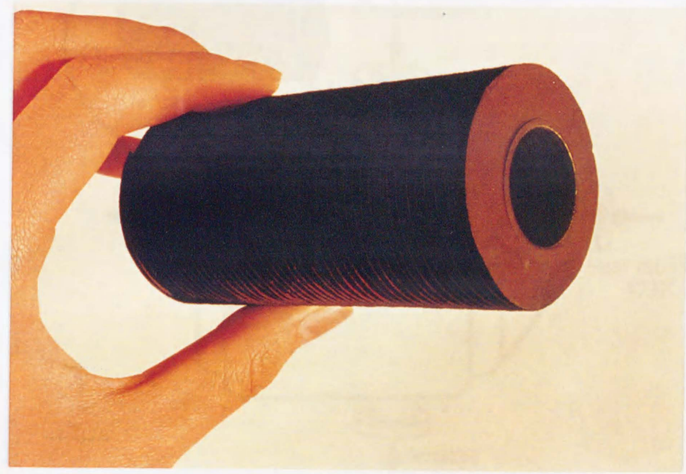

Fig. 8.7 A type of fin-tube catalyst whose fin surface has been modified into Pt catalyst

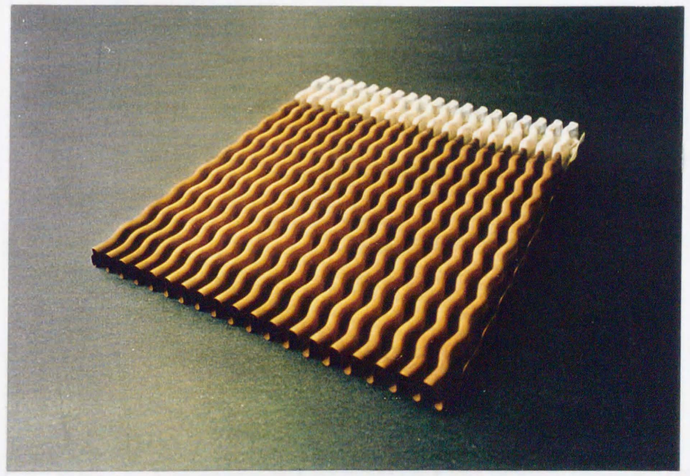

Fig. 8.9 A corrugated aluminum plate whose surface has been modified into Pt catalyst

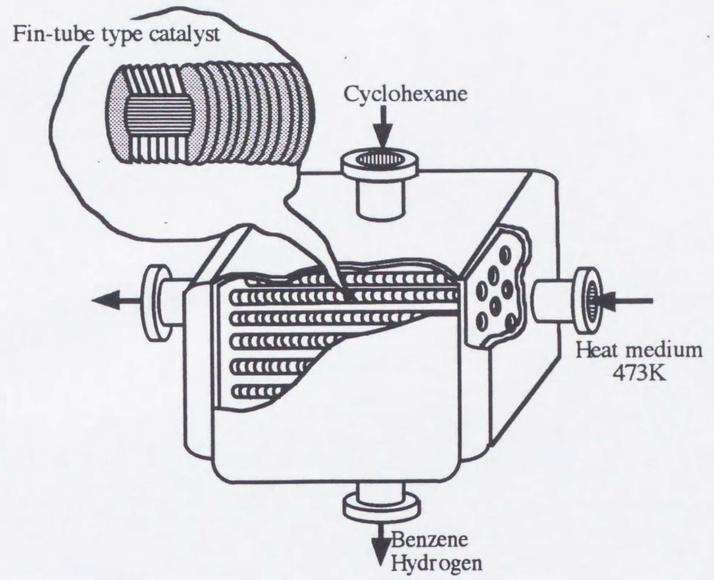

Fig. 8.8 A conceptional model of fin-tube reactor with heat exchanger function

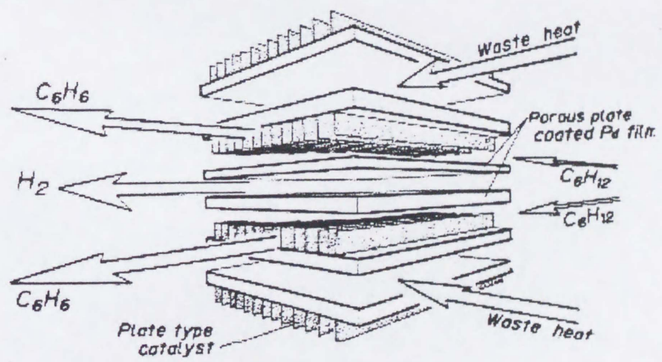

Fig. 8.10 A reactor with heat exchanger and product separator functions

Chapter

9

Performance Of Cyclohexane/Benzene/Hydrogen Chemical Heat Pump With Tube Wall Reactors

INTRODUCTION

A chemical heat pump with the reaction couple of cyclohexane dehydrogenation at 473 K and benzene hydrogenation at 623 K (cyclohexane/benzene/hydrogen chemical heat pump, CBH-CHP) has been proposed to pump up industrial waste heat and to back up the UT-3 thermochemical hydrogen process as a heat and hydrogen storage system 1)2). The chemical reaction is expressed in equation (9.1).

$$C_6H_{12} + 206\ kJ/mole \underset{623K,1.6MPa}{\overset{473K,0.1MPa}{\rightleftharpoons}} C_6H_6 + 3H_2 \qquad (9.1)$$

A high coefficient of performance (COP) of over 3.0 and also high thermal efficiency of more than 80 % are needed for the utilization of CBH-CHP 1).

In the CHP, thermal energy transfers into chemical energy through endothermic reaction at low temperature and the chemical energy turns into thermal energy at high temperature through exothermic reaction. Then, this system can store thermal energy or deplete thermal energy by controlling the endothermic or exothermic chemical reactions. The system performance (COP and thermal efficiency) under heat storage and heat pump operating modes have never been studied. In this chapter, following items were studied for CBH-CHP with 100 kW output of exothermic reactor by using a process simulator, ASPEN plus.

1) Estimate the effects of the use of tube wall reactor for the CBH-CHP
2) Propose the new process flow which shows constant COP and thermal efficiency under heat storage and heat pump operating modes
3) Calculate the performance change in transient state between heat storage

and heat release operating modes

4) Fix the operating parameters to control the CBH-CHP system.

1 METHOD OF SIMULATION

1.1 Process simulator, ASPEN plus

ASPEN PLUS (Ver.8.5-6, ASPEN TECH. JAPAN) was used to estimate process performances. Model manager employed a personal computer (IBM compatible, CPU 486DX2/66 MHz, RAM 16 MB, HD 580 MB).

1.2 Process flow of CBH-CHP

Output of exothermic reactor was 100 kW in this study. Classical CBH-CHP system used one flash after the endothermic reactor to reduce compression work. Hydrogen and organic substances are separated in this flash. In this case, one more flash after the exothermic reactor is installed to facilitate the endothermic reaction. The separated hydrogen is compressed and supplied to exothermic reactor. In heat storage operating mode, hydrogen is discharged from the hydrogen gas line to hydrogen tank to control the exothermic reactor, on the other hand, hydrogen is charged into the exothermic reactor to promote the exothermic reaction. The process flow is shown in **figure 9.1**.

This new process is composed of two reactors, two flashes, three heat exchangers, five pumps. Block #1 R1 is an endothermic reactor and R2 is exothermic reactor. In this process, pressure loss of both reactors is zero, using TWR. In order to reduce the work of compressor flashes F1 and F2 are installed. H1,H2, H3 and H4 are heat exchangers to recover latent heat. Streams ID (SID) 20-25 are hydrogen gas lines. SID24 goes to the hydrogen storage tank or UT-3 cycle , and SID25 comes from the hydrogen storage tank or UT-3 cycle.

1.3 Process performance

The heat ratio of the heat pump is defined as the ratio of the heat supplied (composed of the endothermic reaction heat) and the heat upgraded by the cycle (exothermic reaction heat at R2).

$$\Psi = \frac{\textit{Heat upgrated} \quad (\textit{Exothermic reaction heat})}{\textit{Heat supplied} \quad (\textit{Endothermic reaction heat})} \tag{9.2}$$

The COP (Coefficient of performance) is given by the ratio of the removed high temperature heat to the energy supplied to the compressors.

$$COP = \frac{\textit{Removed high temperature heat}}{\textit{The energy supplied to the compressor}} \tag{9.3}$$

COP : Coefficient of Performance

2 RESULTS AND DISCUSSION

2.1 Pressure drop and system performance

The conventional fixed-bed reactor has a large pressure drop. The effect of pressure drop of the reactors on COP and thermal efficiency are studied here.

Effects of pressure drop of exothermic reactor on system performances (COP and thermal efficiency) are shown in **figure 9.2.** COP decreased with pressure drop of the exothermic reactor. This is because exhaust pressure of the compressor increases with the pressure drop, and energy consumption increases with the pressure.

In this process the effect of the pressure drop of endothermic reactor on the performance were negligible, since inlet pressure of the endothermic

reactor, which is reaction pressure plus pressure drop, can be controlled by the pump, which is located after high pressure separation drum, from 2.0 MPa to 0.1 MPa. On the other hand, the size of the endothermic reactor tends to increase with pressure drop.

From the view point of system performance and reactor size, tube wall reactor which has low pressure loss is suited for the CBH-CHP system.

2.2 Reaction pressure of exothermic reactor

Figure 9.3 shows the effect of pressure of exothermic reaction on system performance. The temperature of exothermic reaction was 623 K. Conversion of endothermic reaction was assumed to be chemical equilibrium conversion. The result of the simulation was that the COP showed a peak at 1.4-1.6 MPa.

At low pressure, compression work of unit volume is small but total mole flow rate is large, because equilibrium conversion is low. Therefore, total compression work is large and the COP is small. At high pressure, total mole flow is small, since equilibrium conversion is high, but the compression work per unit volume is large. Then, total compression work increased and the COP decreased. Therefore, the optimum pressure of exothermic reactor was 1.6 MPa.

2.3 Reaction conditions of endothermic reactor

The effect of pressure of endothermic reactor on system performance is shown in **figure 9.4**. Conversion of output of endothermic reactor was assumed to achieve equilibrium. The COP increased slightly with the decrease of pressure of endothermic reactor. It was not desirable to keep the reactor pressure low, because the reactor volume increased linearly and the increment of COP was lower than 2.

If a membrane tube which separates generated hydrogen is installed in the endothermic reactor, cyclohexane dehydrogenation can progress irrespective of the equilibrium. **Figure 9.5** shows the relationships between

the conversion of cyclohexane dehydrogenation and system performance. The performance under equilibrium conditions is low, the COP is 0.9 and the thermal efficiency is 0.12. But, beyond the equilibrium, if the reaction progresses up to 40 mol%, COP increases to 4.3 and thermal efficiency also increases to 80 %. Therefore, an endothermic reactor with the hydrogen separation function (a membrane reactor) is necessary to realize this CBH-CHP process.

2.4 System performance under heat storage or heat release

Operation conditions of both reactors were determined by the calculation results above-mentioned. The conditions are as follows:

1) Pressure of endothermic reaction was 0.1 MPa
2) Dehydrogenation conversion was 40 mol%
3) Pressure of exothermic reaction was 1.6 MPa
4) Hydrogenation progresses to the equilibrium conversion.

The state of heat storage If hydrogen is purged out from the process by SID24, benzene hydrogenation in the exothermic reactor is controlled, then concentration of benzene in the process increases. In this condition, endothermic reaction heat at 473 K produces chemical substances such as benzene and hydrogen.

The state of heat release On the other hand, if hydrogen is introduced into the process by **SID25**, benzene hydrogenation in the exothermic reactor progresses at 623 K, then benzene concentration is decreased.

Therefore, benzene concentration is an important factor to know whether the process is in a state of heat storage or in a state of heat release. **Figure 9.6** shows system performance changes with concentration of benzene at the inlet gas of endothermic reactor. COP and thermal efficiency are almost constant in spite of benzene concentration. This is because unreacted hydrogen is separated after the exothermic reactor and cyclohexane dehydrogenation can take place in a high benzene concentration. Therefore,

the system performance is high, both in the state of heat storage and heat release.

2.5 Process dynamics of CBH-CHP cycle

Dynamic change of CBH-CHP between the state of heat storage and the state of heat release were calculated.

1) Heat release operating mode

Figure 9.7 shows the transient state of heat release operating mode by introducing hydrogen into the process via SID25. Initial concentration of benzene at SID1 is 60 mol% and initial mole flow of benzene is 0.5 mol/s. Effects of hydrogen mole flow on concentration of benzene, heat input capacity of endothermic reactor and heat output capacity of exothermic reactor are shown in this figure. Benzene hydrogenation regresses due to an excess of hydrogen, and the following are shown:

1) Heat output capacity shows the highest point at 230 kW and there is a rapid fall to 100 kW
2) Benzene concentration falls right down from 60 mol% to the lowest point of 10 mol% after 1 time constant.
3) Heat input capacity increases slightly.

After 4 time constants, this CHP shows that dynamic steady state under benzene concentration is 10 mol % and hydrogen mole flow is 3 mol/s.

2) Heat storage operating mode

Figure 9.8 shows the transient state of heat storage operating mode by releasing hydrogen via SID24. Initial concentration of benzene at **SID1** and initial mole flow of hydrogen at **SID20** are 10 mol% and 3.5 mol/s, respectively. Effects of hydrogen mole flow on concentration of benzene, heat input capacity of endothermic reactor at 473 K and heat output capacity at 623 K are shown in this figure. Benzene hydrogenation is controlled by the shortage of hydrogen, and the following are shown:

1) Heat output capacity shows the lowest point at 60 kW. After that it increases rapidly and is steady at 100 kW after 12 time constants.
2) There is an immediate sharp increase of benzene concentration. The rise brings the benzene concentration to 60 mol% after 12 time constant.
3) Heat input capacity decreases slightly.

After 12 time constants, this CHP shows dynamic steady state under benzene concentration is 60 mol% and hydrogen mole flow is 0.5 mol/s. This time constant is 12 times longer than that of heat release operating mode, because hydrogen is separated after exothermic reactor and some hydrogen is consumed for benzene hydrogenation. It is possible to shorten the time constant by separating hydrogen at hydrogen separator of endothermic reactor.

2.6 Operating parameters for heat storage and heat release

It is shown that the flow rate of hydrogen can control the state of heat storage or heat release as I have been describing. Under dynamic steady state, effects of total mass flow and hydrogen mole flow on the heat output capacity and benzene concentration were calculated in **figure 9.9**. Total mass flow is controlled by the pump and the compressor which are located after the endothermic reactor. The hydrogen mole flow is controlled by the compressor which is placed after the exothermic reactor. It is possible to keep the heat output constant by controlling the hydrogen mass flow when the concentration of benzene at SID1 is between 2 mol% and 10 mol%. When the concentration of benzene is between 20 mol% and 90 mol%, it is possible to keep the heat output constant by controlling the total mole flow. In practical use, the concentration of benzene is considered between 10 mol% and 80 mol%, and controlling of total mass flow is required.

CONCLUSIONS

In this paper, the system performance of new flow of CBH-CHP was studied and the following items were established.

1) System performance (COP and thermal efficiency) decreased with the pressure drop of reactors. Tube wall reactor whose pressure drop is negligible is needed for the chemical heat pump.

2) A new flow sheet for the CBH-CHP process was proposed. This new process installed two flashes to separate hydrogen. The system storages waste heat at 473 K as benzene and hydrogen. The system releases heat at 623 K by benzene hydrogenation. This process shows constant high performance under both heat storage and a heat release operating modes.

3) Dynamic change between the heat storage operating mode and the heat release operating rate was studied. It is shown that the flow rate of hydrogen can control the state of heat storage or heat release.

4) Operating parameters for heat storage and heat release mode were studied. Under dynamic steady state, effects of total mass flow and hydrogen mole flow on the heat output capacity and benzene concentration were calculated. When the concentration of benzene is between 20 mol% and 90 mol%, it is possible to keep the heat output constant by controlling the total mole flow. In practical use, the concentration of benzene is considered between 10 mol% and 80 mol% and controlling of total mass flow is recommended.

REFERENCES

1) Kameyama, H.: Proc. World Congress III of Chemical Engineering, Tokyo, p.649, 1986

2) Cacciola, G., Y. I. Aristov, G. Restuccia and V. N. Parmon: Hydrogen Energy, 18, 8, p.673(1993)

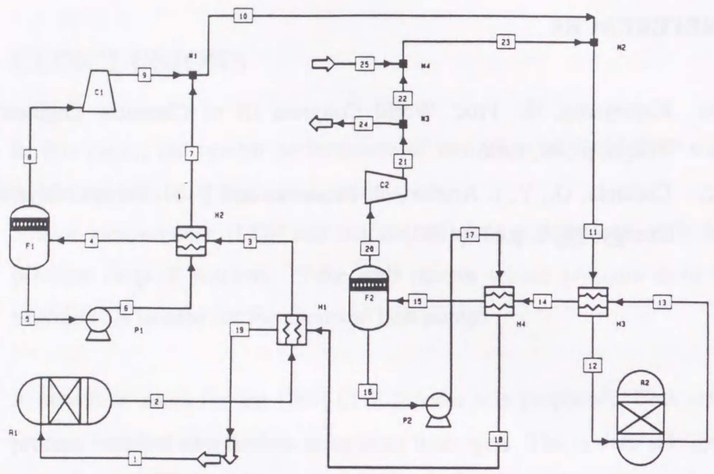

Fig.9.1 A new flow sheet for the CBH-CHP process

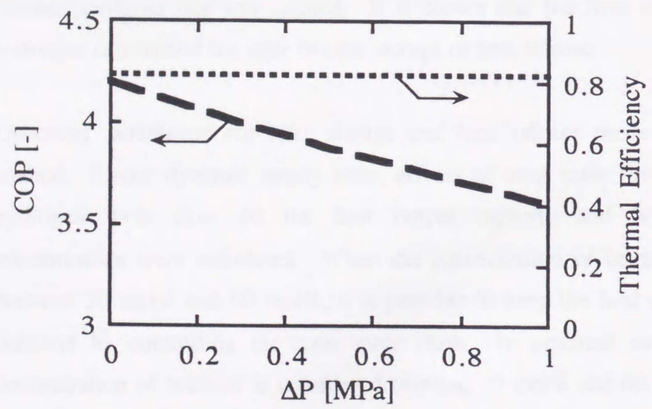

Fig. 9.2 Relationship between pressure drop in the exothermic reactor and system performance thermal efficiency and COP

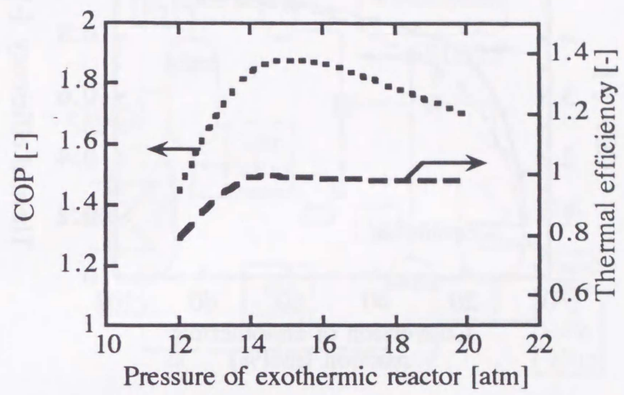

Fig. 9.3 System performance change with pressure of exothermic reactor

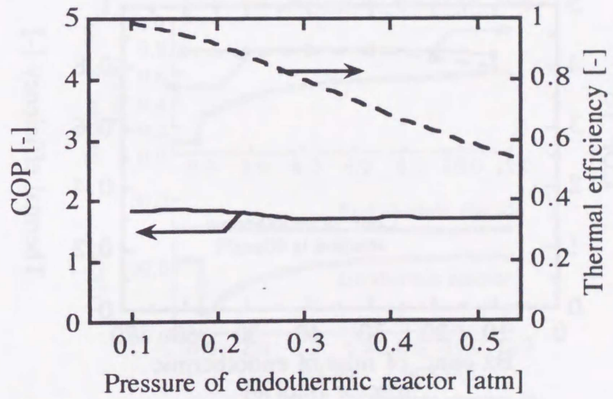

Fig. 9.4 System performance change with pressure of endothermic reactor

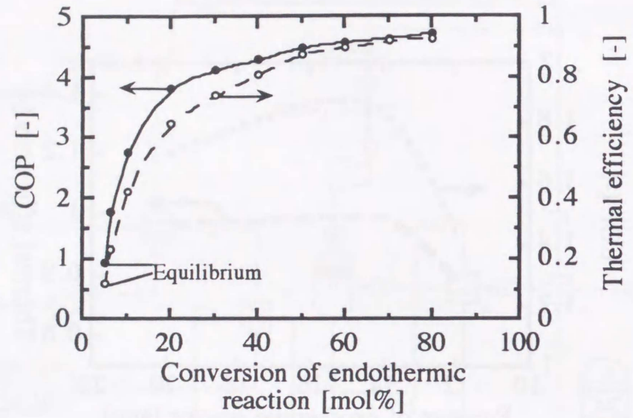

Fig. 9.5 Relationships between endothermic reaction conversion and thermal efficiency, COP

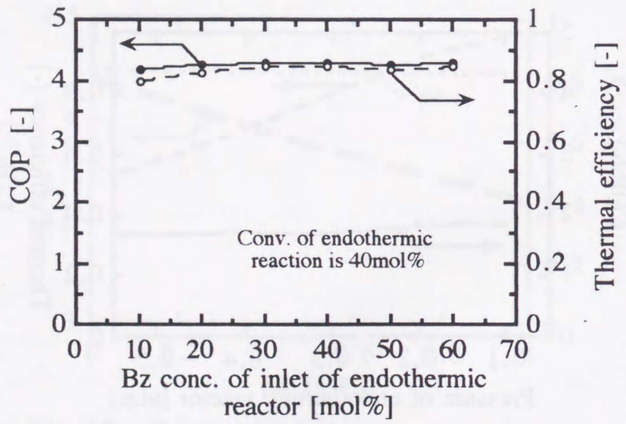

Fig. 9.6 Relationships between benzene concentration and thermal efficiency, COP

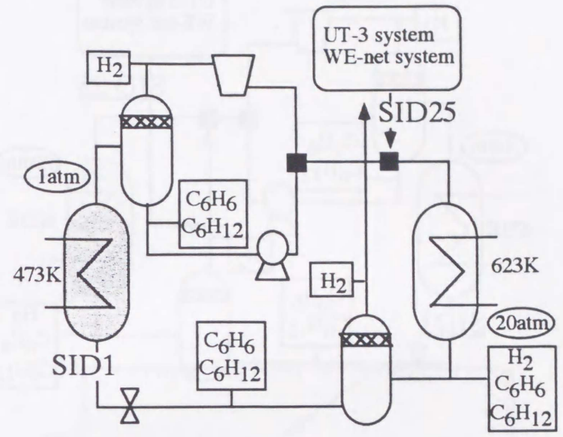

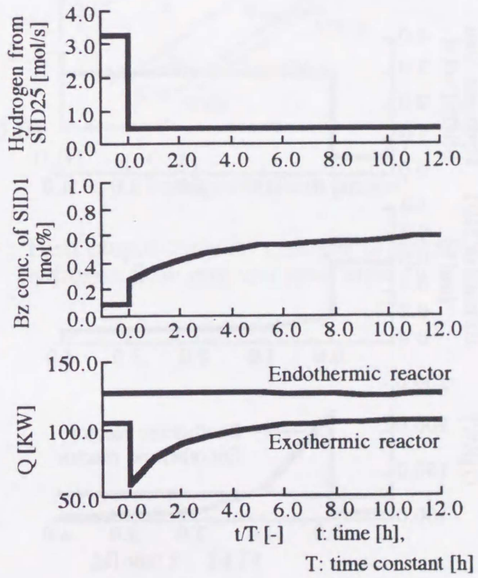

Fig. 9.7 Changes in Q, benzene conc. and ΔH_2 with time in the transient state of heat storage mode

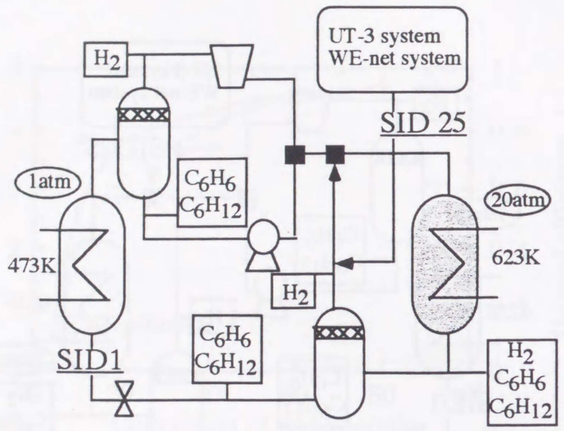

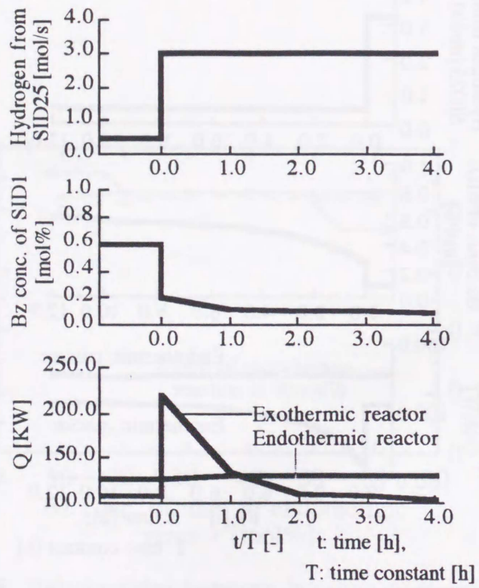

Fig. 9.8 Changes in Q, benzene conc. and ΔH_2 with time in the transient state of heat pump mode

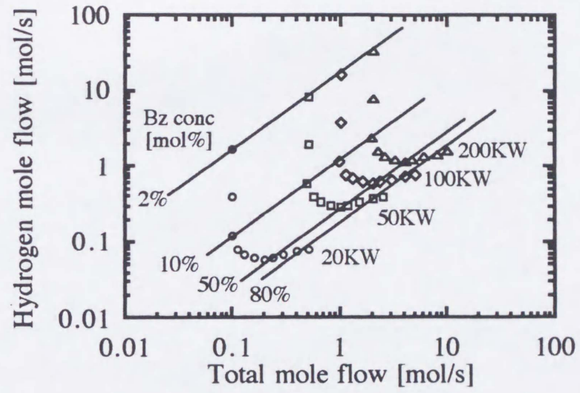

Fig. 9.9 Heat output capacity changes of benzene conc. with hydrogen flow rate and total mass flow rate

Chapter

10

Conclusions

1. CONCLUSIONS

Main purpose of this doctor thesis is preparation of plate type catalyst and design of tube wall type reactor for practical use of the CBH-CHP. Preparation of plate type catalyst, design of tube wall reactor and advanced process flow of CBH CHP system were studied. Followings have been studied in advance of practical usage of these technique.

PART 1 REPARATION OF THE PLATE TYPE CATALYST

Preparation method, effectiveness factor and durability of plate type catalyst were studied in **Chapters 2-5**.

Chapter 2 The Preparation Method Of The Plate Type Catalyst Using Chromic Acid

A thin-layered catalyst supported on a metal plate is one of the ideal types of catalysts, making it possible to design a compact reactor. A reactor equipped with this type of catalyst can serve as a heat exchanger since the catalyst is expected to exhibit high thermal conductivity and low pressure loss. A $Pt/Al_2O_3/Al$ plate type catalyst was prepared by anodic oxidation (AO) of a commercial aluminum plate, followed by hot-water treatment (HWT) in chloroplatinic acid solution. Alumina layer as catalyst support is produced by AO and the BET surface area of the alumina is increased, and simultaneously Pt as a catalyst species is impregnated by HWT. The conditions for preparing a catalyst film of any thickness under 30 μm were established. The amount of Pt supported per BET surface area of alumina was 170-180 $\mu g/m^2$, which corresponds to 3 wt% of alumina, and the dispersion of Pt was around 0.5, regardless of the thickness of the alumina film. Catalyst with 30 μm of alumina film showed a constant reaction rate per apparent surface area of 3.5 $mol/(h \cdot m^2)$ for cyclohexane

dehydrogenation at C_6H_{12}/N_2=1/10, 1 atm and 473 K for 130 hours.

Chapter 3 Preparation Method Of The Plate Type Catalyst Using Oxalic Acid

The purpose of this chapter is to explain preparation of a plate type catalyst with high catalytic reactivity for utilization. The preparation method of the plate type catalyst was examined by using oxalic acid solution for anodic oxidation (AO). In AO process, an alumina layer with more than 350 μm in thickness was formed. Porosity of the alumina layer was increased to 0.79 by pore widening or a long period of anodic oxidation. Impregnated platinum within the anodized alumina layer increased with the porosity. The maximum content of platinum per apparent surface area was 15.8 g-Pt/m^2 and this was 5 times larger than the previous catalyst. Platinum dispersion of each catalyst was about 0.5. Reactivity of cyclohexane dehydrogenation increased with catalyst content. The highest reactivity after 20 h was about 12 mol/(h·m^2) and this was 3 times as high as the previously reported catalyst. It was clear that the reactivity achieved the target reactivity.

Chapter 4 Effectiveness Factor Of The Plate Type Catalyst

The effectiveness factor of the $Pt/Al_2O_3/Al$ plate type catalysts were studied theoretically and experimentally. The investigated Pt/Al_2O_3 catalyst layer, which was prepared by anodic oxidation and followed hot water treatment, had a porous structure and a narrow pore size distribution. Porosity of the catalyst was about 0.5 and the mean of the pore radius was about 2 nm. Reaction rate of the cyclohexane dehydrogenation increased with thickness of Pt/Al_2O_3 catalyst layer but it raised to a peak because diffusion of reactant into the catalyst layer was the controlling step and the effectiveness factor decreased with the thickness. The reaction rate is governed by the effective diffusion coefficient and the reaction rate constant. The reaction rate constant can be improved by augmentation of the Pt content and Pt dispersion. The reaction rate constant will be also improved by a

large effective diffusion coefficient due to a large pore radius.

Chapter 5 Deactivation And Durability Of The Plate Type Catalyst

The cyclohexane/Benzene/Hydrogen chemical heat pump system has been proposed to store and upgrade waste heat. In this system, it is required that catalysts have high heat transfer performance, high selectivity and long lifetime in the endothermic and the exothermic reactor. In this chapter, the catalyst deactivation mechanism of $Pt/Al_2O_3/Al$ plate type catalysts in the endothermic reaction is studied. The main cause of catalyst deactivation was fouling by carbonaceous deposits. Sintering, migration and loss of active species were not observed. The reactivity of a refreshed catalyst was as high as for fresh catalysts. The proposed model of catalyst deactivation matched the experimental results well. In the model, the carbonaceous deposits narrow the micro pores, and the mass transfer of the reactants into the catalyst pores becomes rate controlling. Then, the reaction rate goes down with the reaction time. In the long-life test of a tube type catalyst, the catalyst showed a steady reactivity during the reaction time from 50 h to 200 h, but deactivation gradually proceeded to reach the value of 40% reduction of steady reactivity after the reaction time of 1000 h.

PART 2 DESIGN OF THE WALL TYPE REACTOR

Mass transfer in the tube wall reactor, simulation of tube wall reactor and performance of the tube wall reactor were studied in **Chapters 6-8**.

Chapter 6 Mass Transfer In Tube Wall Reactor Developing Laminar Flow

Radial mass transfer is experimentally studied while developing laminar flow in a tube wall reactor. Total reaction rate of tube wall catalyst is

decided by radial mass transfer in boundary layer and catalytic reaction rate. The radial mass transfer was controlling the total reaction rate at low space velocity under 3000 h^{-1}. To cancel the mass transfer's control, it is important to decrease the thickness of boundary layer. Static mixers were inserted in the tube wall catalyst. The results of this showed that the static mixers accelerate mass transfer and reaction rate is controlling step at low space velocity.

Chapter 7 Simulation Of Tube Wall Reactors

Feasibility study of tube wall reactor was undertaken using simulation. In a tube wall reactor, endothermic or exothermic reaction takes place with the reaction heat recovered or supplied simultaneously through the reactor wall. The reactor wall is expected to be made of $Pt/Al_2O_3/Al$ plate type catalyst with high thermal conductivity.

Reaction mechanism of dehydrogenation of cyclohexane was discovered. This reaction rate was controlled by adsorption rate of cyclohexane molecules to catalyst sites. Using the equation of this reaction rate, conversion and temperature distributions in tube wall reactor and in fixed bed reactor were calculated. Temperature and conversion distributions in the tube wall reactor are narrower than in the fixed bed reactor. The wall type reactor is preferable for use in chemical heat pumps.

It was showed that a compact tube wall reactor was able to be designed by reducing the diameter of the reactor tube and by increasing catalyst thickness.

In some cases, there is no need for a feed preheater for tube wall reactor. This affords cost down and flexibility for process design.

Chapter 8 Design and Performance of Tube Wall Reactors

The cyclohexane/benzene/hydrogen chemical heat pump (CHP) cycle is a hopeful way to back up the UT-3 system or the WE-NET system for heat and hydrogen storage. To realize the CHP system, a tube wall type reactor

(TWR) has been proposed to transform thermal energy into chemical energy efficiently. The catalyst volume in the TWR was 6 times smaller, and the pressure drop was 100 times smaller, than those of a classical fixed bed reactor (FBR). For reactor performance over 42 kW the TWR also became smaller than the FBR. It will be possible to design a high performance TWR by improving the reactivity. The catalyst layers have been formed on the surfaces of fin-tube and fin-plate type heat exchangers.

PART 3 CHEMICAL HEAT PUMP SYSTEM WITH TUBE WALL REACTOR

Performance of cyclohexane/benzene/hydrogen chemical heat pump system including heat storage/release operating mode were studied. Operating parameters were also studied in **Chapter 9**.

Chapter 9 Performance Of Cyclohexane/Benzene/Hydrogen Chemical Heat Pump With Tube Wall Reactors

The new process flow of the cyclohexane/benzene/hydrogen chemical heat pump (CBH-CHP) system has been proposed. Tube wall reactor is suited for the CBH-CHP, since coefficient of performance of the CBH-CHP is diminished by pressure drop of the reactors. In the new process, conversion of cyclohexane dehydrogenation in the endothermic reactor is an important factor in the performance. When the conversion goes up to 40 mol%, the thermal efficiency is 80 % and the coefficient of performance (COP) is 4.3. In the state of heat storage by dehydrogenation of cyclohexane at 473 K, concentration of benzene in the liquid line is high, on the other hand, concentration is low under heat release at 623 K. The COP and the thermal efficiency are stable under heat storage and heat release operating mode. Heat storage and heat release mode were controlled by supply and elimination of hydrogen from the system. The output of the CBH-CHP can be kept stable by controlling total mass flow.

2. LIST OF TECHNICAL PAPERS RELATED TO THIS THESIS

CHAPTER 2

(1) Murata, K., K. Yamamoto and H. Kameyama: Study of Method of Preparing a Plate-Type Catalyst by Anodic Oxidation and Hot-Water Treatment, *Kagaku Kogaku Ronbunshu*, 19, 1, pp.41-47(1993)

CHAPTER 3

(2) Murata, K. and H. Kameyama: Application of the Anodized Alumina Plate to the Wall Type Catalyst, *Hyoumen Gijutsu*, 47, 2, pp.173-177 (1996)

CHAPTER 4

(3) Murata, K. and H. Kameyama: Effectiveness Factor of $Pt/Al_2O_3/Al$ Plate Type Catalyst, submitted to *Hyoumen Gijutsu*

CHAPTER 5

(4) Murata, K. and H. Kameyama: Deactivation and Durability of the $Pt/Al_2O_3/Al$ Plate type catalyst for the Chemical Heat Pump, under preparation

CHAPTER 7

(5) Murata, K. and H. Kameyama: A Study of a Tube-Wall Reactor with Heat Exchanger Function, *Kagaku Kogaku Ronbunshu* , 19, 5, pp.849-855 (1993)

CHAPTER 8

(6) Murata, K., K. Yamamoto and H. Kameyama: Performance of a Tube Wall Type Reactor for Transforming Heat Energy Into Chemical

Energy Efficiently, Int. J. Hydrogen, 21, 3, pp.201-205 (1996)

ANOTHER PAPERS RELATED

(7) Terai, S., K. Murata, K. Yamamoto and H. Kameyama; *Kagaku Kogaku Ronbunshu*, 21, 6, pp.1069-1074 (1995)

3. REVIEWS

(1) H. Kameyama, M. Inoue, R. Yamanaka and K. Murata, " *Pure-to jou shokubai zairyou no kaihatsu*": Chemical Engineering, 36, 2, pp.42-47 (1991)

(2) K. Murata and H. Kameyama; "The transformation of anodic oxide layer on aluminum into catalyst layer", *Alutopia*, 23, 10, pp.9-15 (1993)

(3) H. Kameyama, K. Murata, S. Terai and Y. Toyoshima, "Development of plate type catalyst with anodic oxidation film on aluminum", *Hyoumen Gijutu*, 46, 5, pp.37-40 (1995)

4. PATENTS

(1) 連続触媒体の製造方法、及びその方法によって得られた連続触媒体を用いた低濃度有機物の酸化方法： 出願番号 2-235271

5. PRESENTATIONS IN INTERNATIONAL CONFERENCES

(1) K. Murata, Y. Toyoshima, S. Terai, K. Yamamoto and H. Kameyama, "Experimental and Simulative study on Chemical Heat Pump with Reaction Couple of Cyclohexane Dehydrogenation and Benzene Hydrogenation for Effective Use of Industrial Waste Heat or Solar Energy", Int. Symposium on CO_2 fixation and Efficient Utilization of Energy, p.177 (1992)

(2) K. Murata, K. Yamamoto and H. Kameyama,"Performance of a Tube Wall Reactor Transforming Heat Energy into Chemical Energy Efficiently" , The 10th World Hydrogen Energy Conference, p.1537- (1994)

(3) K. Murata and H. Kameyama, "Performances of Chemical Heat Pump with Reaction Couple of Benzene Hydrogenation and Cyclohexane Dehydrogenation", International Hydrogen and Clean Energy Symposium '95, p.313- (1995)

(4) K. Murata, P. Gastauer and H. Kameyama "Combination of the Isopropanol/Acetone/Hydrogen cycle and the Cyclohexane/Benzene/ Hydrogen Chemical Heat Pump System: Proposal and Evaluation", International Symposium on Energy, Environment and Economics, (1995)

6. PRESENTATIONS IN INTERNAL CONFERENCES

1) Murata K. and H. Kameuyama :Preprints of the 23rd Autumn Meeting of The Soc. of Chem. Engrs. Japan, SO113 (1990)

2) Mutata K., M. Inoue and H.Kameyama: Preprints of the 56th Annual Meeting of The Soc. of Chem. Engrs. JAPAN, L311,(1991)

3) Murata K. and H. Kameuyama, and K. Yamamoto :Preprints of the 24th Autumn Meeting of The Soc. of Chem. Engrs. Japan, M304 (1991)

4) Ichimura S., K. Murata, K. Yamamoto, T. Kabe and H.Kameyama: Preprints of the 57th Annual Meeting of The Soc. of Chem. Engrs. JAPAN, O124, (1992)

5) Murata K., S. Terai, K. Yamamoto and H. Kameuyama :Preprints of the 25th Autumn Meeting of The Soc. of Chem. Engrs. Japan, C310 (1992)

6) Mutata K., S. Terai, K. Yamamoto and H.Kameyama: Preprints of the 58th Annual Meeting of The Soc. of Chem. Engrs. JAPAN, F114, (1993)

7) Murata K., K. Yamamoto and H. Kameuyama :Preprints of the 26th Autumn Meeting of The Soc. of Chem. Engrs. Japan, P103 (1993)

8) Mutata K., K. Yamamoto and H.Kameyama: Preprints of the 59th Annual Meeting of The Soc. of Chem. Engrs. JAPAN, A205, (1994)

9) Murata K., K. Yamamoto and H. Kameuyama :Preprints of the 27th

Autumn Meeting of The Soc. of Chem. Engrs. Japan, (1994)

10) Mutata K. and H.Kameyama: Preprints of the 60th Annual Meeting of The Soc. of Chem. Engrs. JAPAN, I120, (1995)

11) Mutata K. and H.Kameyama: Preprints of the 60th Annual Meeting of The Soc. of Chem. Engrs. JAPAN, B205, (1995)

APPENDIX 2

Review of studies on tube wall reactors and preparation of plate type catalysts

In this part, studies on tube wall reactor and preparation of plate type catalysts were reviewed.

1 Shapes of wall type reactors

Some shape of wall type reactors have been proposed and studied for a long time. Tube wall type catalyst is popular shape (**Fig. 1a**). Catalyst layer was formed on the outside wall or inside wall. Analysis of mass transfer in the reactor has been carried out using this type of catalyst [1,5-17,19,20,24-28,31-35,37-39,46-48,51,52,54,57,60]. In another cases, double tube wall type catalyst (**Fig. 1a**) [26,37,49] and duct type reactor (**Fig. 2a**) [2,39-42,45,53,55,56,61] were used to accelerate mass transfer. Inside surface of exhaust pipe of motorcycle (**Fig. 3a**) [36] and the surface of fin-tube, fin-plate (**Figs. 8.7, 8.9**) [2,41], plate [22,23,30] and another types [43,44] can be catalyzed. Then, kinds of reaction and reaction conditions is important to select a kind of tube wall reactor.

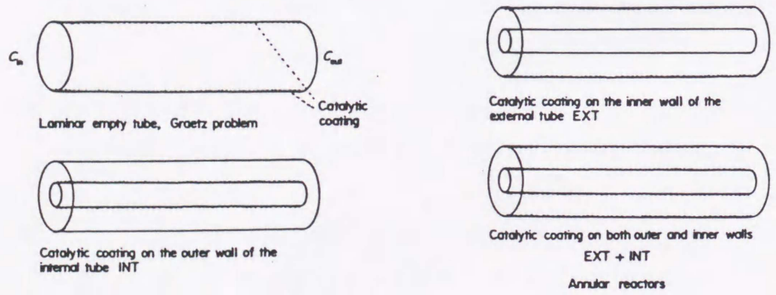

Figure 1a Illustration of tube and annular reactor

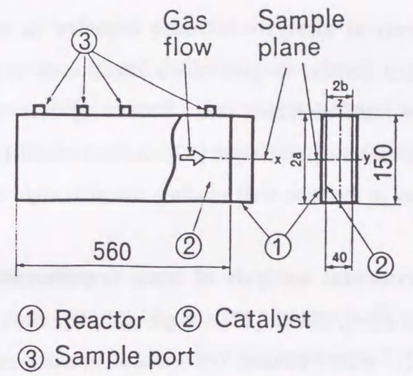

Figure 2a Illustration of duct type reactor

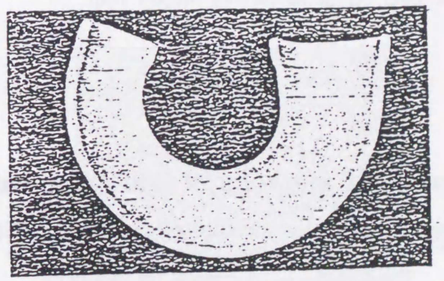

エキゾーストパイプの内面にコーティングした触媒

Figure 3a Photograph of spray catalyst which is formed on inside surface of exhaust pipe

2 Mass transfer in tube wall reactors

Studies on mass transfer in tube wall reactors were classified in three parts.

I Theoretical analysis of mass transfer in tube wall reactors

The first scholar to give much attention to mass transfer in tube wall reactor was Damköhler [12]. Baron [5], Kasaoka [34], Katz [35], Lupa [37] Johnstone [29] Siegel [50] and Satterfield [46] were studied on mass transfer in the tube wall reactors theoretically. (- 1960 s)

II Experimental analysis of mass transfer in tube wall reactors

Arashi [3,4], Field [17], Inoue [27,28], Shitaokoshi [47] and Smith [51,52] were studied of mass transfer in wall type reactors experimentally including theoretical analysis. (- 1980 s)

III Design of tube wall reactors

Anikeev [2], Fukuhara [18], Kameyama [31-33] and Murata [39-41] were studied design of tube wall reactor including theoretical and experimental analysis. They also studied on preparation method of catalyst layer on the surface of reactor wall.

3 Preparation methods of wall type catalysts

In this part, preparation methods of wall type catalysts were reviewed.

I Galvanizing of catalyst metal

This is popular method for preparation of wall type catalysts. Catalyst species such as Ni, V, Cu can be formed on surface of metal wall [1,2,17-20,27,28,34,44,51,53,54]. Catalyst species for this method were limited. Thickness of the catalyst layer is up to several micro meter. In

the case of Ni as catalyst species, BET surface area was 60 m^2/Ni-g. (**Figure 4a**) This method has critical defects of low surface, reactivity and omission of catalyst.

II Spray or coating of catalyst on reactor wall

Spray or coating method [3,4,21,36] has some merits. Any catalyst species can be used by this method. Any shapes of reactor tube can be used. But these methods have critical defects of low surface, reactivity and omission of catalyst (**Figure 5a**).

III Leaching of Raney alloy

Porous catalyst layer is prepared by leaching of raney alloy. Ag [8], Ni [55,56] can be prepared on the surface of the reactor wall. BET surface of prepared catalyst was about 60 m^2-BET/g-Ni. It is possible to prepare a catalyst with bimodal pore structure by optimizing the composition of alloy (**Figure 6a**). In this method, it is difficult to form catalyst layer on surface of several shapes of reactor wall and catalyst layer is detached from metal body easily.

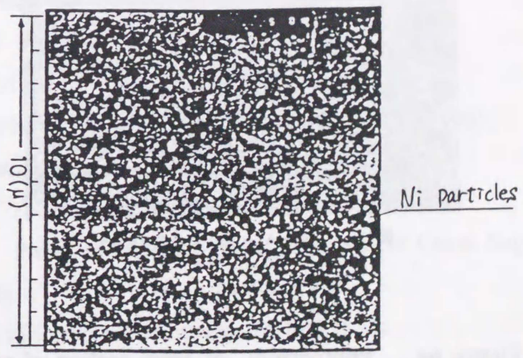

Figure 4a Photograph of prepared catalyst by galvanizing

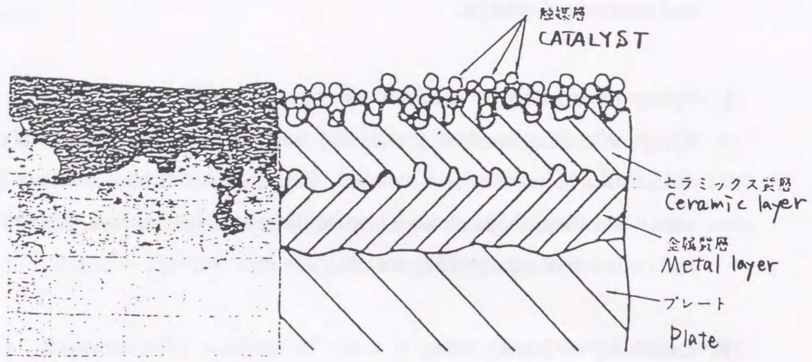

Figure 5a Cross section of coating catalysts

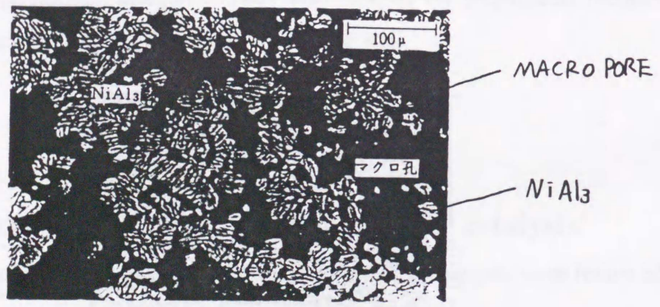

図 12－1 Ni－Al＝40：60 多孔質合金
700℃, 60 min 焼結
10％ NaOHaq 5 min エッチング
×260

Figure 6a Photograph of cross section of catalyst prepared by leaching of Raney alloy

References

1) ALWITT, R. S. : A. I. Ch. E. J., 10, 417(1964)
2) ANIKEEV, V. I. : Prepri. of NEW ENER. SYS. and CONV., 1993, 767(1993)
3) ARASHI, N. : Kagaku Kogaku Ronbunshu, 6, 5, 476(1980)
4) ARASHI, N. : Kagaku Kogaku Ronbunshu, 10, 3, 359(1984)
5) BARON, T. : 125, (1952)
6) BRAUER, H. : Chemie. Ing. Techn., 37, 1107(1965)
7) CACCIOLA, G. : Int. J. Hydrogen Energy, 18, 8, 673(1993)
8) CAMBRON, A. : Can. J. Chem, 34, 665(1956)
9) COLTON, C. K. : A. I. Ch. E. J., 17, 4, 773(1971)
10) COWHERD, C. J. : I&EC Fund., 4, 150(1965)
11) CRIDER, J. E. : A. I. Ch. E. J., 12, 3, 514(1966)
12) DAMKÖHLER : Z. Elektrochem, 42, 846(1936)
13) DRANOFF, J. S. : Maths. Comput., 15, 403(1962)
14) DROTT, D. W. : PH.D. Thesis, (1972)
15) EIGENBERGER, G. : Adv. Chem. Series, 133, 477(1974)
16) FERGUSON, N. B. : A. I. Ch. E. J., 20, 3, 539(1974)
17) FIELD, J. H. : I&EC Prod. Res. Dev., 3, 150(1964)
18) FUKUHARA, T. : Kagaku Kogaku Rinbunshu, 19, 1993)
19) FUNAKOSHI, M. : Kagaku Kogaku Ronbunshu, 5, 609(1979)
20) FUNAKOSHI, M. : Kagaku Kogaku Ronbunshu, 10, 4, 439(1984)
21) GROSS, B. : Plasma Technology, 1969)
22) HASHIOKA, T. : Chem. Lett., 1987, 1067(1987)
23) HAYASHI, H. : Prepri. of 26th Aut. Meet. of the Soc. of Chem. Engng, P107, 285(1993)
24) HORVATH, C. : Biotech. and Bioengng, 14, 885(1972)
25) HORVATH, C. : Chem. Engng Sci., 28, 375(1973)
26) HOUZELOT, J. L. : Chem. Engng Sci., 32, 1465(1977)

27) INOUE, H. : Kagaku Kogaku Ronbunshu, 5, 6, 609(1979)
28) INOUE, H. : Kagaku Kogaku Ronbunshu, 6, 1, 98(1980)
29) JOHNSTONE, H. F. : I & EC, 46, 4, 702(1954)
30) KAKINUMA, Y. : Prepri. of 59th Anu. Meet. of the Soc. of Chem. Engng, (1994)
31) KAMEYAMA, H. : Kagaku Kogaku, 49, 12, 928(1985)
32) KAMEYAMA, H. : Chem. Engng, 34, 4, 58(1989)
33) KAMEYAMA, H. : Chem. Engng, 36, 2, 42(1991)
34) KASAOKA, S. : Kagaku Kogaku Ronbunshu, 33, 6, 69(1969)
35) KATZ, S. : Chem. Engng Sci., 10, 202(1959)
36) KUBO, O. : 自動車技術, 47, 5, 70(1993)
37) LUPA, A. J. : Chem. Eng. Sci., 21, 861(1966)
38) LYCZKOWSKI, R. D. : A. I. Ch. E. J., 17, 497(1971)
39) MURATA, K. : Kagaku Kogaku Ronbunshu, 19, 1, 41(1993)
40) MURATA, K. : Kagaku Kogaku Ronbunshu, 19, 5, 849(1993)
41) MURATA, K. : ALUTOPIA, 23, 10, 9(1993)
42) NAGASAWA, T. : Kagaku Kogaku Ronbunshu, 20, 1, 131(1994)
43) NIIYAMA, H. : Catalyst, 34, 5, 364(1992)
44) PETERS, H. : USA pattent, 3353923, (1967)
45) SATOH, A. : Prepri. of 26th Aut. Meet. of the Soc. of Chem. Engng, P118, 295(1993)
46) SATTERFIELD, C. N. : A. I. Ch. E. Journal, 9, 2, 168(1963)
47) SATTERFIELD, C. N. : I. &E. C. Fund, 2, 257(1963)
48) SHINDO, Y. : Kagaku Kogaku Ronbunshu, 15, 6, 1138(1989)
49) SHITAOKOSHI, S. : Kagaku Kogaku Ronbunshu, 7, 2, 178(1981)
50) SIEGEL, R. : Appl. Scienrt. Res., A7, 386(1958)
51) SMITH, T. G. : Chem. Eng. Sci., 30, 2-E, 221(1975)
52) SMITH, T. G. : Chem. Eng. Sci., 31, 1071(1976)
53) SOLBRIG, C. W. : A. I. Ch. E. Journal, 13, 2, 346(1967)
54) SUNEJA, S. K. : A. I. Ch. E. J., 18, 1, 194(1972)
55) TAKEOKA : Kagaku Kogaku, 45, 433(1981)

56) TAKEOKA : Hyoumen, 24, 143(1986)
57) TONOOKA, Y. : Kagaku Kogaku Ronbunshu, 3, 2, 166(1977)
58) ULRICHSON, D. N. : Ind. Eng. Chem. Fund., 4, 2(1965)
59) WHITE, A. G. : U. S. Patent Office, 3011958, 1961)
60) WISSLER, E. H. : Chem. Engng Sci., 17, 937(1962)
61) YAMASEKI, K. : kagaku Kogaku Ronbunshu, 17, 2, 267(1991)